GA-4434

DIFFERENTIAL NEUTRON THERMALIZATION

Annual Summary Report, October 1, 1962 through September 30, 1963

By
W. L. Whittemore

October 15, 1963

General Atomic Division
General Dynamics Corporation
San Diego, California

UNITED STATES ATOMIC ENERGY COMMISSION • DIVISION OF TECHNICAL INFORMATION

DISCLAIMER

LEGAL NOTICE

Printed in USA. Price $2.00. Available from the Office of Technical Services, Department of Commerce, Washington 25, D. C.

USAEC Division of Technical Information Extension, Oak Ridge, Tennessee

GENERAL ATOMIC

DIVISION OF

GENERAL DYNAMICS

JOHN JAY HOPKINS LABORATORY FOR PURE AND APPLIED SCIENCE

P.O. BOX 608, SAN DIEGO 12, CALIFORNIA

GA-4434

PHYSICS

(TID-4500, 26th Ed.)

DIFFERENTIAL NEUTRON THERMALIZATION

ANNUAL SUMMARY REPORT
October 1, 1962 through September 30, 1963

Work done by:

S. Boehm
C. S. Choi
J. Hamrick
A. K. Hom
D. Parks
P. Schofield
W. L. Whittemore
K. Zimmermann

Report written by:

W. L. Whittemore

Contract AT(04-3)-167
Project Agreement No. 10
U. S. Atomic Energy Commission
General Atomic Project No. 220

October 15, 1963

FOREWORD

This annual summary report was prepared by General Dynamics/ General Atomic Division, San Diego, California, on USAEC contract AT(04-3)-167, Project Agreement No. 10, titled "Differential Neutron Thermalization." Dr. W. L. Whittemore is the General Atomic principal investigator on this project.

This report covers research conducted during the period of October 1, 1962 through September 30, 1963. The General Atomic project number is 220.

ABSTRACT

A large-aperture rotating mechnical chopper has been successfully incorporated in a neutron velocity selector at the General Atomic electron linear accelerator. During the present contract year, a system has been completed and put into full use to study the inelastic scattering of monoenergetic neutrons in a variety of materials. The scattering into various angular directions between 30 deg and 150 deg has been studied for incident neutrons with energies between 0.009 ev and 0.40 ev. Because of the uniqueness of the facility and its ability to study details of single scattering events with neutrons having energies significantly higher than are available with reactor-based experiments, most of the later work was done for $E_o > 0.20$ ev. The exact incident energy was chosen to optimize the ability to study various chemical rotation and vibration levels in this higher energy region. The technical details of the experimental apparatus are abundantly discussed. Numerous details are given for neutron interactions in liquid methane, liquid para-hydrogen, zirconium hydride, and polyethylene. A separate section is devoted to (1) a comparison of neutron moderation in liquid methane and liquid para-hydrogen, (2) details of the chemical binding of H atoms in zirconium hydride, and (3) some specific neutron interactions in polyethylene with specific references to the observation of interactions with the high-lying vibrational and rotational levels.

THIS PAGE

WAS INTENTIONALLY

LEFT BLANK

CONTENTS

THIS PAGE

WAS INTENTIONALLY

LEFT BLANK

FIGURES

FIGURES (Cont.)

FIGURES (Cont.)

I. INTRODUCTION

The experimental and theoretical work carried out during this reporting period continues the fundamental studies of the interaction mechanisms by which neutrons exchange energy with moderator materials. Above ~1.0 ev, these interactions may be regarded as collisions of neutrons with free atoms; however, at lower energies they must be regarded in terms of the excitation of molecular thermal motions determined by binding forces. A problem of neutron thermalization, therefore, is concerned with the distribution of energy levels and the probability of excitation by neutron collision. In particular, differential neutron thermalization is concerned with specific neutron interactions with these various energy levels. In the earlier phases of this contract, interest was directed toward very-low-temperature moderators in order to produce better sources of neutrons for the linear accelerator velocity selector and to promote a better understanding of cold neutron sources in general. As this contract has progressed, and particularly during this present contract year, interest has shifted to the specific details of the scattering kernel $\sigma(E_o, E, \theta, T)$ for several moderator substances and particularly for the higher values of $E_o (> 0.10$ ev).

During the earlier part of the present contract period, a completely new and considerably enlarged scattering set-up was established. As a result, the versatile General Atomic neutron velocity selector has been put into satisfactory operation at the linear accelerator (Linac). Considerably expanded flight paths have been provided where appropriate, and a major change in the experimental set-up has been made by adding massive amounts of neutron and gamma ray shielding where most appropriate. As a result, considerable improvement has been obtained not only in the energy resolution of the incident neutrons but also in the substantial reduction of the perennial gamma-flash problem in the neutron detectors. With the new neutron velocity selector, it is possible to study a number of different scattered neutron beams simultaneously. This is permitted by simultaneous use of several counter banks and a multiple input adapter which is used in conjunction with the Technical Measurements Corporation 1024 channel analyzer. As a result of these changes, far more efficient use is made of Linac running time since numerous individual scattering patterns are obtained simultaneously.

The previous Annual Summary Report[1] contained a detailed discussion of the advantages of the present neutron velocity selector compared with the reactor-based counterpart where four choppers are required to accomplish the work now substantially performed by a single rotating chopper. It seems appropriate, at this point, to indicate another substantial advantage provided by the neutron velocity selector operated at Linac which is the possibility of studying neutron interactions for incident neutrons with energies ≤ 1.0 ev. This opens up the entire range of chemical and crystal binding forces. For incident neutron energies >1.0 ev, atoms can be considered free in their interactions with the incident neutrons. For the energy region from ~ 1.0 ev down to thermal energies, one has the exceedingly complex problem of chemical binding forces where the atoms cannot be considered to be either tightly bound or completely loose. Experimental work on this problem at reactors is limited by low incident neutron energies ($\lesssim 0.1$ ev); consequently, the major effects of chemical rotations and vibrations cannot be investigated there. In the present work, a large body of new information is presented on a number of these higher-lying energy levels and their interactions with neutrons.

II. EXPERIMENTAL TECHNIQUES

The method of utilizing an electron linear accelerator with a neutron velocity selector to perform measurements of neutron inelastic scattering were discussed in the last annual summary report.[1] The exact details of the system currently used to perform the measurements are sufficiently different from those of the system used during last year's contract period to warrant the detailed treatment given below.

2.1 NEUTRON VELOCITY SELECTOR

The experimental area used for neutron inelastic scattering is much the same as during the previous contract period. However, considerable readjustments within this area have been made. Figure 1 shows a new, modified floor plan giving the important details of the new neutron velocity selector. Of particular interest to this experiment is the relative size of the various flight paths. An inspection of Fig. 1 shows that the incident energy resolution is determined by a 6 m flight path between the neutron source moderator and the neutron chopper. From the scattering well position for the scattering sample to the individual neutron detectors, there is a flight path of the order of 2 m. The scattered neutron energies are determined by time-of-flight techniques over this 8 m distance.

In going to the longer flight path of 6 m, instead of the former 3 m, there has been no sacrifice of intensity for a number of reasons. The neutron source moderator has been made sufficiently large to cover effectively the same solid angle as previously covered with the much smaller flight path. Specifically, this means that, in place of the former neutron source moderator which was essentially 6 in. x 12 in., the present neutron source moderator is 12 in. x 24 in. in lateral extent. A U-238 electron-converter target is used to produce neutrons and has been observed to give a factor of 2 improvement over a W target. The 6 m drift tube is filled with argon gas in place of nitrogen, lessening the scattering loss. The degree to which the details have been worked out with regard to providing adequate intensity in the new, revised set-up is indicated by the fact that the over-all intensity of neutrons selected by the chopper is now somewhat greater than with the older set-up, even though the flight path has been increased from 3 m to 6 m.

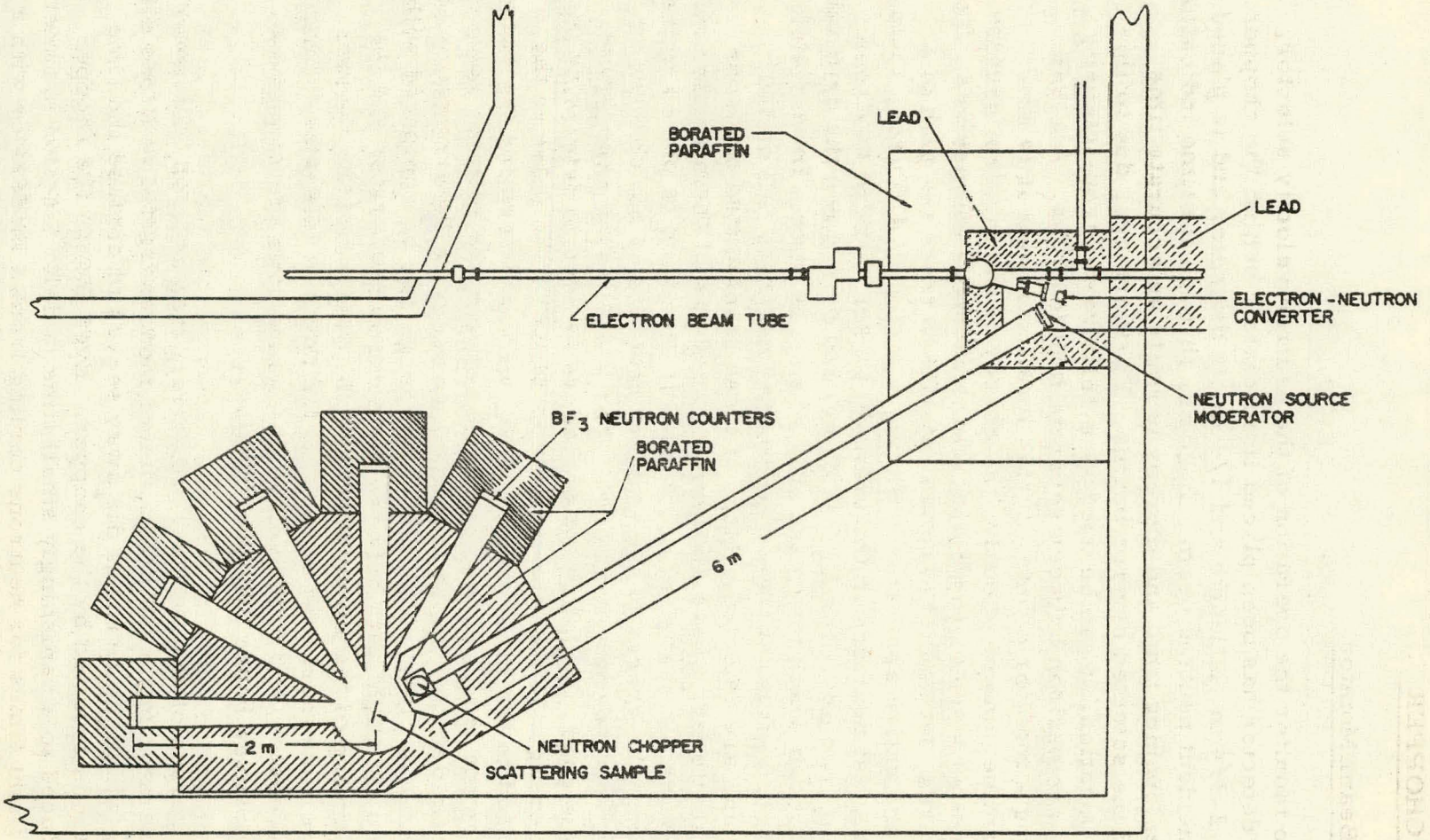

Fig. 1--The experimental arrangement for the neutron velocity selector and scattering apparatus, showing part of the experimental room at the General Atomic electron linear accelerator facility

2.2 NEUTRON CHOPPER

2.2.1 Neutron Beam Monitor

In order to monitor the operation of the neutron velocity selector, a small neutron detector has been placed immediately behind the chopper. This detector is 2-3/4 in. in length and 1/4 in. in diameter and is placed directly in the incident neutron beam. It gives, through its time indication, the exact chopper opening time and thereby permits an accurate time determination of the selected neutron beams. Furthermore, due to this detector's ideal location, it can be used as a relative-neutron-intensity monitor to allow comparison between separate neutron runs. Another advantage of using a monitor counter at this location is that it is now possible to determine, unambiguously, the energy of the incident neutron, using recorded output time-of-flight data on the neutrons themselves. To show how this works, let us digress momentarily to trace the path of a neutron through the entire apparatus. During a period of 4.5 μsec, incident electrons produce fast neutrons in the uranium target. These neutrons moderate in one or two μsec (for $E_o > 0.25$ ev) and drift down the drift tube to the chopper, through which they pass only when it is open. Immediately thereafter, a small fraction of these transmitted neutrons fall on the monitor counter and are detected. Most of these transmitted neutrons progress to the scatterer, where appropriate numbers of them scatter into the various detectors for scattered neutrons. If vanadium is placed in the scattering position, the energy of the incident neutrons is not changed in scattering; only the direction is changed. For a scattering experiment where vanadium is used, the following procedure is used to determine the incident neutron energy. From the time dependence of the pulse in the monitor counter and in the main counter bank, we can determine the exact flight time. Since the length of the flight path between the monitor counter and one of the main detector banks is known, an accurate determination of the neutron velocity is made. The resulting energy can be compared with that deduced from the flight path between the neutron moderator and the chopper and the timing of the Linac burst and the opening of the chopper. (In the latter case, one must take account of the neutron "die-away" time in the source moderator.) The above two determinations are consistent, except for uncertainties in the "die-away" time.

In earlier phases of the contract, relatively long neutron "die-away" times in the moderator made the production of monoenergetic neutrons difficult. This time during which the neutrons die away serves to confuse the time of flight for neutrons selected by the chopper. Even though the chopper time may be reduced to a vanishingly small time (a delta function in time), the variation in flight times for neutrons coming from a moderator with a long die-away time is sufficient to produce a big variation in incident

neutron energy. The average flight time is difficult to determine under such circumstances, since we know only the estimated die-away time. However, use of the monitor counter and the detector bank for neutrons scattered by vanadium provides a unique and unambiguous determination of this average incident energy, with no undertainty due to such quantities as neutron die-away time. Incidentially, use of this technique has now verified previous measurements on neutron die-away times in moderators. Furthermore, thanks to this improved method for energy determination, fewer diagnostic studies of potential moderators have now to be made than would otherwise be necessary.

2.2.2 Considerations of New Chopper Inserts

The neutron monitor counter placed immediately behind the neutron chopper has been used to measure the relative intensities of neutrons selected by the neutron velocity selector. Figure 2 shows the results obtained with this chopper; no corrections have been made for neutron counter efficiencies. From Fig. 2, it is seen immediately that adequate intensities for neutron inelastic scattering measurements exist well above 0.5 ev, since it is known that adequate intensity exists for measurements with neutrons $\leq$0.4 ev. The failure of the slit system for neutron energies $>$0.4 ev is due to the fact that this system depends entirely on the use of cadmium and nickel to stop neutrons. A new slit system, using additional hydrogenous scatterer in place of the nickel-cadmium scatterer absorber, will surely extend the upper limit considerably beyond 0.4 ev. However, due to strength considerations, it will be difficult to fabricate a neutron scatterer from a plastic material as thin as the present 0.011 in. cadmium-nickel separators in the rotating slit system. Since this neutron absorbing material must be somewhat thicker to gain sufficient strength for use in the rotating chopper, improving the chopper by use of such material will decrease somewhat the transmitted intensity of the slit system, because the relative ratio of absorber to open channels will be smaller. Some of this lost transmission efficiency will be recovered by the use of properly curved slits instead of straight slits. Table 1 indicates some of the pertinent information with regard to the effective improvement produced through the use of slightly curved slits, instead of straight slits, for the selection of neutrons in the energy region above 0.2 ev.

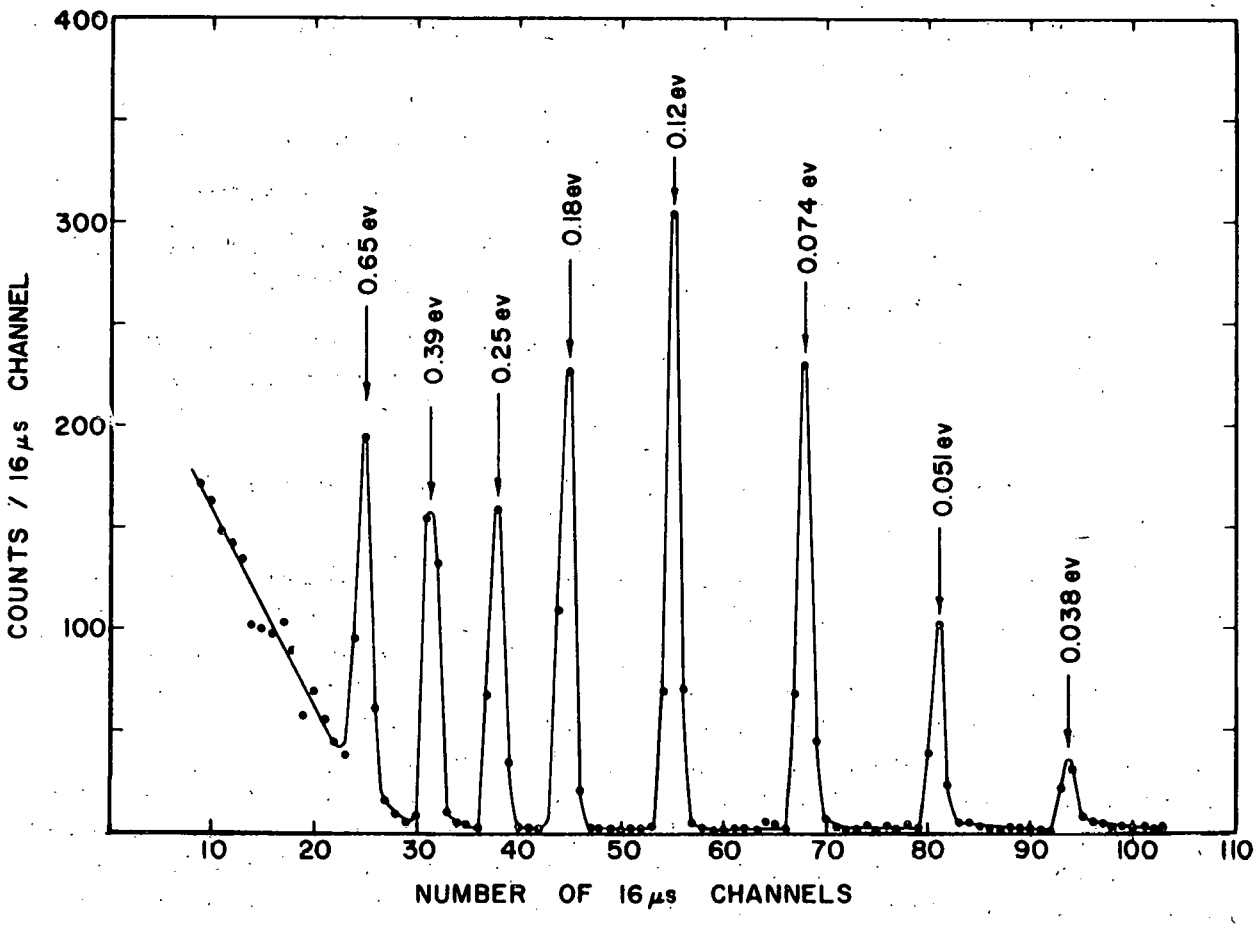

Fig. 2--Composite representation of the operation of the mechanical neutron chopper. Each individual pulse was obtained by properly phasing the chopper to select the desired energy. The detector is a 1/4 in. diameter BF_3 counter placed immediately behind the chopper. The pulse width represents the chopper-open time. Background is not deducted and no correction for counter efficiency is included. Note that the background is very low for $E_o < 0.4$ ev, whereas the Cd shutters in the chopper begin to fail for $E_o > 0.4$ ev.

Table 1

RELATIONS BETWEEN OPTIMUM CURVATURE AND FRACTIONAL TRANSMISSION FOR STRAIGHT SLITS* FOR VARIOUS INCIDENT NEUTRON ENERGIES AT CHOPPER SPEED OF 180 RPS

E_o (ev)	ρ (in.)	s (in.)	T
.50	126	.016	.68
.25	86	.023	.54
.10	77	.026	.48
.05	54	.037	.26
.025	38	.052	0

E_o = incident neutron energies

$\rho = v_o/2\omega$ = optimum curvature

s = maximum deviation of the curved slit from a straight slit

T = ratio of straight-slit transmission to curved-slit transmission

*Straight slits have a spacing of 0.05 in. and a length of 4 in.

The construction of a new chopper slit system will have three main improvements as its goal. On the one hand, it is necessary to increase the amount of absorbing and scattering material in the beam to effectively "chop" the incident beam for incident neutron energies > 0.4 ev. Secondly, it becomes useful to incorporate curved slits for these larger energies, because a gain in intensity of as much as 30 percent may be achieved, particularly if the individual channel widths in the slit system are narrower than used in the current system. Thirdly, the slit system and/or collimators will be made narrower, or the rotor system will be rotated at a higher speed, or a combination of these two will be used to decrease the effective width at half maximum of the incident neutron pulse. As detailed in the last annual summary report,[1] the relationship between the pertinent quantities governing the effective opening time is given by

$$\alpha_1 + \alpha_2 = 2\omega t_{\frac{1}{2}} \qquad (1)$$

where

α_1 = the angular aperature of the collimator system,

α_2 = the individual angular aperture of the individual slits in the the chopper,

ω = the angular rotational speed of the rotor, and

$t_{\frac{1}{2}}$ = the width at half maximum of the transmitted beam.

Rotating the present chopper at twice the present rotational speed would be the simplest way to reduce the transmitted beam width; unfortunately,

this would require rotation speeds of over 21,000 rpm and is entirely out of the question for the present rotor. However, we believe that rotational speeds up to 15,000 rpm are possible with the present system (with only minor mechanical modifications) which would thus achieve an effective open time of the order of 2/3 the present effective time, or about 14 μsec. It is not useful to decrease α_1 or α_2 individually by large amounts because of a large resultant sacrifice in intensity. The present value of α_1 approximately equals α_2 and is an optimum choice. A suitable change will decrease both quantitites. The new design will probably reduce $(\alpha_1+\alpha_2)$ by $\sim 1/\sqrt{2}$ and call for an increase in ω by $\sim\sqrt{2}$. The over-all change in $t_{\frac{1}{2}}$ will thus be a factor of about 2. The resulting pulse width will then be quite comparable with the Linac pulse time of 4.5 μsec plus a 2 μsec die-away time.

2.2.3 Electron-Neutron Converter and Neutron Moderator

During the present contract year, a new electron target encorporating U-238 was installed. The gain in over-all ouput compared with the use of a tungsten target was a factor of 2. The cooling rate for this target is six gallons of water per minute circulating in a closed system. No fission products have been detected in the water. The individual uranium discs, 1-1/2 in. in diameter and 1/8 in. thick, were clad in thin stainless steel envelopes, carefully welded shut. A series of these dics was arranged coaxially, perpendicular to the incident beam. A large slug of tungsten acted as the final back-up to the electron beam. Figure 3 shows the details of this uranium holder.

The neutron moderator is placed in as close proximity to the electron neutron converter as possible and has recently been in the form of a slab of water 1-1/2 in. thick with a lateral extent of 12 in. x 24 in. Since this moderator is very close to the electron target where a considerable amount of thermal heat is produced, water is circulated continuously at a rate of two gallons per minute through the aluminum-jacketed moderator holder. For some of the experiments, this water moderator was replaced by 1-1/2 in. of polyethylene. The neutron flux observed in the neutron velocity selector was lower by a factor of approximately 2 when polyethylene was used. This is in agreement with our earlier conclusion that polyethylene is a poorer moderator than water.

2.2.4 Motor Speed Control

The rotating neutron chopper is powered by a 1 hp, series-wound 110 v electric motor. This motor has a variable speed ranging from considerably less than 60 rps to more than 180 rps. During most of the present contract year, the speed has been controlled manually by the use of a Variac. Small drifts in motor speed are corrected by adjusting motor input voltage in increments of the order of 1/2 v, achieved in

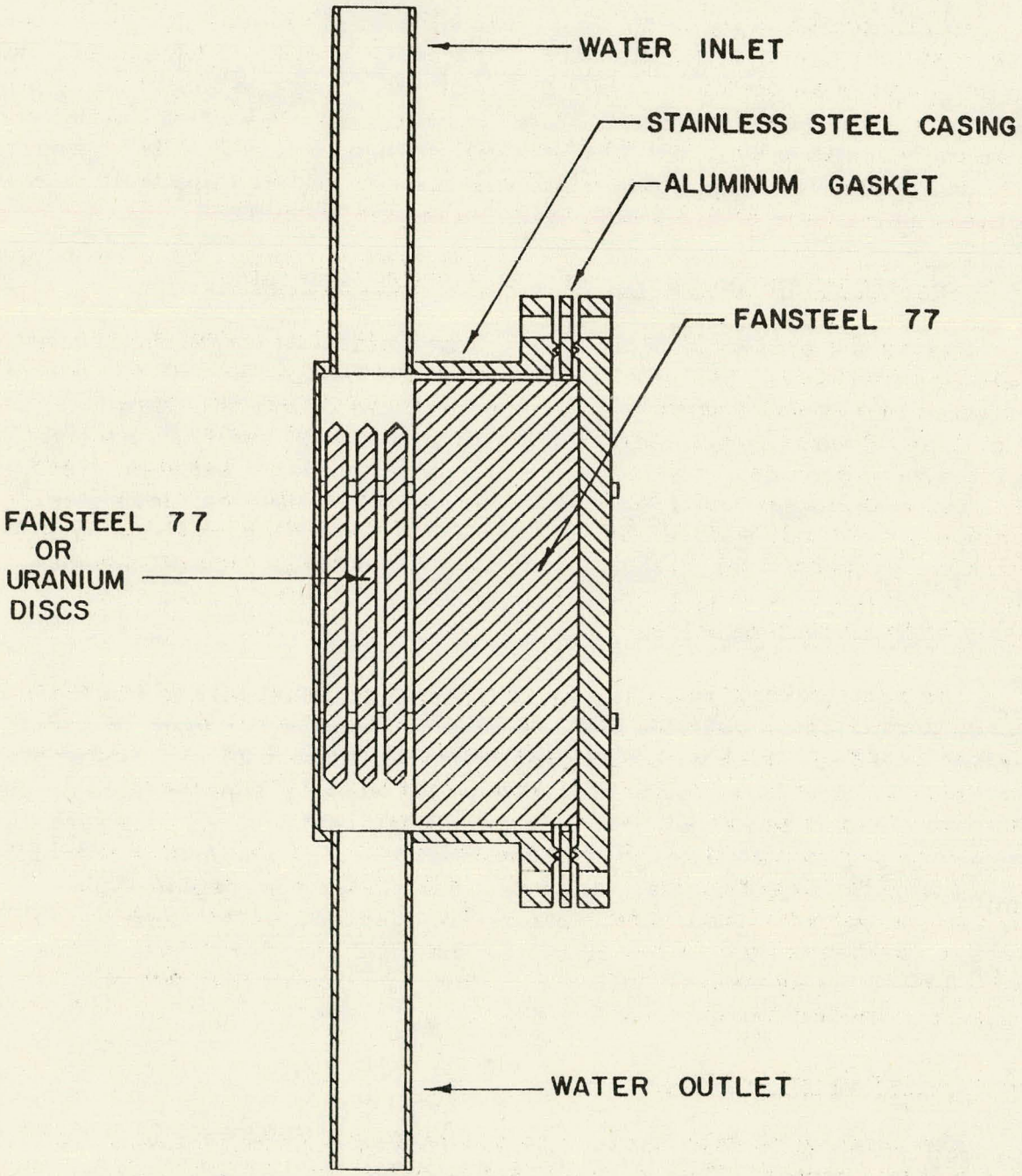

Fig. 3--Cross section of the electron-neutron converter

about 1 or 2 sec. The period of the motor is continuously monitored electronically. It is observed that fluctuations in this period of about ±1 μsec occur regularly, with only an occasional excursion of ±3 or 4 μsec. An electronic Servo system, which has been installed recently and is currently being improved, uses solar light cells to sense the lights from the scaler of the electronic period counter. Except for a dead band, arbitrarily taken as ±1 μsec, automatic adjustments on the ac input voltage correct small deviations in the period. At present, it is anticipated that larger variations in the period will automatically signal the operator to make manual adjustments in fine speed control of the motor. A variation of 2 μsec in the period of the motor corresponds to $\Delta E/E \approx 0.006$ for incident neutrons of 0.4 ev. The width of the chopper pulse itself corresponds to an incident energy resolution of $\Delta E/E \approx 0.06$. It is thus seen that the additional error caused by the usual drift in motor period is about 1/10 of the resolution of the chopper itself. Consequently, for the present, this system is entirely satisfactory.

2.2.5 Multi-Input Adapter for TMS Time-Of-Flight Analyzer

An exceedingtly flexible adapter, which has been fabricated for use with the TMC time-of-flight analyzer, permits the use of up to 8 separate input channels for the simultaneous recording of time-of-flight data. The details of this analyzer are being published elsewhere[2] but will be summarized in some detail here. The basic point to note is that there is no essential restriction in counting rate in any of the multiple input channels. This means that no special additional correction need be made for counting rate loss in one channel because another channel has recorded an incoming pulse during a single burst from the Linac.

The economics of Linac operation encourage making neutron scattering measurements at several angles simultaneously. It was decided to use the memory splitting feature of the TMC-1024 time-of-flight analyzer to accomplish this. The external-memory-control mode of operation permits division of the core memory array into 8 sub-groups of 128 channels each, or 4 sub-groups of 256 channels each. When suitable signals are applied to the instrument's memory location connector, the signals are transferred into the proper address bits by the arithmetic reset pulse in the CN-1024 digital computer. A trigger circuit for each of 8 detectors, followed by a diode matrix and 3 flip-flop circuits, provides the memory locations signals in our adaptor. This method carries a severe limitation, however. To be certain of error-free storage, only one detected neutron can be processed during each pulse from the Linac because the address bits can be set from the memory location connector but they cannot be reset. Strictly speaking, more than one pulse per address-cycle time could be accomodated if the later pulse occurred in a higher numbered sub-group. These restrictions were intolerable in this case.

One solution is to modify the CN-1024 rather severely. The last three address bits, corresponding to the routing portion of the address scaler, could be slaved to the three flip-flops in the adaptor. Diode coupling into the collectors of the 2^7, 2^8, and 2^9 transistor binary circuits could accomplish this slaving. However, this method is mechanically awkward due to the lack of spare pins on the scaler plug-in cards. In view of this, an alternative solution was adopted.

During the analyzer's 16 μsec memory-cycle time, an address-advance pulse is generated in the 211 time-of-flight plug-in unit to artificially advance the address scaler. The counts lost during the memory cycle are thus replaced. This allows the scaler to start from the count it would have contained had it not been stopped by the input pulse. The address advance signal occurs immediately after the count is added to the appropriate channel. It is quite simple to take this pulse and use it to reset the 2^7, 2^8, and 2^9 address bits. At the expiration of the fixed 16 μsec memory-cycle time, the routing portion of the address scaler has thus been reset and is capable of accepting new commands. The memory subgroup corresponding to the particular adaptor input receiving a neutron pulse can therefor be selected unambiguously by using the eight states of the above mentioned flip-flops to generate the ground signals required at the memory location connector. The input signal to the 211 input is delayed slightly to allow the flip-flop circuits to assume their new states. Provision was made to accept either the -50 v pulses from a Hamner N-301 discriminator or +8 v pulses from a transistor gating unit.

III. SCATTERING OF NEUTRONS BY LIQUID HYDROGEN AND LIQUID METHANE

3.1 SOME CONSIDERATIONS OF NEUTRON SCATTERING IN LIQUID PARA-HYDROGEN

During this contract period, additional experimental work has been performed on neutron scattering in liquid para-hydrogen. The major effort in this direction was aimed at the very-low-energy inelastic scattering. Neutrons with energies of the order of 0.009 ev incident on liquid hydrogen should reveal considerable liquid state effects in the hydrogen. Previous data obtained for the total cross section as well as neutron spectra from specimens of liquid para-hydrogen also reflect liquid state effects. As part of the effort to understand scattering in liquid hydrogen, the total cross section was evaluated using both Sjölander's and Sarma's treatment for the total scattering cross section.

3.1.1 Computed Total Cross Section for Para-Hydrogen

Since no complete theory for the total scattering cross section of hydrogen in the liquid phase exists, it seems reasonable to evaluate the best possible gaseous total cross section and to make comparisons from this. The theory of Sarma[3] has been evaluated using a digital computer to give the total cross section as a function of neutron energy for para-hydrogen. Since this cross section is dependent on the temperature of the liquid hydrogen, two temperatures were used for this evaluation, namely 0.3°K and 20.4°K. The theoretical results for these two temperatures are shown in Fig. 4.

Sjölander's[4] closed form representation for the total cross section of gaseous para-hydrogen has also been used to check the energy dependence of the total cross section. Sjölander's results per molecule are given as

$$\sigma(E) = \sigma_o \left[\left(1+\frac{1}{2}\frac{kT}{ME}\right) \mathrm{erf}\left(\frac{ME}{kT}\right)^{\frac{1}{2}} + \left(\frac{kT}{\pi ME}\right)^{\frac{1}{2}} \exp(-ME/kT) \right], \qquad (2)$$

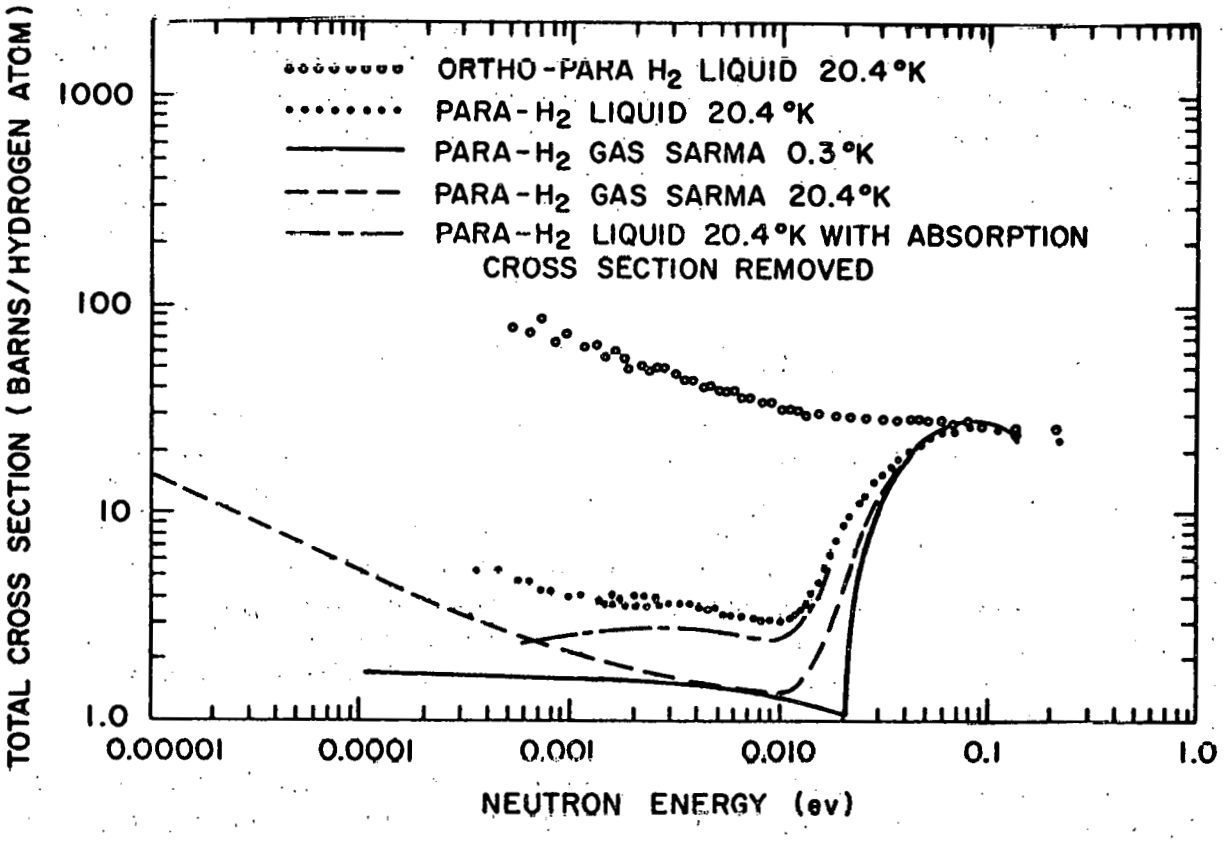

Fig. 4--Liquid hydrogen cross section as a function of neutron energy. The experimental data for an ortho-para mixture and para-hydrogen are compared with theoretical curves for gaseous hydrogen at 0.3°K and 20.4°K.

where

$$M = 2$$

$$\mathrm{erf}x = \frac{2}{\pi^{\frac{1}{2}}} \int_{o}^{x} \exp(-y^2)\, dy$$

$$\sigma_o = \frac{16}{9}\pi \times 16\left(\frac{a_s}{4} + \frac{3a_t}{4}\right)^2$$

$$= \frac{4}{9} \times 64\pi \sum_c \; ; \quad \sum_c = 3.52 \times 10^{-2} \text{ barn} \; .$$

This particular function has been evaluated for the same temperatures used for Sarma's theory. The agreement between the two approaches is satisfactory. Figure 4 also shows, for the Sarma case of 20.4°K, the manner in which the cross section goes over into its "1/v" dependence for the low-energy incident neutrons. It is particularly useful to note that the total cross section for incident energies <0.010 ev is much smaller for the gaseous hydrogen case than for the liquid hydrogen experimental results. This is a liquid state effect which will be treated in Section 3.1.2.

It is probably also useful to point out that the broadening of the energy region over which excitation of the first rotational level takes place is a molecular effect and not necessarily a solid state effect. Figure 4 shows that, for 0.3°K, the onset of the excitation of the first rotation level is extremely sharp. The energies of neutron for which, for gaseous hydrogen, excitation of the first level takes place at 20.4°K, extend from 0.01 to >0.02 ev. This can be readily explained as a Doppler broadening by noting that the broadening of the resonance is approximately equal to $(K^2T/2)^{\frac{1}{2}}$, where K is the momentum transfer for such collisions of neutrons and hydrogen molecules and T is the average kinetic energy of the molecules. Evaluation of this quantity shows that the resonance is easily spread by something of the order of 0.01 ev, which is sufficient to explain the observed predicted results without recourse to liquid state effects.

3.1.2 Some Considerations of Liquid State Properties of Para-Hydrogen

It has been pointed out in some of our previous reports that the widths of the scattered distributions for liquid para-hydrogen were broader than predicted by Sarma's theory. Figure 5 shows a typical scattering distribution for liquid para-hydrogen for an incident neutron energy of 0.065 ev. It is readily seen that the predicted gaseous scattering distribution is substantially narrower than observed. Egelstaff, at the Chalk River Symposium (September, 1962),[5] suggested that the higher

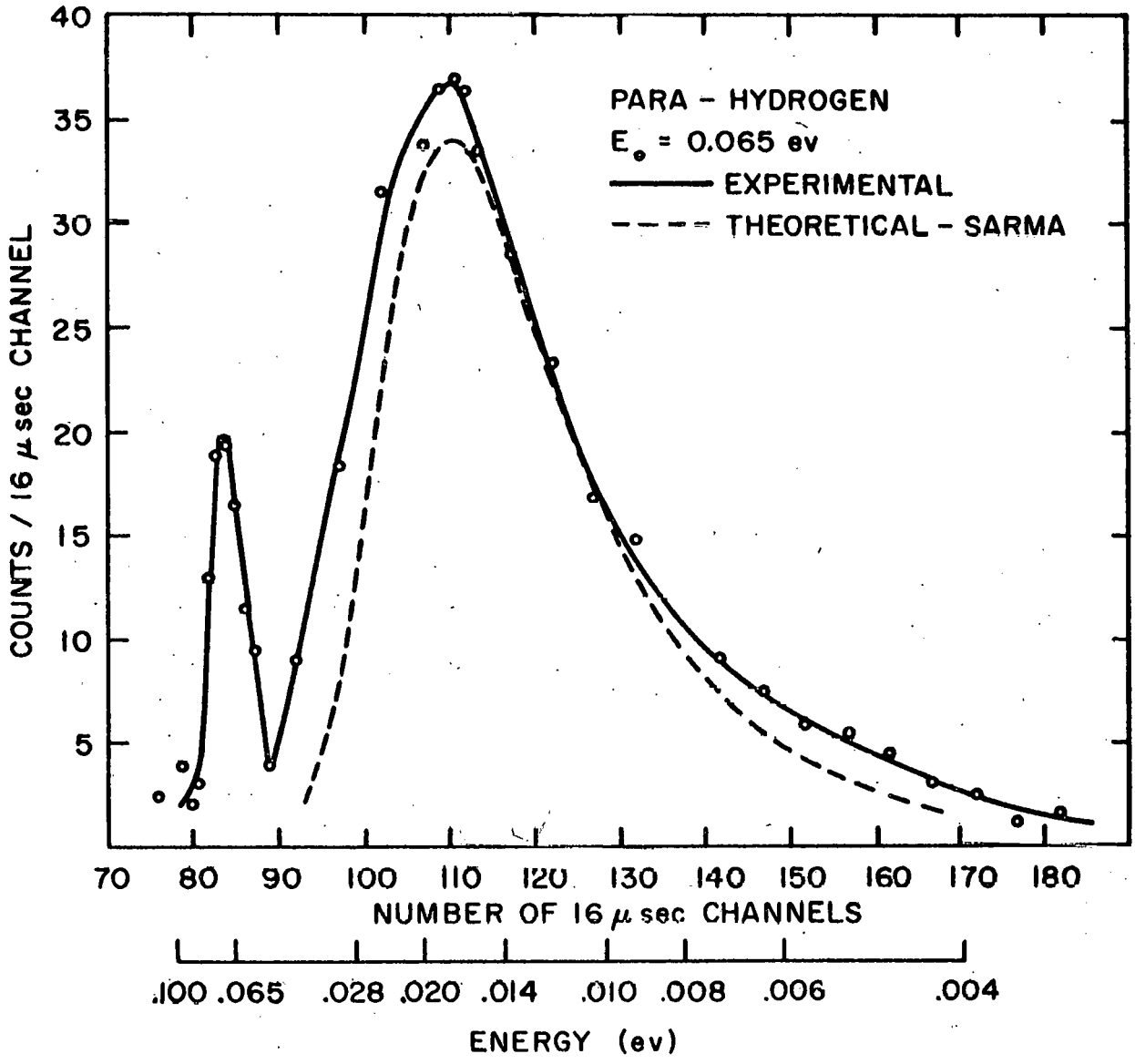

Fig. 5--A time-of-flight scattering distribution for neutrons of 0.065 ev scattered at 90 deg by liquid para-hydrogen. Also shown is a theoretical curve computed for gaseous hydrogen from the theory of Sarma.

average energy of the molecules in the liquid state should broaden the scattered neutron distribution beyond that expected for a gas. To make a first estimate of this effect, let us proceed as follows. Sarma has computed that the shape of the differential scattering distribtuion should be given as

$$\exp\left\{-m\frac{\left[\hbar\omega-(E_{j'}-E_j)-\hbar^2K^2/4m\right]^2}{k_\beta T\hbar^2K^2}\right\} \qquad (3)$$

The quantities in this equation are, for the most part self-explanatory; however, a complete description of the origin of this equation as well as of all the terms is given in Eq. (6) in Ref. 1. Schofield points out that if the molecules are not free and, in fact, have an Einstein energy $h\nu$ which is considerably larger than $k_\beta T$, then $k_\beta T$ in Eq. (3) should be replaced by something similar to

$$\tfrac{1}{2}h\nu\coth(h\nu/2k_\beta T) \quad ,$$

which, for the present case, $\approx 2k_\beta T$. Of course, something more sophisticated would need to be done to make a complete correction for the liquid state effects. However, the important point to note is that replacing $k_\beta T$ in Eq. (3) by approximately $2k_\beta T$ implies that the width of the distribution is increased by about $\sqrt{2}$ ($\approx$40 percent). This is in line with the observation of Egelstaff.[5]

The preceding consideration shows that the molecular effects in the liquid state are important for determining neutron interactions with the lower energy neutrons. A similar deduction can be made strictly on the basis of the measured total cross section. In Fig. 4, we have already shown that the measured liquid total scattering cross section is considerably larger than the predicted gaseous total cross section. The somewhat strange behavior of the total cross section for liquid para-hydrogen is only partially understood from the behavior of the gaseous hydrogen cross section. In particular, it should be noted that the observed scattering cross section σ_{ob} of liquid para-hydrogen is relatively independent of neutron energy E_o in the range $0.0004<E_o<0.010$ ev, in contrast with the cross section for gaseous hydrogen. It should also be noted that σ_{ob} is larger than 2x1.7b , the very-low-temperature gaseous para-hydrogen molecular cross section σ_o for extremely slow neutrons. These facts together indicate that the hydrogen molecules are bound together in larger scattering complexes and do not freely rotate and translate. A simple relation exists between m, the mass of the scattering complex; m, the neutron mass; and M, the mass of the scattering nucleus (=2m for

para-hydrogen molecules), provided that the neutron energy is simultaneously larger than kT (0.0017 ev) and smaller than an equivalent Debye temperature which has been shown to be approximately 0.007 ev.[6] This relation is expressed as

$$\sigma_{ob} = \sigma_o\left[(1+m/M)/(1+m/\mathfrak{M})\right]^2. \qquad (4)$$

Since the cross section in question is relatively independent of the neutron energy over an extended range, including the above restricted energy range, application of this equation may be justified and gives $\mathfrak{M}/M$ approximately 3 for the data of Fig. 4; this indicates that, on the average, about 3 molecules of para-hydrogen are bound together. From the point of view of neutron moderation, a neutron scattering against a larger hydrogenous mass should lose less energy on the average because of the larger effective mass of the recoiling particle. In this presentation, one sees two quite different aspects of the experimental problem, both pointing to the tendency of molecules in liquid para-hydrogen to cluster.

3.2 COMPARISON OF NEUTRON INTERACTION IN LIQUID METHANE AND LIQUID PARA-HYDROGEN

The interest in inelastic scattering of neutrons in liquid methane and liquid hydrogen stems in large measure from an interest in the use of these substances as moderating materials for cold neutrons. A number of preliminary investigations have been conducted with this goal in view, although a complete study has not yet been performed on either substance. Complete inelastic scattering measurements for very cold neutrons, as well as for neutrons having all other incident energies, have not yet been published for either substance; however, partial data from the present experiments does exist for selected incident energies and for a restricted range of scattering angles. In 1961, Webb[7] published a paper on some considerations of the use of liquid methane and liquid hydrogen in producing cold neutrons; he based his results mainly on the cold spectra of neutrons emerging from these two moderators. Although Webb treated only the spectra for liquid methane and liquid hydrogen, it appears to us that the information contained in the total cross section can be useful in arriving at general conclusions concerning the relative merits of these two cold-neutron sources. The inelastic scattering data will, of course, be most useful in this respect. The purpose of this section (Sec. 3.2) is the consideration of our data on the total scattering cross section, the neutron spectra, and the inelastic neutron scattering in liquid hydrogen and liquid methane.

3.2.1 Experimental Data on Neutron Spectra

In previous publications,[8] [9] we have presented experimental results on the neutron spectra generated in specimens of liquid methane and liquid para-hydrogen. Figures 6 and 7 contain some of these data. These spectra illustrate a significant difference between liquid hydrogen and liquid methane. The specimens were 6 in. in diameter and more than 6 in. high, and thus contained several interaction path lengths. They were excited from all sides by an external source of fast neutrons.

It will be noted from Fig. 6 that, for a liquid para-hydrogen, the average temperature of the Maxwellian curve best fitting the data is about 31°K, whereas the temperature of freely boiling liquid hydrogen is known to be 20.4°K. Thus, the neutrons are not in thermal equilibrium with liquid hydrogen. Solid para-hydrogen is not much more effective than liquid hydrogen in producing cold neutrons. It appears that the energy exchange processes for very slow neutrons in liquid and solid hydrogen are hindered.

In contrast with the preceding situation, Fig. 7 shows that neutrons are in thermal equilibrium with liquid methane. This is indicated by the fact that the average temperature of liquid methane is 111°K ($\approx$0.009 ev) and the average temperature of the neutrons, as indicated by the best Maxwellian curve fitted to the data, is about the same. Furthermore, if liquid methane is cooled to the temperature of boiling liquid hydrogen (20.4°K), the neutrons are again in thermal equilibrium with the colder methane. In contrast to the situation with liquid para-hydrogen, it would appear that the individual methane molecule rotates most freely in either the liquid or the solid phase. From these data, it appears that liquid or solid methane is superior to liquid hydrogen as a source of cold neutrons with $E < 0.010$ ev.

3.2.2 Total Scattering Cross Section

The total scattering cross sections have been measured for liquid para-hydrogen and liquid and solid methane and are presented in Figs. 4 and 8. These data have been reported in an earlier work.[9] The important feature of the scattering cross section for liquid para-hydrogen, shown in Fig. 4, is that it decreases to a very low value for neutron energies less than $\approx$0.010 ev and remains roughly constant with decreasing energy. This small cross section for a neutron energy which is less than that for excitation of the first rotational level, has to do with a coherence of the scattering from the two hydrogen atoms bound in the molecule and has been extensively studied experimentally[10] for gaseous hydrogen. Also shown in Fig. 4 is the theoretical cross section for gaseous hydrogen computed from the theoretical work of Sarma[3] and Sjölander[4].

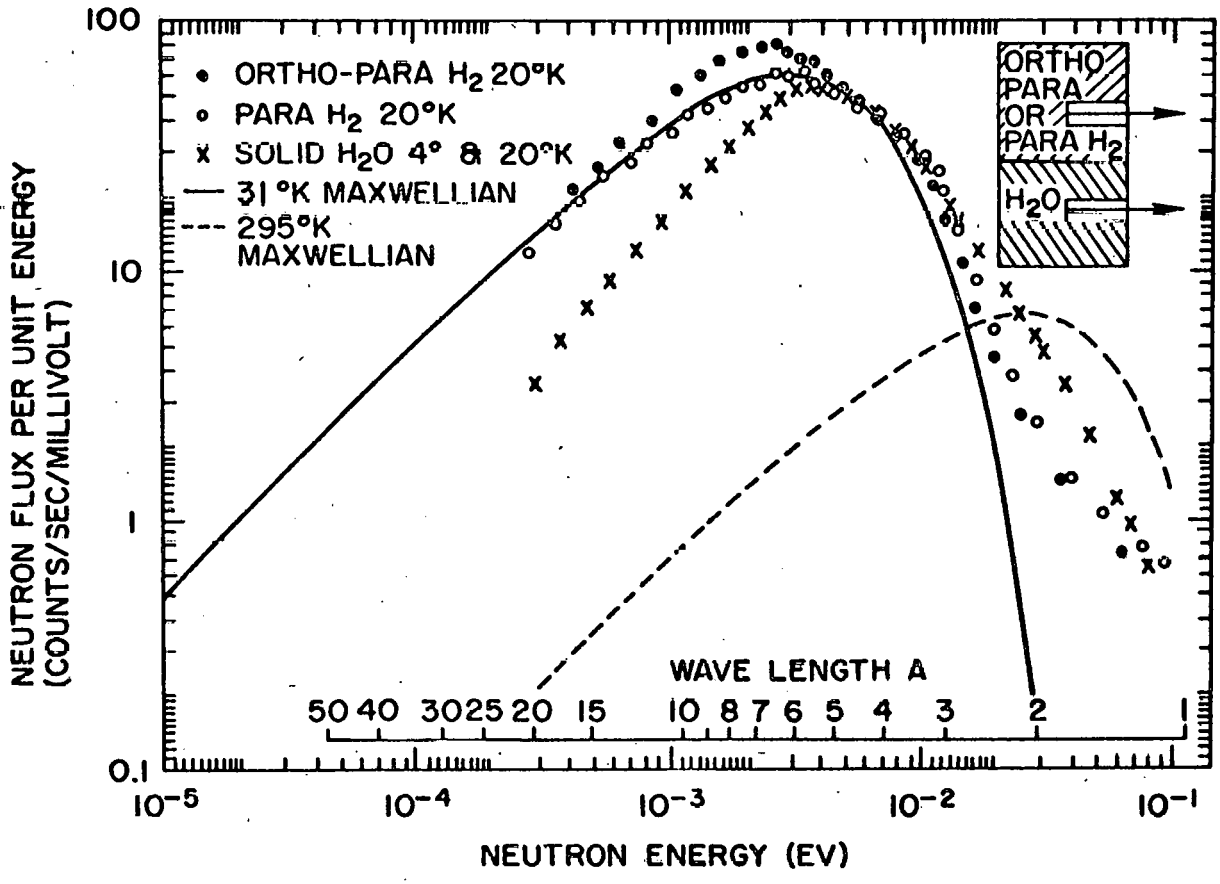

Fig. 6--Neutron spectra from specimens of liquid hydrogen and ice at 4°K and 20°K. Also shown are theoretical Maxwell distributions for 31°K and 295°K. Note that the para-hydrogen spectrum has a characteristic temperature of about 31°K.

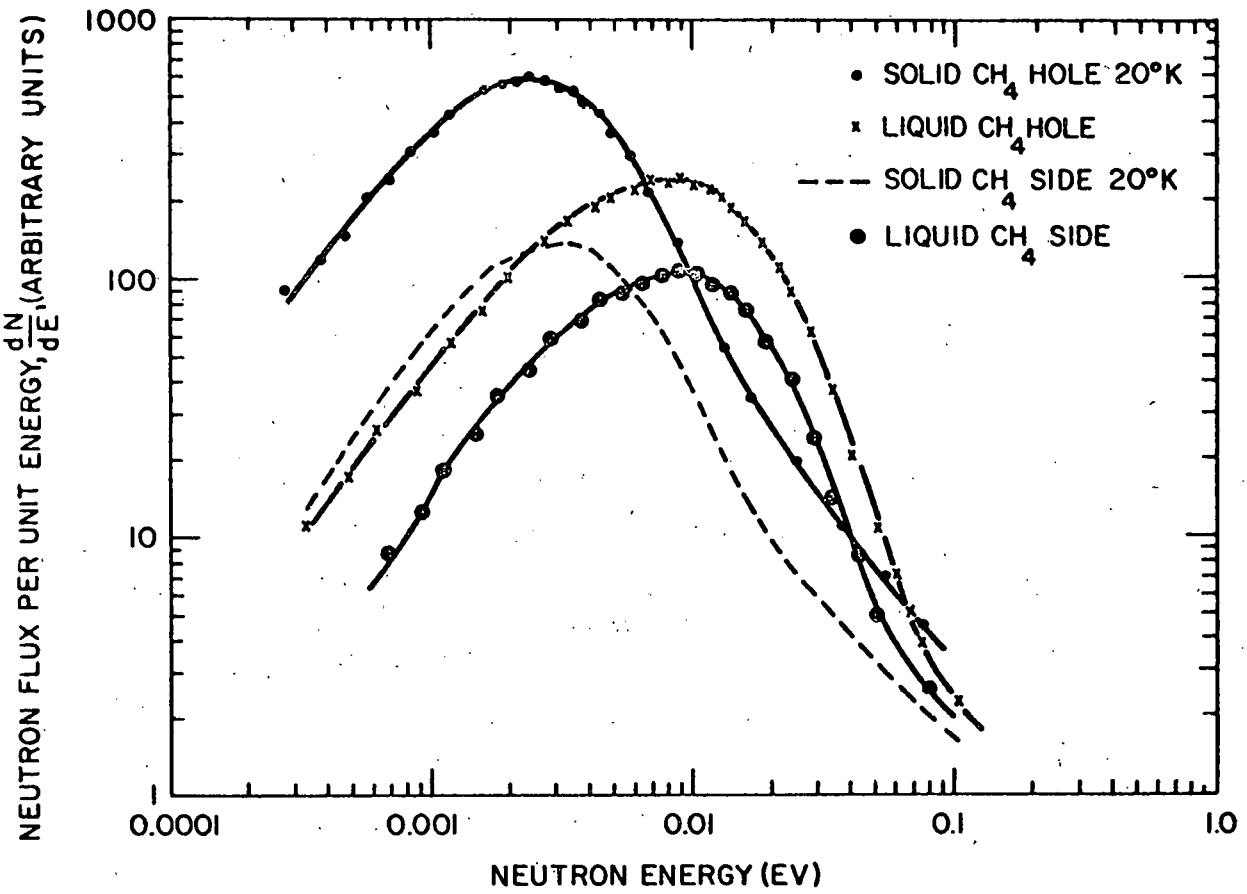

Fig. 7--Neutron spectra from specimens of liquid and solid methane. Hole and side refer to spectra taken from a re-entrant hole and the side surface, respectively. Note that solid methane gives a colder spectrum than the warmer liquid.

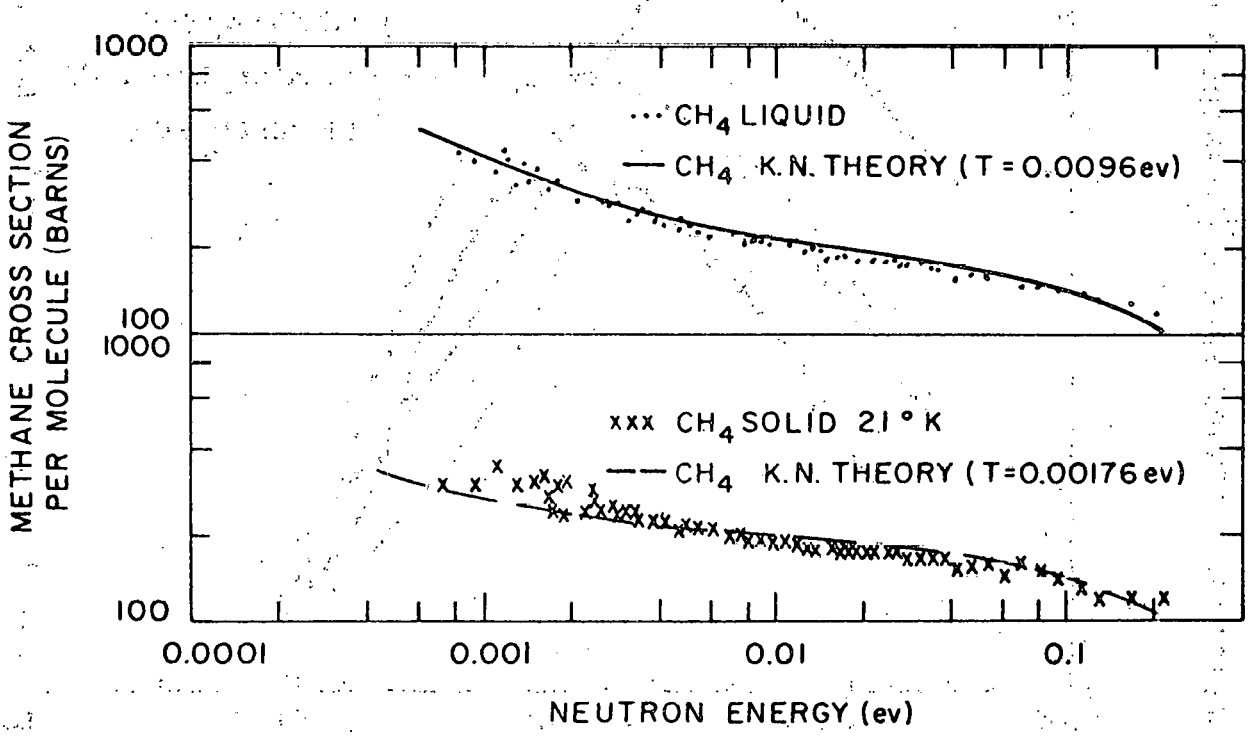

Fig. 8--Cross section of liquid and solid methane versus neutron energy. Also shown are calculations based on the Krieger-Nelkin theory for the liquid and solid cases.

The somewhat strange behavior of the total cross section for liquid para-hydrogen has already been treated in Section 3.1.2. It will be remembered that, from the point of view of neutron moderation, a neutron scattering against the larger hydrogenous mass should lose less energy on the average because of the larger effective mass of the recoiling particle. It has already been noted that the spectrum of cold neutrons produced in liquid para-hydrogen indicates a reduction in neutron interactions for $E_o < 0.010$ ev.

The cross section for liquid methane shown in Fig. 8 is much the same as for any hydrogenous material. As can be readily noted, the cross section monotonically increases as the neutron energy decreases. Rogalska[11] recently published a measured cross-section curve for liquid methane which agrees well with our previous results.[9] He has shown that the Krieger-Nelkin (K.N.) theory explains his experimental curve adequately and thus concludes that the methane molecule freely rotates in the liquid phase except possibly for the very slowest neutrons studied. In Fig. 8, we have compared the (K. N.) theory with both the liquid- and solid-methane experimental data. The formulation of this theory[12] for the present case can be given as follows:

$$\sigma(E_o) = \sigma_f \frac{2\bar{\omega}}{E_o} \left\{ \operatorname{erf} C^{\frac{1}{2}} - (1-p)^{\frac{1}{2}} e^{-Cp} \operatorname{erf} \left[C^{\frac{1}{2}} (1-p)^{\frac{1}{2}} \right] \right\} , \qquad (5)$$

where σ_f = the free-proton cross section (20.4 barns),

T = the temperature in ev,

$\bar{\omega}$ = the effective vibration frequency in ev,

$$C = E_o \left(T \frac{m}{\overline{m}_H} \right)^{-1} ; \quad p = \left(1 + \frac{\alpha^2}{4\beta} \right)^{-1} ; \quad \alpha = \frac{m + \overline{m}_H}{mT} ;$$

$$\beta = \frac{\overline{m}_H}{2m\bar{\omega}T} ; \quad \frac{m}{\overline{m}_H} = 0.2944 ; \quad \bar{\omega} = 0.1656 \text{ ev.}$$

The (K.N.) theory is being applied in a region where its accuracy may be doubtful. It applied strictly for $kT \gg 0.0006$ ev and $(E_o kT)^{\frac{1}{2}} \gg 0.0006$ ev. For $kT = 0.0017$ ev (20.4°K) and the lower incident neutron energies, the inequalities are not great. For solid methane, the calculation involved the same parameters as for liquid methane except for the lower temperature (20.4°K). The predicted cross section is noticeably too small in the energy region below $E_o = 0.002$ ev. This disagreement is not surprising since $E_{rot} \sim E_o$, where E_{rot} is the rotational level separation. The (K. N.) theory assumes that $E_{rot} \ll E_o$. The relatively good agreement in the region

above 0.003 ev, where the assumption is valid, probably indicates that the methane molecule rotates reasonably freely in the solid phase for the neutron energies used in this experiment.

From a comparison of these two cross sections and without any additional data, one would expect liquid hydrogen to require a considerably larger moderating volume to produce neutrons below 0.01 ev, in contrast to liquid methane whose cross section continuously rises with decreasing neutron energies. However, the much larger cross section of methane creates a geometrical problem when liquid methane is used as a neutron source, since the slow neutrons cannot emerge from the center of a large specimen. For this case, a re-entrant hole must be employed.

3.2.3 Inelastic Scattering

The inelastic scattering by liquid hydrogen and liquid methane provides a particularly significant basis upon which to compare these two substances. When the inelastic scattering is combined with the total cross section to give a computed value for the logarithmic energy decrement, as described in Section 3.2.4, one is able to predict quantitative differences in the expected relative moderating powers of these two substances.

Liquid Hydrogen - Figure 5 gives an example of the inelastic scattering of liquid hydrogen. These and other results for liquid-hydrogen scattering have been published.[13] It will be noted that the general appearances of the scattered spectra for both of these incident neutron energies (0.05 and 0.17 ev) are much the same and represent a considerable decrease in the energy of the scattered neutron. As a matter of some interest, the average outgoing energy E for scattering at 90 deg is related to the incident energy E_o by $E = 1/3(E_o - 2\Delta)$, where Δ is the energy of an excited rotational level. Even if the incident energy is less than 2Δ for the first rotational level and no excitation is possible, the average outgoing energy for scattering at 90 deg is still $(1/3)E_o$, owing to the energy taken up by the recoiling molecule. A scattering measurement was also performed for liquid hydrogen for an incident energy of 0.009 ev. The results from this study were of limited value because of a large background. It would appear that the probability for scattering is smaller at this lower incident energy than one would predict on the basis of the total cross section shown in Fig. 4; however, it also appears that the energy transfer is still roughly $(2/3)E_o$, as for the larger values of E_o. If subsequent measurements confirm this somewhat surprising result, it will probably mean that the scattering for these very low-incident-energy neutrons is much more peaked in the forward direction than would be expected on the basis of Sarma's calculations for gaseous hydrogen. This would result in average energy transfers which are smaller than expected for free hydrogen molecules.

From the scattering in liquid para-hydrogen, one notes that a large probability exists for relatively large energy transfers for $E_o > 0.010$ ev and that a small probability exists for energy transfers for $E_o < 0.010$ ev. One also notes that the magnitude of some of the energy transfers for $E_o < 0.010$ ev is still relatively large, although the recoiling mass may be two or three times larger than a single molecule, as shown in Section 3.1.2.

Liquid Methane - Figure 9 shows the scattering at 90 deg from liquid methane for a variety of incident energies ranging from 0.12 ev down to 0.009 ev. The scattering from liquid methane is much the same as that from other bound-hydrogen systems, with the exception of the hydrogen molecule. Attention should be called to the fact that the major amount of scattering is "quasi"-elastic and is peaked around the incident energy E_o rather than at $1/3(E_o - 2\Delta)$, as is the case with liquid hydrogen. For each of the cases studied, a substantial fraction of the neutrons also suffers large energy transfers. For an incident energy of 0.009 ev, a majority of these transfers represents energy gain. Further examination of this particular scattering pattern is useful.

The temperature of liquid methane is 111°K, so kT corresponds to ≈ 0.009 ev. Neutrons with $E_o = 0.009$ ev should, on the average, gain energy from collisions with liquid methane, since the average kinetic energy of the molecules is of the order of $(3/2)kT$ or 0.013 ev. Even through the average neutron energy is increased in single collisions with liquid methane, it should be noted that a large fraction of the neutrons suffers energy loss. These give rise to a substantial tail for energy loss processes in liquid methane. For this reason, liquid methane (even at its relatively higher ambient temperature in contrast with that of liquid hydrogen) should provide a large population of neutrons in the energy region below 0.010 ev, primarily because of its wide variety of energy exchange processes associated with the closely spaced rotational levels in methane.

3.2.4 Discussion

A quantitative comparison of the moderation characteristics of liquid hydrogen and liquid methane is contained in the slowing down power $\xi\sigma$ where σ is the cross section for scattering $(E_o \rightarrow E)$ and $\xi = \ln E_o/E$, the logarithmic energy decrement. The average $\xi\sigma$ over all angles and final energy states is given as

$$\overline{\xi\sigma} = \int_{\Omega}\int_{E} \sigma(E_o \rightarrow E_f,\ \theta) \ln\left[E_o/E_f(\theta)\right] dE\, d\Omega \qquad (6)$$

Thus for each substance the average slowing down power so defined is a function of only one parameter, the incident neutron energy E_o.

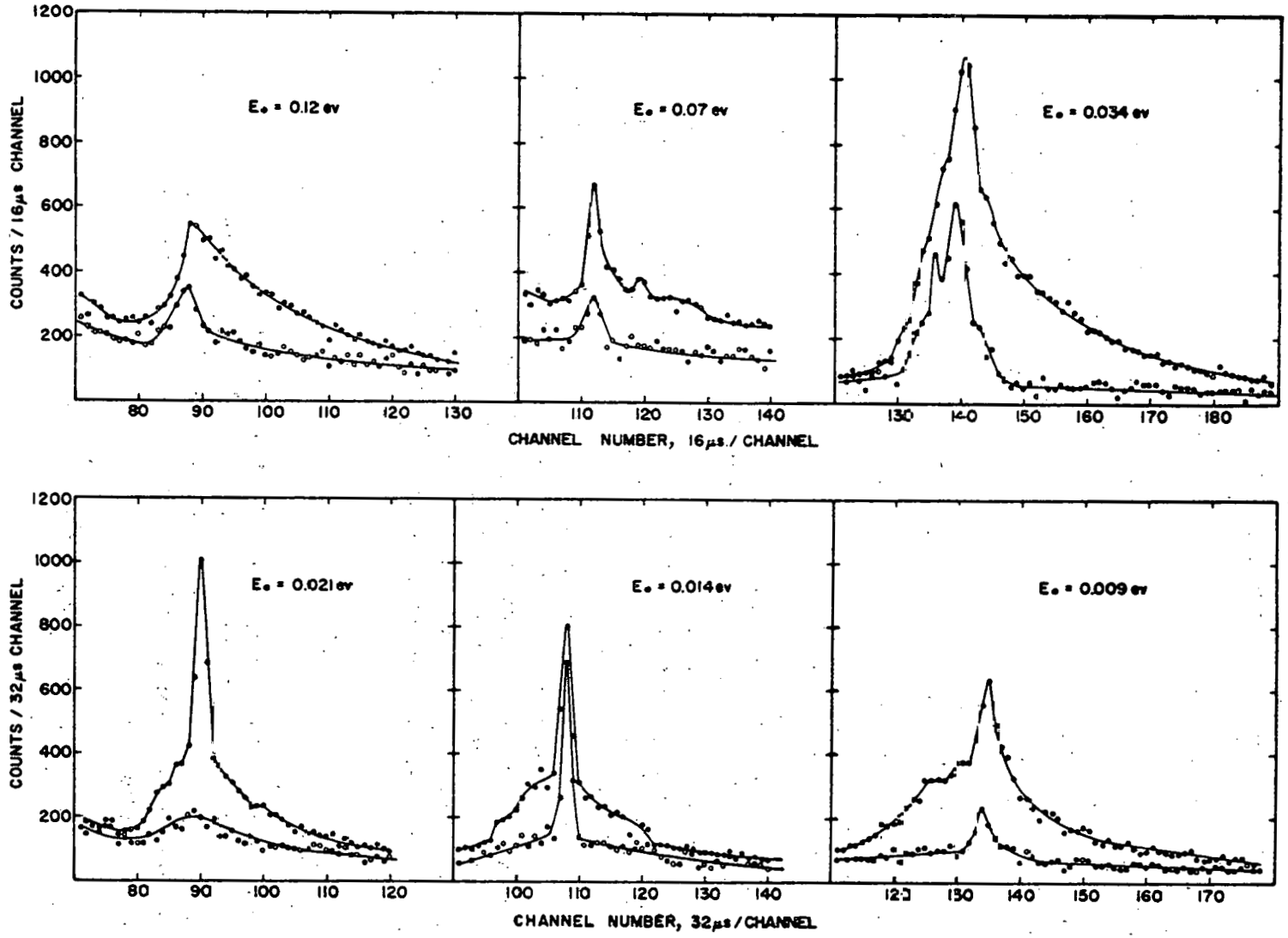

Fig. 9--Time-of-flight scattering distributions for neutrons of various energies scattered at 90 deg by liquid methane. Also shown are the respective backgrounds produced by the aluminum container and cryostat.

Since the present measurements were made only for scattering at 90 deg, it is not possible to integrate the experimental values over all angles as indicated in Eq. (6). However, 90 deg is a fairly typical scattering angle, and this data will be used with the total cross section to provide a basis for comparing methane with hydrogen. Figure 10 shows the experimental values of ξ where ξ is averaged over all final energies for scattering at 90 deg and σ is the total scattering cross section. The experimental values of $\xi\sigma$ thus computed will be in error, but the relative values should be meaningful, since the shapes of the angular distributions for liquid methane and liquid para-hydrogen probably do not differ greatly. Sarma's work[3] on gaseous hydrogen permits a theoretical calculation of $\overline{\xi\sigma}$ properly averaged over all final energies and scattering angles. Bouquet[14] has computed more numerous values of $\xi\sigma$ which agree well with our calculations. These results are displayed in Fig. 10 and are not very different from those determined from the experimental data.

Figure 10 provides the following comparison of scattering by liquid hydrogen and liquid methane. Liquid para-hydrogen is a better moderator for the higher neutron energies, probably deriving from the fact that the cross section is large and that all neutrons undergoing scattering from liquid hydrogen must give up a considerable amount of recoil energy to the recoiling molecule. For a relatively heavy mass such as liquid methane (compared with the hydrogen molecule), the recoil energy of the whole molecule is rather small. Consequently, many of the outgoing neutrons scattered by methane have an energy approximately equal to the incident neutron energy, which results in little energy loss for much of the scattering. As the incident neutron energy decreases below 0.025 ev, the moderation powers for the two substances are comparable until an energy around 0.010 ev is reached. For this lower energy region, the situation is complicated. For methane, $\xi\sigma$ becomes <u>negative</u>, indicating that neutrons gain energy for $E_o < 0.013$ ev. The value of $\xi\sigma$ for para-hydrogen does not become negative but rather becomes very small, mainly because of the small cross section. The experimental data indicate that $\xi\sigma$ may be considerably smaller for liquid hydrogen than is expected for gaseous hydrogen. If subsequent measurements substantiate this fact, then liquid hydrogen should be classed as a relatively poor source of very cold neutrons because of the absence of low-lying inelastic energy levels. On the other hand, in liquid methane the broad energy spread for the scattered neutrons with low-incident energies more than makes up for the fact that the <u>average</u> neutron energy is increased rather than decreased. Evidence for a copious low-energy tail is contained in the neutron spectra data shown in Figs. 6 and 7.

In order to render more quantitative the difference in moderating power of liquid methane and of liquid para-hydrogen, much more precise data need to be obtained on inelastic scattering for both of these substances.

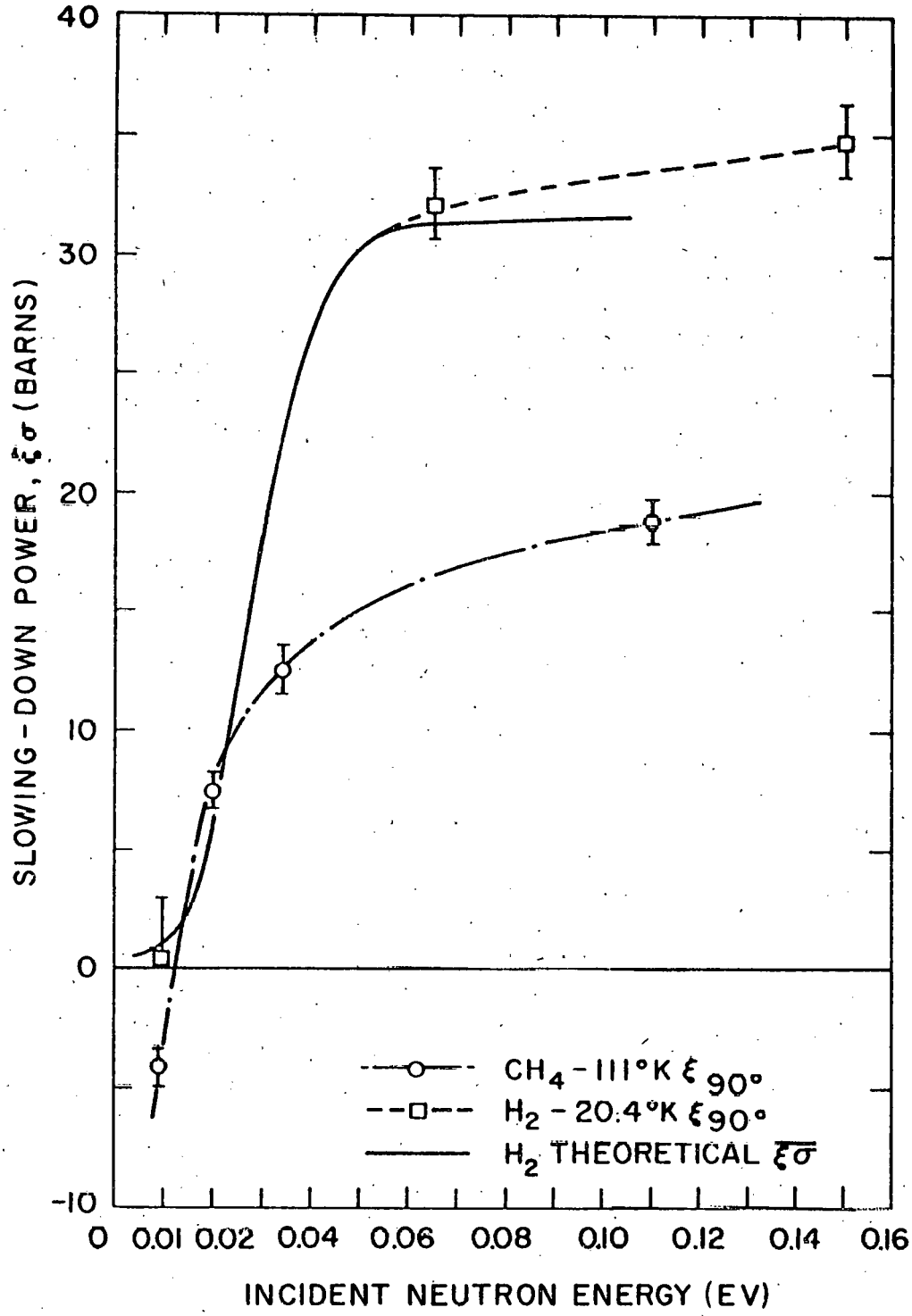

Fig. 10--Variation of the slowing down power with incident neutron energy for liquid methane and liquid para-hydrogen. The experimental data are based on inelastic scattering measurements at 90 deg, whereas the theoretical curve is averaged over all values of scattering angle and final neutron energies.

In particular, detailed data will be needed for incident energies below 0.010 ev, so that a detailed calculation can be made. When such data become available, a detailed space-dependent neutron spectrum can be computed which will take into account all aspects of the moderation, including the observed geometrical dependence of the source.

THIS PAGE

WAS INTENTIONALLY

LEFT BLANK

IV. NEUTRON INTERACTIONS IN ZIRCONIUM HYDRIDE

Zirconium hydride is an example of a neutron moderator with rather unique properties. Instead of a large and overlapping continuum of energy exchange mechanisms, ZrH has unique and well-separated energy levels. Since the hydrogen atom is bound within a tetrahedron of zirconium atoms, in the first approximation the hydrogen is an isotropic, harmonic oscillator. In the present program, the first measurements of neutron scattering in ZrH were made to verify the general features of hydrogen binding. The total scattering cross section and the inelastic scattering of cold neutrons substantiated the concept of a hydrogen atom bound with distinct oscillator levels. Subsequently other measurements were made in other laboratories to specify, in somewhat greater detail, the exact nature of the binding of hydrogen in ZrH. The most detailed of these were performed by Brockhouse.[15] Although his measurements on the first level substantiated our earlier results obtained from the scattering of cold neutrons, his measurements on the second level disagreed with our earlier published results and indicated a much broader width.

With the advent of our present neutron velocity selector, which provides monoenergetic neutrons with energies up to 0.4 ev, a suitable technique became available for investigating the interaction of incident high energy neutrons on ZrH. Some of the results of this investigation are presented in the following subsections.

4.1 PREVIOUS EXPERIMENTAL RESULTS ON THIS PROGRAM

4.1.1 Total Scattering Cross Section

Fermi[16] was one of the first to point out that the total scattering cross section will reflect specific details of harmonic binding of hydrogen atoms in a crystal. Figure 11 shows a theoretical representation of the notions presented by Fermi. It is seen that for multiples of the harmonic frequency $h\nu$, sharp minima appear in the total cross section. A precision measurement of the total cross section in ZrH was made, using a Brookhaven neutron spectrometer, with results as shown in Fig. 12. An analysis of these experimental data in terms of the theory of Fermi gives a value for $h\nu$ of 0.137 ev for the oscillator level in ZrH. A further examination of Fig. 12 indicates that the theory and experiment deviate in some details around the first and second oscillator levels in ZrH. The deviation is

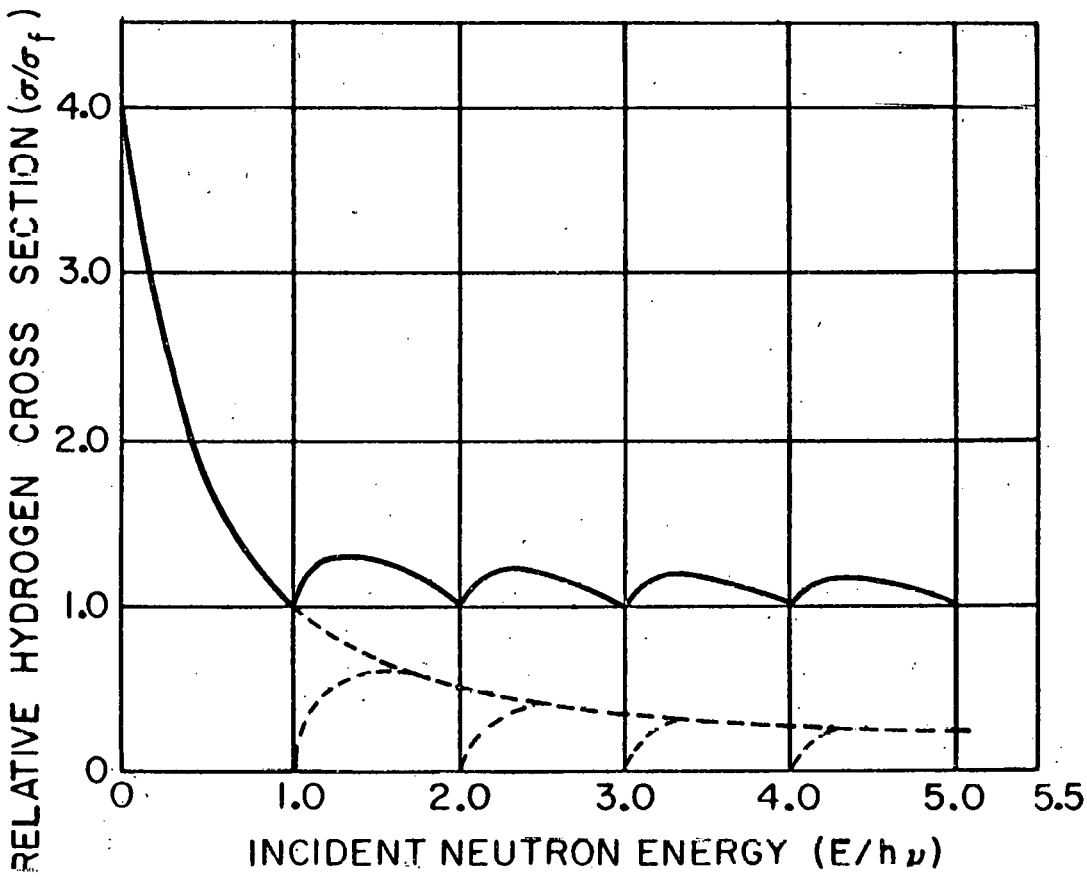

Fig. 11--Theoretical neutron cross section of bound proton, with frequency ν of isotropic harmonic oscillation.

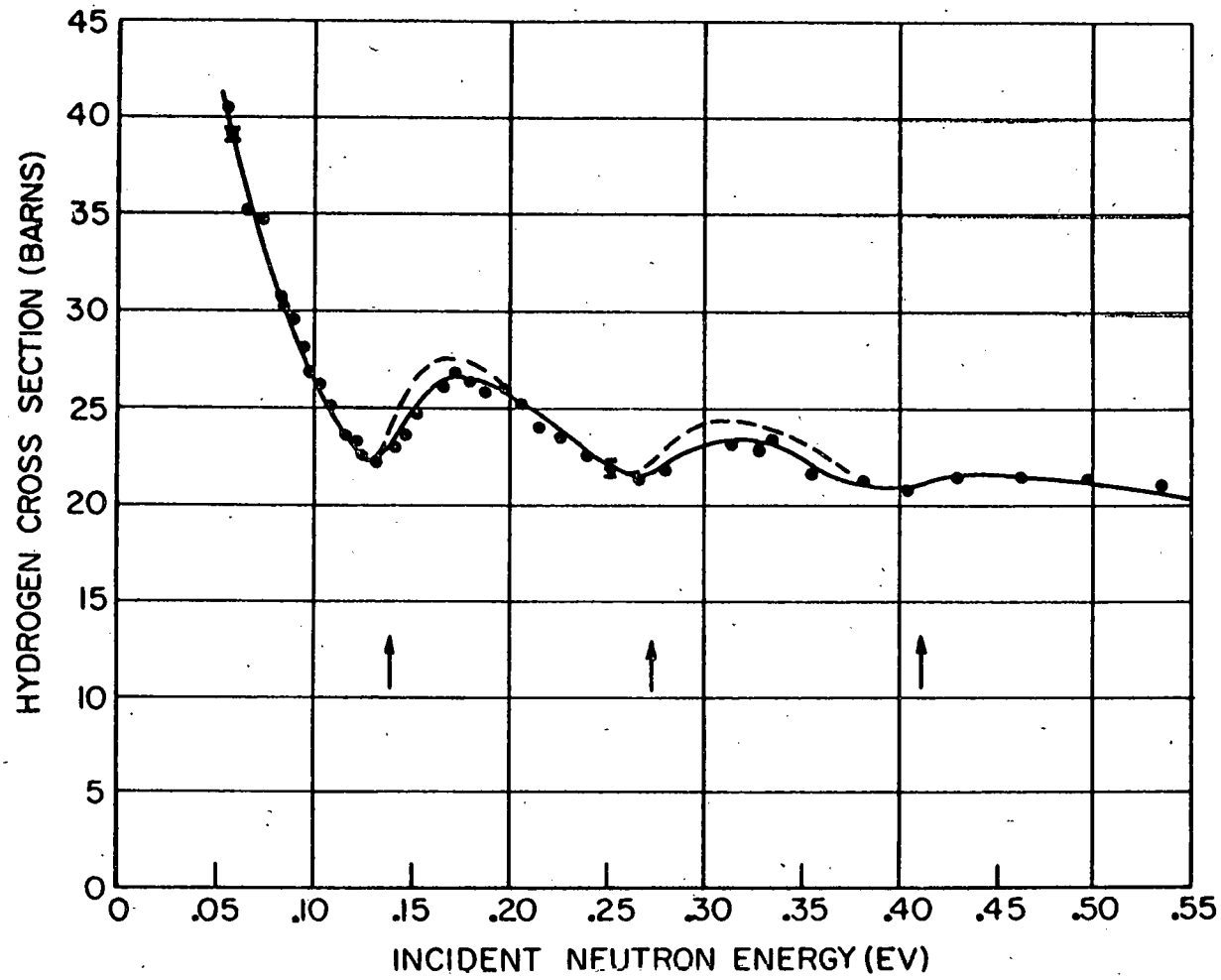

Fig. 12. The solid curve gives the total neutron cross section of hydrogen in $ZrH_{1.5}$ obtained from total cross section by subtracting the constant cross section of zirconium. The Fermi theoretical curve corrected for Doppler broadening has been fitted to the above data with $h\nu = 0.137$ ev and agrees with the experimental curve except as shown by the dashed curve.

greater for the second level, indicating that the isotropic harmonic oscillator model used for the theoretical curve is not completely accurate.

4.1.2 Scattering of Low Energy Neutrons by Zirconium Hydride

Previous work[10] has shown that the total neutron cross section of hydrogen in ZrH depends significantly on the energy of the incident neutron. For incident neutrons with lower energy ($<h\nu$), one expects that, as the incident energy is decreased, the cross section of hydrogen bound as an harmonic oscillator should, to the first approximation, increase to the fully bound hydrogen cross section of 80.4 barns. The slow increase of the total cross section above the value for a fully bound hydrogen atom is due to inelastic scattering from the acoustical modes and is determined by the frequency distribution in the solid.

To compute the cross section of zirconium hydride, we have used the results of Marshall and Stuart[17] with appropriate modifications for the case of a bound hydrogen atom and assumed a Debye frequency distribution for the acoustical modes. For this computation, there are three factors to be considered: (1) a Debye-Waller factor due to optical vibrations; (2) inelastic scattering from acoustical modes; and (3) diffraction effects in zirconium. The latter are small and can be approximately corrected for by subtracting the observed elastic cross section for zirconium for neutron energies above the Bragg cutoff. On this basis, we derived the following expression for the total cross section σ:

$$\sigma = \sigma_b f\left(\frac{E}{h\nu}\right)\left[1+A_1(x,t)\frac{m}{M}+A_2(x,t)\left(\frac{m}{M}\right)^2+A_3(x,t)\left(\frac{m}{M}\right)^3+\ldots\right] \qquad (7)$$

where

σ_b = 81.4 barns/H atom (bound cross section)

$x = (E/\theta)^{\frac{1}{2}}$

$t = T/\theta$

θ = Debye temperature

E = incident neutron energy

T = temperature of scatterer

m = neutron mass (1)

M = Effective mass of hydrogen atom in the lattice. (It is taken as 91 in this calculation, but a mass of 200 is probably better.)

$f(E/h\nu) = \left(1-e^{-4E/h\nu}\right)\frac{4E}{h\nu}$

$h\nu$ = energy of Einstein level. (0.13 ev was used for ZrH in this calculation; however, more recent measurements indicate that 0.140 ev is a better value.)

The parameters A_1, A_2, A_3 in this expression have been computed and tabulated by Marshall and Stuart.[17]

During the measurement, the sample was kept at room temperature. The only remaining parameter subject to choice is the Debye temperature to be assumed for the ZrH lattice. The cross sections have been computed for three different assumptions of reasonable Debye temperatures: 197°K (0.0170 ev), 296°K (0.0255 ev), and 370°K (0.0319 ev). A comparison of theoretical and experimental results (see Fig. 13) shows that they are in quite good qualitative and quantitative agreement, in regard both to the shape and to the absolute magnitude of the curve. However, the predicted cross section is found to be relatively insensitive to the choice of Debye temperature for the lattice; consequently, the agreement between experiment and theory may be regarded as real rather than resulting from a fortuitous choice of Debye frequency.

4.1.3 Cold Neutron Investigation of Inelastic Scattering in Zirconium Hydride

Cold neutrons from a beryllium-filtered reactor source have been used to study the inelastic scattering of neutrons by ZrH. We have published[18] some experimental results from such a study. Figure 14 shows the effect of temperature on the scattering from hydrogen in ZrH. In general, cold neutron scattering from bound levels as high as those in ZrH is difficult to achieve by the energy gain technique because of the very small population of these higher-lying levels due to the Boltzmann population factor $e^{-h\nu/kT}$. One saving feature for this scattering is that the cross section for energy gain is proportional to $(E/E_o)^{\frac{1}{2}}$ where, for cold neutron experiments, E, the final energy, is of the order of 0.14 ev and E_o is of the order of 0.003 ev. This feature is insufficient to compensate for the Boltzmann factor, however, and the higher lying levels in ZrH can be observed only if the specimen is heated. Figure 14 shows that for room temperatures, the second level in ZrH does not give any appreciable scattering. Raising the temperature to about 693°K raises the population of both the first and second levels and makes possible the observation of scattering from the second level. By studying the change in population of the first level as a function of temperature, it was possible to evaluate $h\nu$ through the use of the Boltzmann factor $e^{-h\nu/kT}$. This particular measurement gave a value of 0.130±0.005 ev. This value is somewhat lower than the value 0.137 ev obtained from analysis of the total scattering cross section.

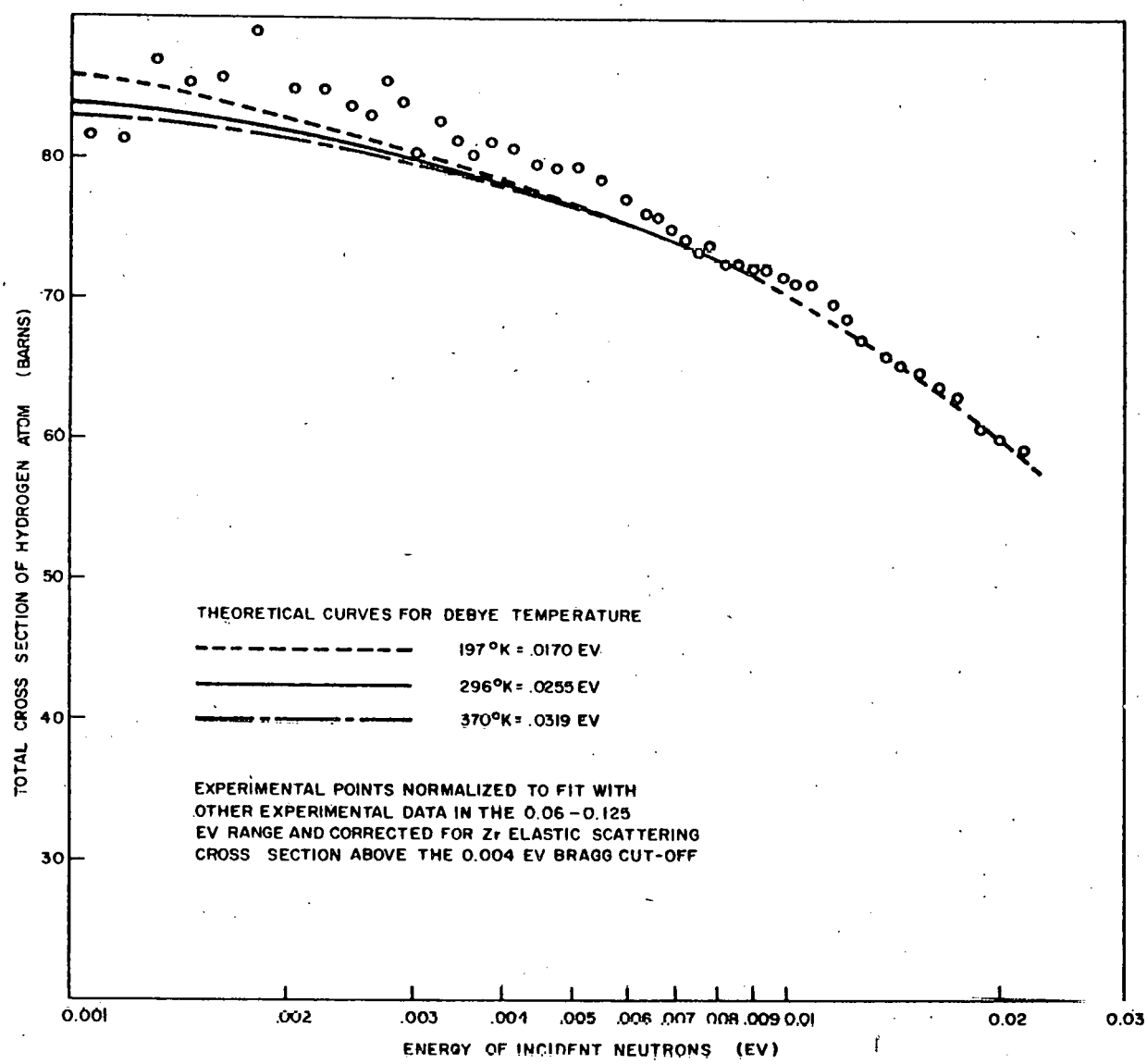

Fig. 13--Cross section of H in ZrH at low energy

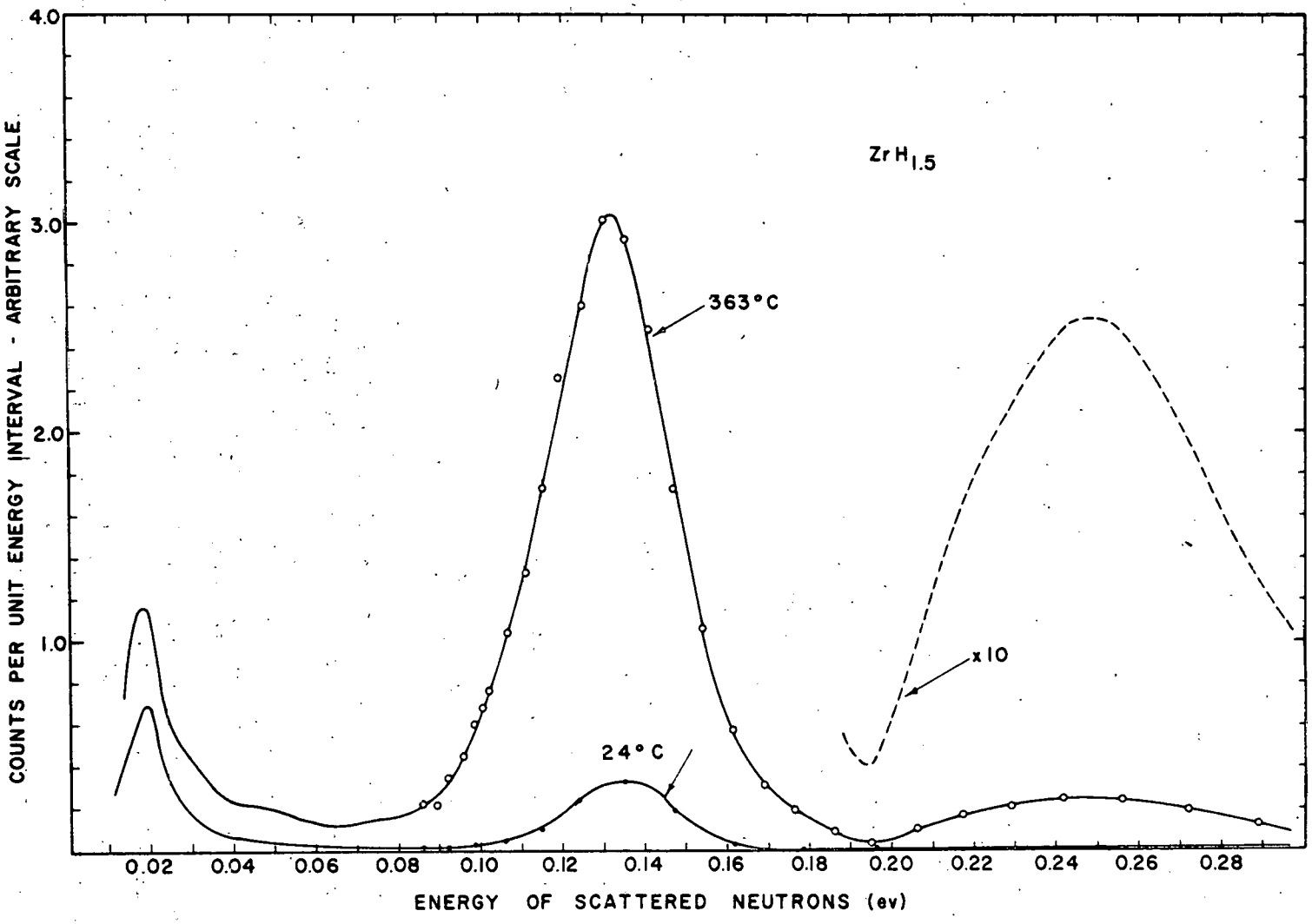

Fig. 14--Scattering of cold neutrons at θ = 90 deg by $ZrH_{1.6}$. Note that the width of the first bound level in ZrH increases with temperature and that the second bound level has an intensity which is difficult to measure at room temperature.

The variation of the width of the first and second bound level in ZrH as a function of scattering angle is an indicator of the nature of binding. Earlier in this program, observations were made only at 90 deg; therefore, no firm conclusion could be reached concerning the nature of the binding. However, from the data in Fig. 14, we observe that the width at half maximum of the first harmonic level for ZrH at room temperature is of the order of 0.030 ev. Raising the temperature to about 636°K gives a width for this level of about 0.04 ev. For this elevated temperature, the width of the second harmonic level is about 0.065 ev. From these data, two aspects of the binding in hydrogen can be investigated. The ratio of the widths at half maximum of the second level and the first level is about 1.6. A ratio of $\sqrt{2}$ would be expected if the levels were purely harmonic. Within the accuracy of the experiment, it appeared that the width is somewhat greater for the second level than would be expected for harmonic lattice vibrations.

One can compare the widths of the first level as a function of temperature. The width of the level varies as $(\kappa^2\overline{T}/M)^{\frac{1}{2}}$ where κ is the magnitude of the momentum transfer, M is the effective mass for the acoustic vibrations of the H atoms ($\approx$200), and $(3/2)\overline{T}$ is the average kinetic energy of the hydrogen atoms in a Debye crystal. $\overline{T}$ is given by the expression:

$$\overline{T} = \frac{1}{2}\int \omega\, \rho(\omega) \coth\left(\frac{\omega}{2T}\right) d\omega \ , \qquad (8)$$

where T is the temperature in ev units. Making a high temperature expansion where $\omega/2T$ is small, one finds

$$\overline{T} = T + \frac{\theta^2}{20T} \ , \qquad (9)$$

where θ is the Debye temperature in the same units as T and is about 300°K. From the above, the ratio of the level widths at 300°K and 636°K is predicted to be 1.43. Experimentally, the ratio of the two widths at half maximum is of the order of 1.33, which is in reasonably good agreement with the ratio predicted for pure Doppler broadening.

Considering the observed width of $\approx$0.030 ev at room temperature, we can compute the expected width of the optical band due to the finite mass of the zirconium atoms. Since the relative inherent width $\Delta\omega/\omega$, given by $(1+\frac{m}{M})^{\frac{1}{2}}-1$, is of the order of 0.005 or smaller, depending on whether M is taken as 91 or larger, the inherent line width is of the order of $0.005 \times 0.140 \simeq 0.0007$ ev. This is far smaller than the 0.030 ev measured above and indicates that the width is not due to the finite mass of zirconium atoms.

4.2 INELASTIC SCATTERING FROM ZIRCONIUM HYDRIDE USING ENERGY-LOSS TECHNIQUES

From Section 4.1.3, it is clear that the full range of studies of neutrons interacting with ZrH can be carried out only when high energy incident neutrons are available, because of the effect of the Boltzmann population factor in populating mainly the lowest lying level at room temperature. The present neutron velocity selector provides monoenergetic neutrons with energies up to 0.4 ev. These monoenergetic beams have now been used to study additional characteristics of the binding of hydrogen in ZrH. Since the harmonic frequency in ZrH is of the order of 0.14 ev, these neutrons can be used to study directly the characteristics of the second bound level in ZrH using energy-loss techniques. It will be remembered that the differential inelastic scattering cross section for neutron gain experiments has a factor of $(E/E_o)^{\frac{1}{2}}$ which represents an advantage for energy gain scattering and some disadvantage for energy loss scattering. However, the Boltzmann population factor worked severely against neutron-energy-gain scattering but is not important for energy loss experiments.

4.2.1 Scattering Patterns from Zirconium Hydride - Experimental Results

Scattering patterns have been obtained for a variety of incident neutron energies and scattering angles by utilizing the neutron velocity selector to provide monoenergetic incident neutrons. Some of the experimental conditions were set up to optimize conditions for examining characteristics of the first or second harmonic level in ZrH. Other scattering patterns were selected to provide general information for the derivation of the generalized Scattering Law representation of neutron interactions in ZrH.

The selection of optimum conditions for studying the first or second scattering level in ZrH requires attention to multiple scattering effects. From the information shown in Fig. 12, one sees that for neutron energies greater than about 0.09 ev, the cross section of hydrogen bound in ZrH is roughly constant in the range of 20-25 barn. For neutron energies below 0.09 ev, the cross section rises rapidly to much higher values. This fact alone creates a considerable problem in the selection of sample thickness. If an experiment is designed to minimize multiple scattering, this consideration is particularly important. For instance, if incident neutron energies of the order of 0.240 ev are selected and allowed to scatter on a relatively thin (T = 0.9) sample of ZrH, the neutron which has excited the first harmonic level will emerge from the scattering sample with an energy centered around 0.10 ev. The cross section for such a neutron upon leaving the scattering sample is no larger than for the incident neutrons. On the other hand, if an incident energy of about 0.20 ev is

selected for the incident monoenergetic beam and the same inelastic neutron interaction is studied, the outgoing neutron will have an energy centered around 0.06 ev. The multiple scattering effects for such an outgoing neutron are considerably larger than in the former case. If an even smaller incident energy is selected, a situation rapidly develops in which the outgoing neutron has practically no chance of emerging from the ZrH sample without undergoing further scattering. In this regard, we believe that the scattering samples used by Brockhouse[15] were much too thick, since incident energies of the order of 0.15 ev were used with a sample having a transmission of 0.7. The outgoing neutron energy was of the order of 0.003 ev and therefore underwent numerous scattering before emerging from the sample. For the second bound level in ZrH, incident neutron energies of the order of 0.38 ev are selected. The outgoing neutron in these cases also has an energy of the order of 0.10 ev and thereby suffers the same small multiple scattering as before. Figure 15 shows typical time-of-flight results of the neutron scattering by the first bound level in ZrH. Observations were made at 30 deg and 90 deg in a ZrH specimen having a chemical formula $ZrH_{0.5}$. The first measurements in this series were made with a specimen having a thickness of 0.080 in. This gave a transmission of 0.9 for high energy neutrons where the cross section is of the order of 25 barns. All later measurements in the present series were made with finely powdered $ZrH_{2.0}$. The thickness of the specimen was held quite closely to 0.020 in., also giving a transmission of the order of 0.9 for high energy neutrons. The observed width of the harmonic level appears to be exactly the same for the hydrogen in these two different concentrations. The incident energy in this particular case is 0.239 ev. In Fig. 16, one finds similar scattering patterns for $ZrH_{2.0}$ where incident neutron energies of the order of 0.39 ev were selected. Here one sees clear evidence for excitation of the first and second harmonic levels. These data in both Figs. 15 and 16 are particularly useful for studying several aspects of the binding of hydrogen in ZrH. In Fig. 17, we have shown, for comparison purposes, the scattering patterns observed at three scattering angles for a monoenergetic incident neutron beam having selected energies too low to excite the first hydrogen oscillator level. The difference in the scattering pattern for the lower incident energy, which is readily apparent, is directly related to the ability of ZrH to act as an exceedingly fine neutron moderator for incident neutron energies above the energy of the first harmonic level.

4.2.2 Some Considerations of the Nature of Hydrogen Binding in Zirconium Hydride

Because hydrogen is bound in a nearly equilateral tetrahedron of Zr atoms and because the total cross section has been shown to reveal some of the characteristics of harmonic oscillator binding, it seems reasonable to compute some of the theoretical predictions of the expected behavior of

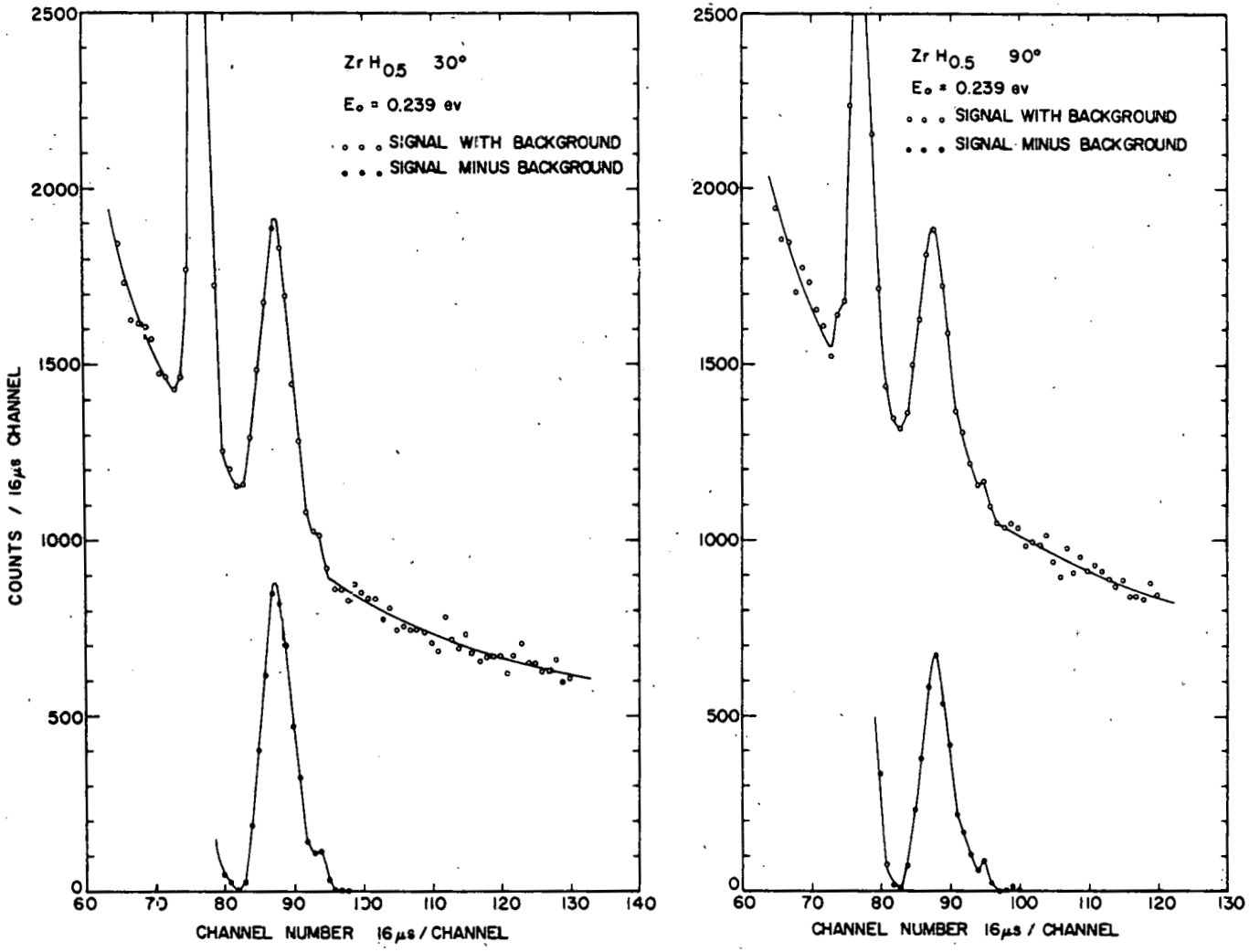

Fig. 15--Time-of-flight scattering data for $ZrH_{0.5}$ with and without background for 300°K at θ = 30 and 90 deg. $E_o = 0.237 \pm 0.006$ ev. No noticeable difference in the width of the scattered distributions is observed for $ZrH_{2.0}$.

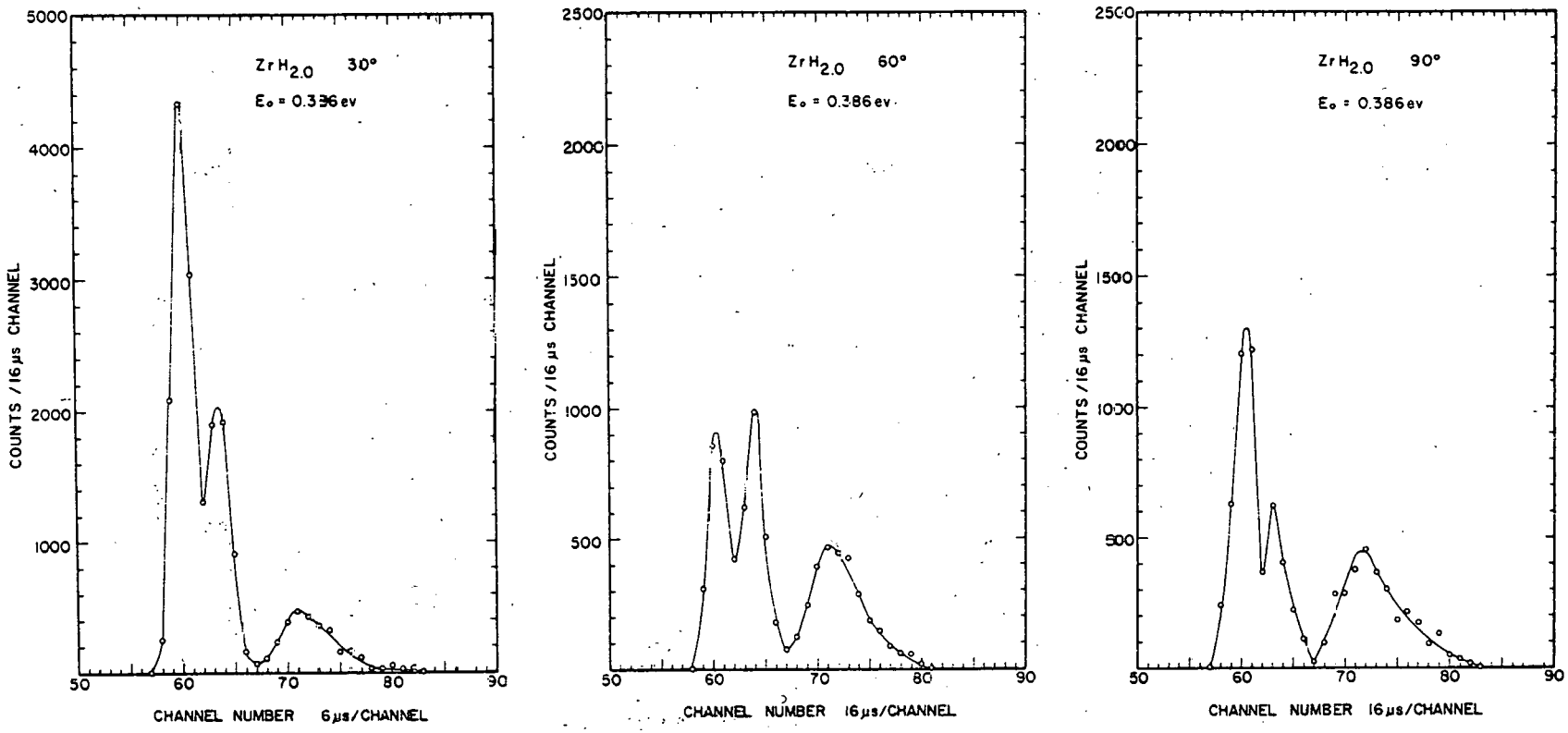

Fig. 16--Time-of-flight scattering data for $ZrH_{2.0}$ for 300°K at θ = 30, 60, and 90 deg. E_o = 0.386 ev. The data are shown with background subtracted.

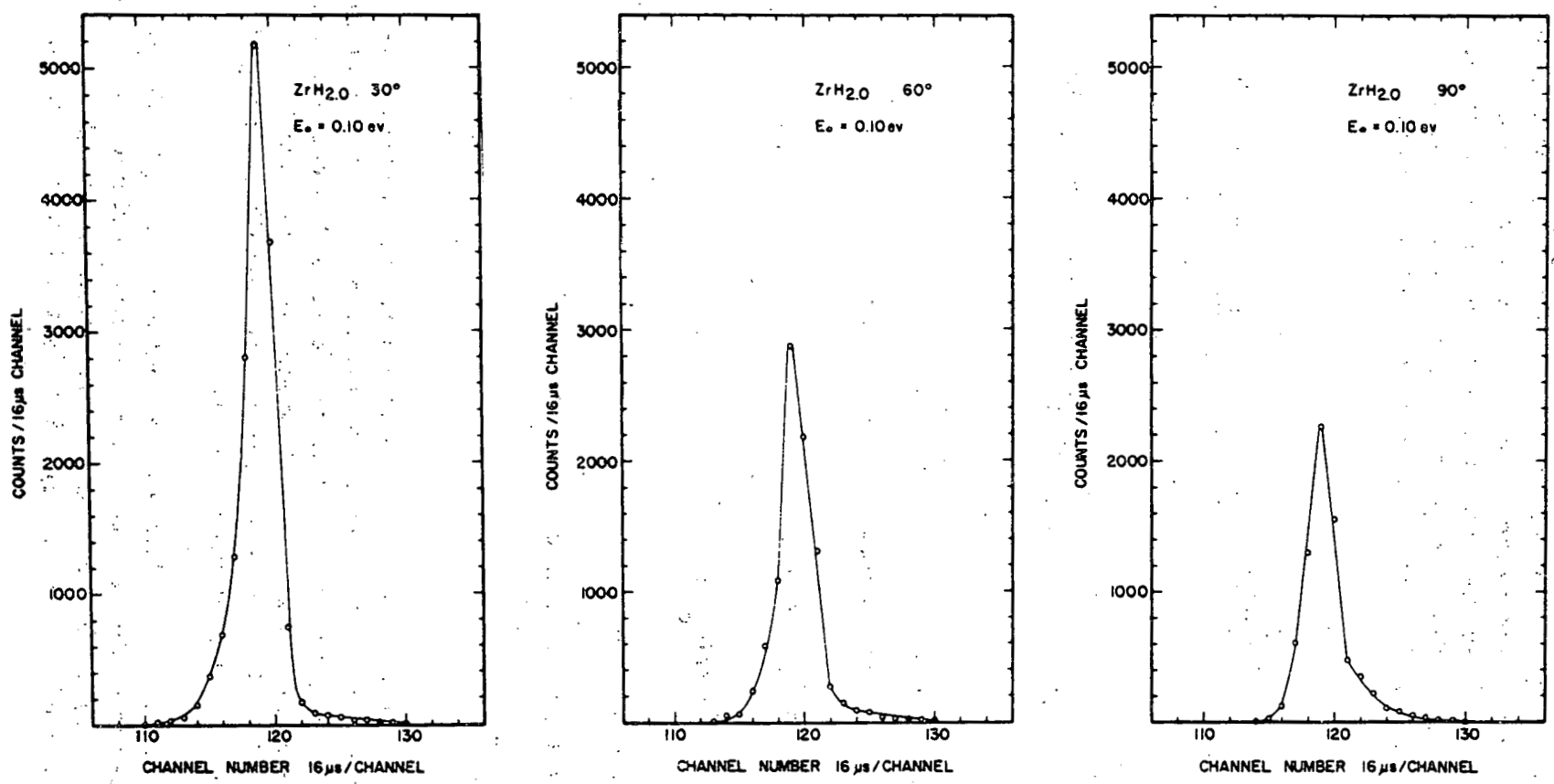

Fig. 17--Time-of-flight scattering data for $ZrH_{2.0}$ with background deducted for 300°K at θ = 30, 60 and 90 deg, respectively. Incident neutron energy (E_o = 0.10 ev) was selected to be too low to excite the first vibrational level of hydrogen. Note that the wings of the quasi-elastic scattering are considerably broader than for the data taken with higher E_o as in Figs. 14 and 15.

a purely harmonic oscillator. The results of these predictions will then be compared directly with experiments, in an effort to ascertain the degree to which ZrH satisfies the assumptions of an isotropic, harmonic oscillator. From a multiphonon expansion, one can write the differential energy-loss cross sections for the first harmonic and second harmonic levels as follows:

$$\frac{d^2\sigma_1}{dEd\Omega} = \frac{\sigma_b}{4\pi}\left(\frac{E}{E_o}\right)^{\frac{1}{2}} \exp\left(-\frac{\kappa^2\alpha}{2}\right) \exp\left(\frac{\omega_o}{2T}\right) I_1\left[\frac{\kappa^2}{2\omega_o \sinh(\omega_o/2T)}\right] \delta\left[(E_o - E) - \omega_o\right] \quad (10)$$

$$\frac{d^2\sigma_2}{dEd\Omega} = \frac{\sigma_b}{4\pi}\left(\frac{E}{E_o}\right)^{\frac{1}{2}} \exp\left(-\frac{\kappa^2\alpha}{2}\right) \exp\left(\frac{\omega_o}{T}\right) I_2\left[\frac{\kappa^2}{2\omega_o \sinh(\omega_o/2T)}\right] \delta\left[(E_o - E) - 2\omega_o\right] \quad (11)$$

where

σ_b = the bound cross section = 80 barns

E, E_o = the final and incident energy, respectively

$\frac{\kappa^2}{2} = E_o + E - 2(E_o E)^{\frac{1}{2}} \cos\theta$, where θ is the scattering angle

$\alpha = \frac{2\bar{n}+1}{\omega_o}$; $\bar{n} = \left[\exp(\omega_o/T) - 1\right]^{-1}$

ω_o = oscillator level in ev

T = sample temperature in ev

$I_n(x)_{x\to 0} = \frac{1}{n!}x^n$

In Figs. 18 and 19, we have shown, as a function of angle between the limits of 30 deg and 120 deg, the theoretical values of the cross section integrated over the energy range for the first and second harmonic levels. Figure 20 shows the theoretical angular dependence of the first harmonic level when the incident neutron energy is 0.239 ev, for which energy it is not possible to excite the second harmonic level.

From such experimental data as are contained in Figs. 15 and 16, it is possible to make the intercomparison of the first and second harmonic level in a number of ways. One can confine attention to a single level (e.g., the first or second excited level) and study its intensity variation as a

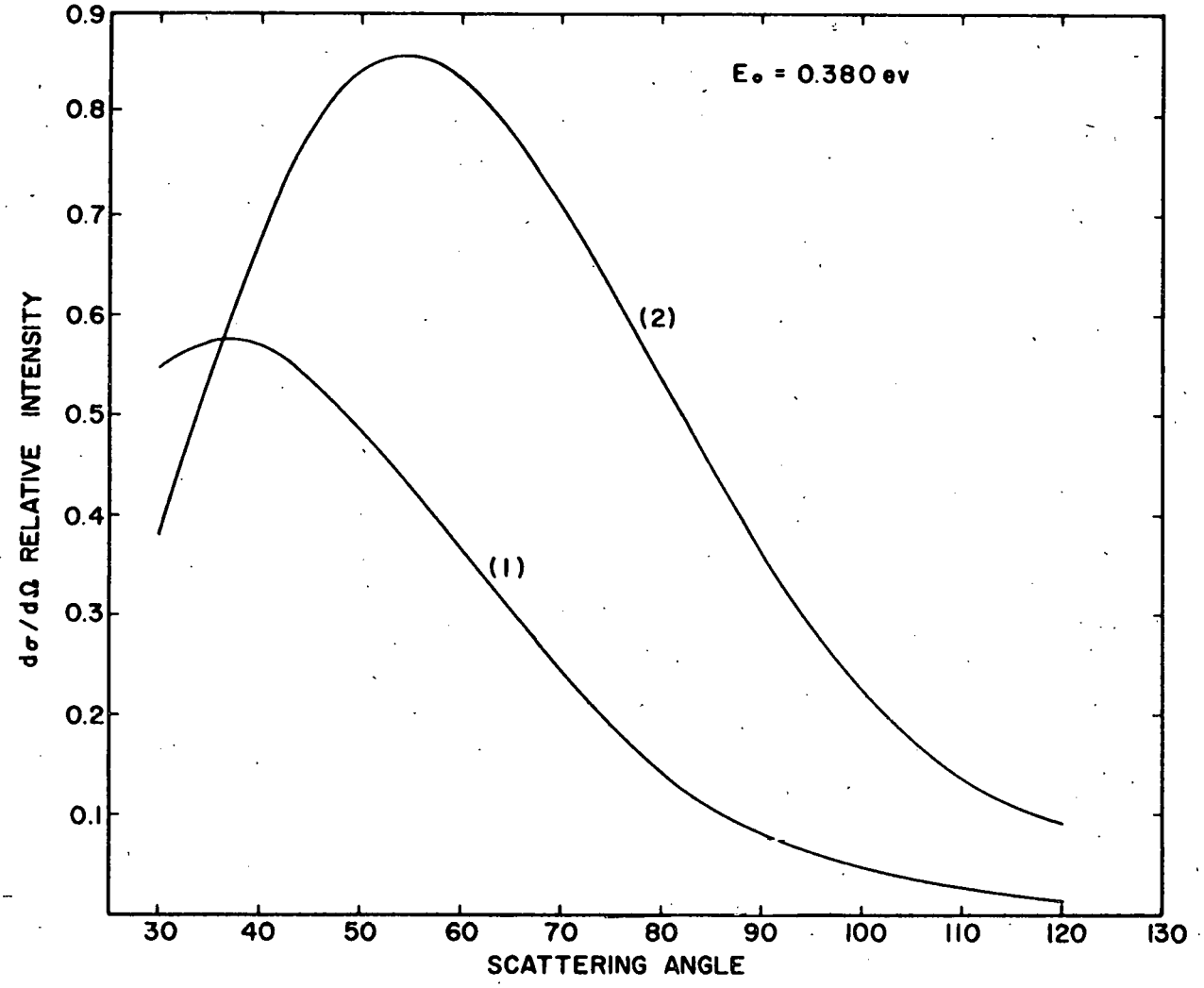

Fig. 18--Theoretical plot of the angular distribution for the partial cross sections for scattering from the first and second bound hydrogen levels in ZrH. E_o = 0.380 ev. A multi-phonon scattering treatment was used.

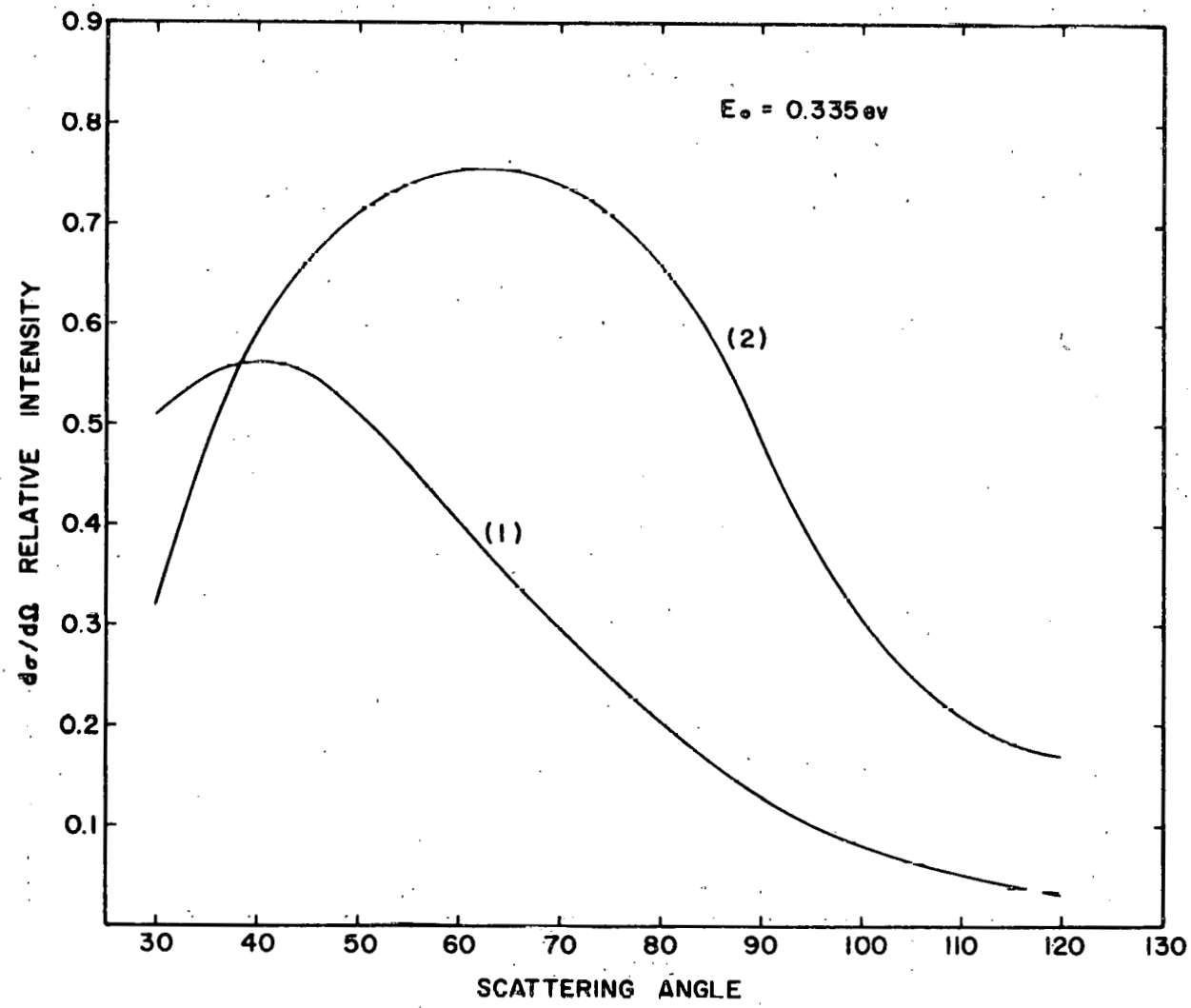

Fig. 19--Theoretical angular distribution for scattering from the first and second level in ZrH. E_o = 0.335 ev. A multi-phonon scattering treatment was used.

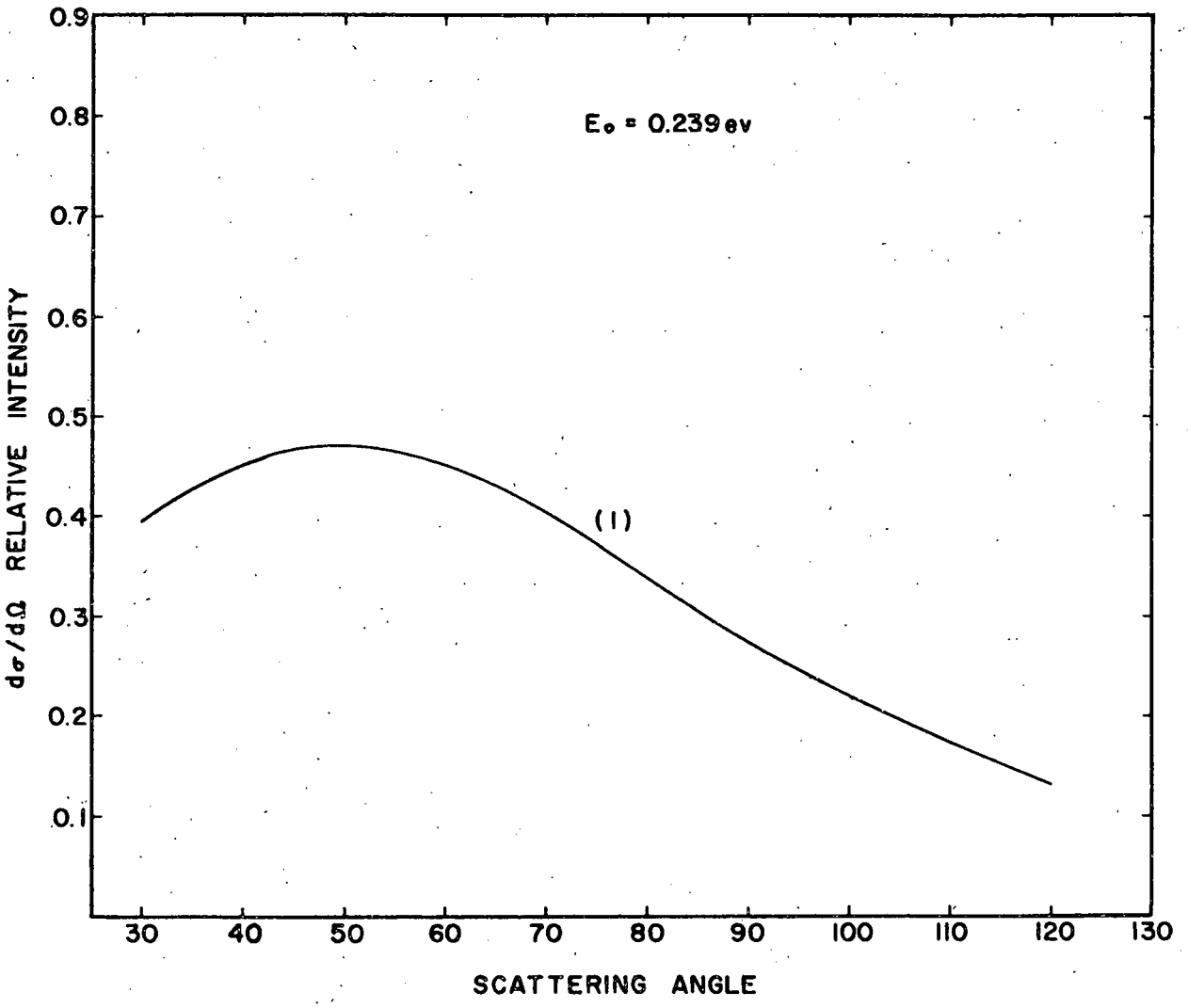

Fig. 20--Theoretical angular distribution for scattering from the first excited level in ZrH. E_o = 0.239 ev. The second level cannot be excited with this incident energy. A multi-phonon scattering treatment was used.

function of angle or one can fix the observation angle and study the intensity ratio of the first to the second level. Both of these approaches have been made for the existing data; however, the comparison which requires the intensity as a function of angle is somewhat less accurate because this presupposes a good determination of the responses of the different counter banks. This has not previously been made on a completely independent basis. Consequently, this comparison is believed to be somewhat more subject to systematic error. Table 2 presents this information as a function of scattering angle for E_o = 0.33 5 ev and 0.386 ev. Table 3 presents the information obtained by comparing the intensity ratio of the first and second levels for fixed observation angles where the individual responses of the counter banks do not enter. The information in Tables 2 and 3 indicates that the binding in $ZrH_{2.0}$ differs from that expected for a purely harmonic crystal. Discrepancies involving factors of three or four are observed in Table 3 and are considered significant.

Table 2

ANGULAR VARIATION OF PARTIAL CROSS SECTION FOR FIRST AND SECOND LEVEL, $\frac{d\sigma_1}{d\Omega}$ AND $\frac{d\sigma_2}{d\Omega}$ RESPECTIVELY. THE DATA ARE NORMALIZED TO UNITY AT 30 DEG.

E_o (ev)	θ (deg)	$\frac{d\sigma_1}{d\Omega}$		$\frac{d\sigma_2}{d\Omega}$	
		Theoretical	Exp.	Theoretical	Exp.
0.335	30	1.00	1.00	1.00	1.00
	60	0.78	--	2.354	--
	90	0.25	0.323	1.53	1.113
0.386	30	1.00	1.00	1.00	1.00
	60	0.67	0.90	2.20	1.42
	90	0.15	0.25	0.95	0.86

Table 3

RATIO OF THE PARTIAL CROSS SECTION FOR THE FIRST $\sigma(\omega_o)$ AND SECOND $\sigma(2\omega_o)$ EXCITATION LEVEL IN ZIRCONIUM HYDRIDE: THE THEORETICAL VALUES ARE EVALUATED FOR A HARMONIC OSCILLATOR

E_o (ev)	θ (deg)	$\sigma(\omega_o)/\sigma(2\omega_o)$ Theoretical	$\sigma(\omega_o)/\sigma(2\omega_o)$ Experimental
.335	30	1.60	2.62
	60	0.53	--
	90	0.26	.75
.386	30	1.44	2.81
	60	0.44	1.28
	90	0.23	0.81

The purely elastic scattering (where the incident and outgoing energies are exactly the same) also provides a test for variations from pure harmonic binding. If the virbrations are strictly harmonic, even through not isotropic, the differential angular scattering of this purely elastic scattering $\frac{d^2\sigma}{dEd\Omega}\Big|_{el}$ is given as follows:

$$\frac{d^2\sigma}{dEd\Omega}\Big|_{el} = \frac{\sigma_b}{4\pi} \exp(-\kappa^2\alpha/2)\,\delta(E_o - E) \quad , \tag{12}$$

where σ_b, κ^2, α, E_o, and E have been previously defined. Using the fact that $E_o \approx E$ and integrating over all values of E, we find that Eq. (12) becomes

$$\frac{d\sigma}{d\Omega}\Big|_{el} = \frac{\sigma_b}{4\pi} \exp(-2E_o\alpha \sin^2\frac{\theta}{2}) \tag{13}$$

From Eq. (13), one sees that the integrated intensity of pure elastic scattering should have a simple angular dependence given essentially as

$$\ln\frac{d\sigma}{d\Omega}\Big|_{el} = K - 2E_o\alpha \sin^2\frac{\theta}{2} \quad , \tag{14}$$

where K is a constant. Thus, a plot on semilog paper of the scattered elastic intensity should give a linear dependence on $\sin^2(\theta/2)$ if the potential well is harmonic. Figure 21 shows the experimental scattering data obtained from the elastic peak for $E_o = 0.386$. The plotted data include a correction for the scattering from the zirconium lattice. This correction has been estimated by comparing the scattering from zirconium with that from vanadium as observed in a separate experiment. The vanadium data are plotted also in Fig. 21 and appear to be isotropic as required for vanadium; the slight deviation is probably due to a slightly non-uniform response of the various detector banks. The resulting scattering from hydrogen atoms does not depend linearly on $\sin^2(\theta/2)$ and is further evidence for deviations from a harmonic potential well.

The width of the energy distribution of scattered neutrons is of interest in the determination of the nature of hydrogen binding in ZrH. From Section 3.1.3, we have already shown that cold-neutron energy-gain scattering has given a scattering width at half maximum of the order of 0.030 ev for the first level and is far larger than the inherent line width due to the finite mass of the zirconium atoms. The widths of the excitation levels are evaluated for the experimental data of Figs. 15 and 16 and are given in Fig. 22. From Fig. 22, one obtains an observed line width of 0.033 ev and 0.055 ev respectively. At present, an extensive investigation of the instrumental resolution is under way.

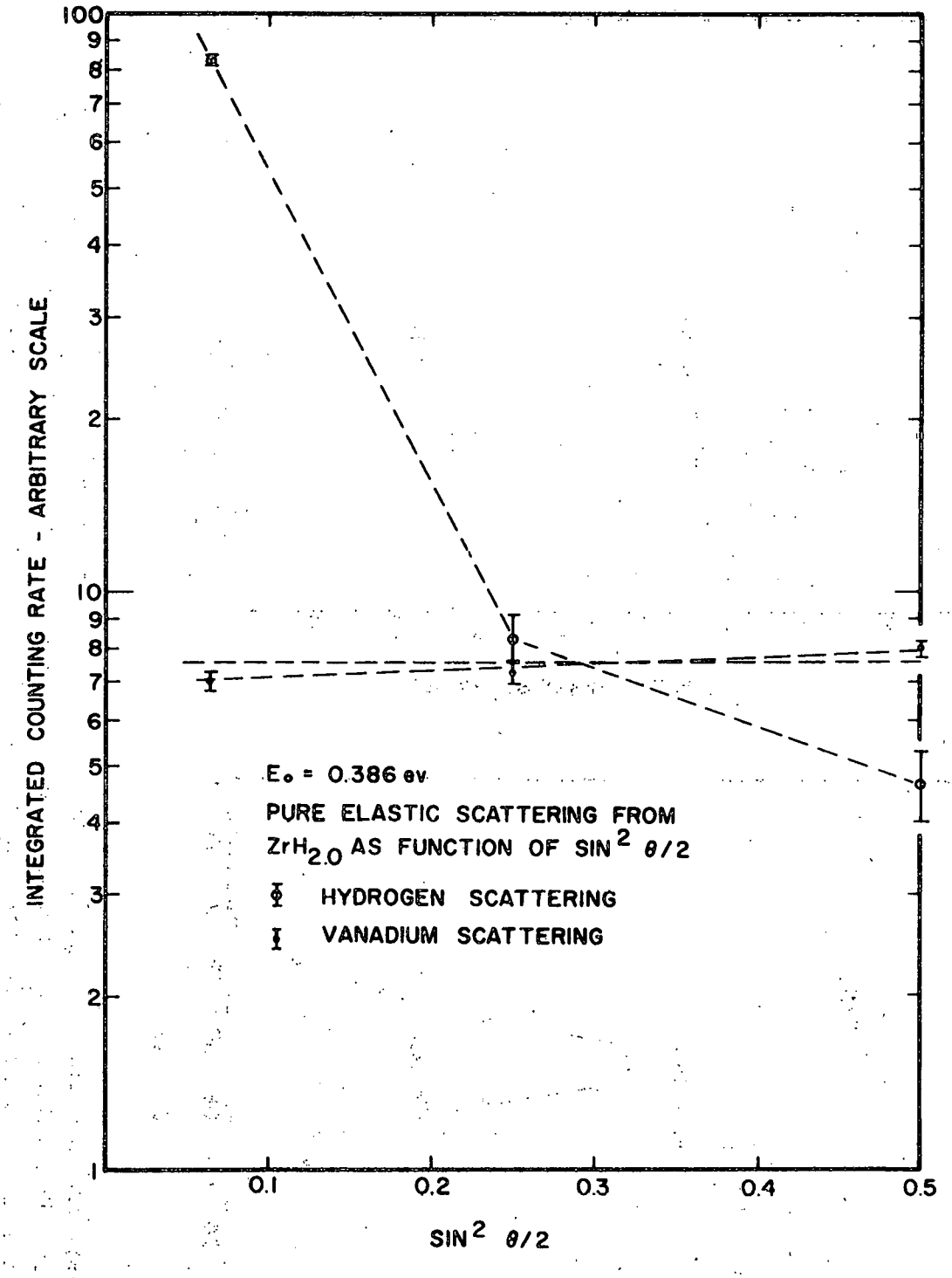

Fig. 21--Angular dependence of purely elastic scattering from hydrogen atoms in $ZrH_{2.0}$. The contribution due to zirconium atoms has been deducted, using the scattering from vanadium as a pattern and adjusting according to cross section. Note that the measured scattering from vanadium appears nearly isotropic, as it is known to be.

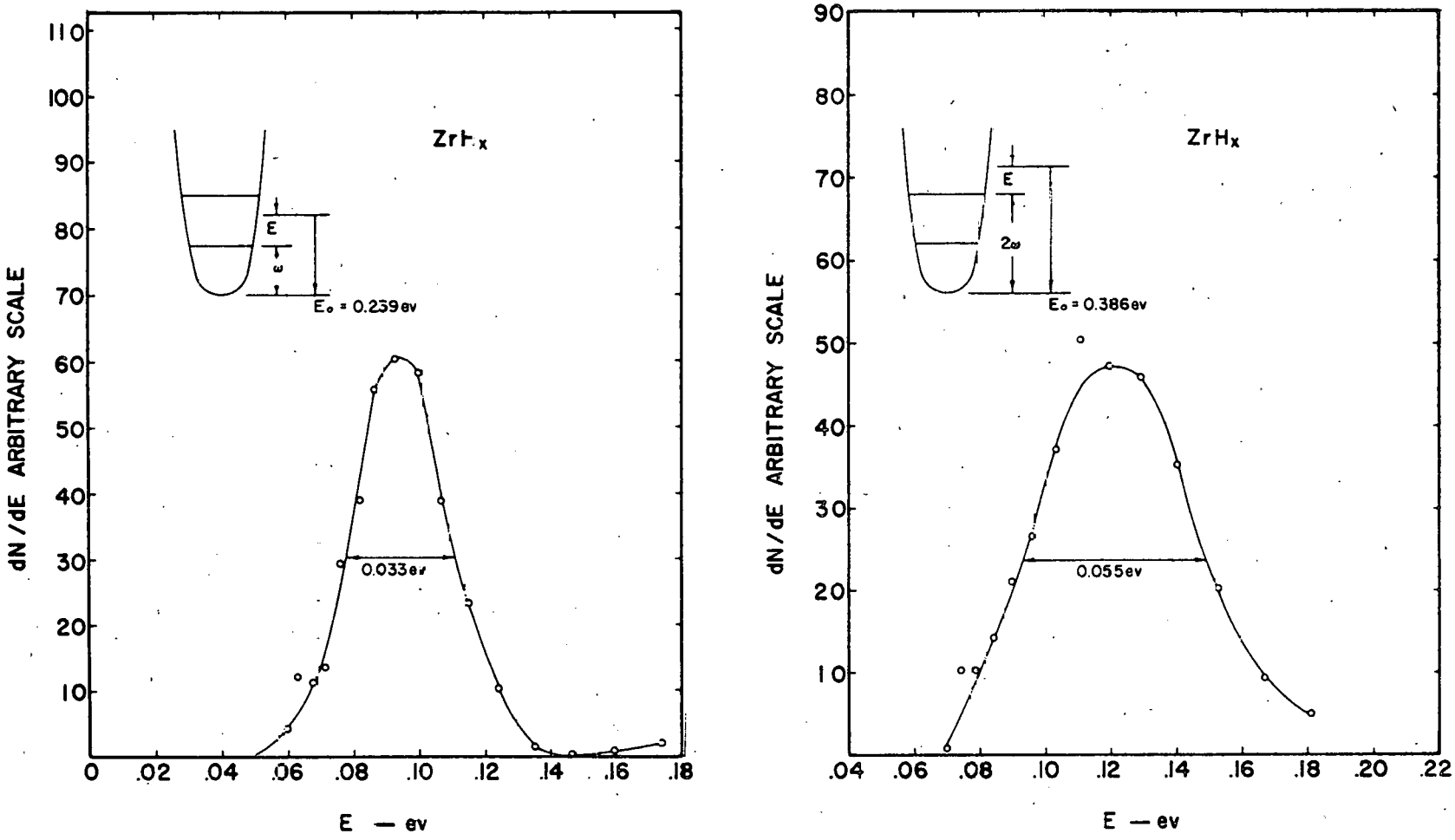

Fig. 22--Distribution in final energy for scattering from the first and second bound levels of H in ZrH. Two values of E_o were chosen; i.e., 0.239 ev and 0.386 ev. The indicated width at half maximum includes instrumental resolution as well as the inherent line width of the first and second bound levels.

In the future, a better evaluation of the resolution effects on the data will be possible. At this writing, the energy resolution for the first level is known to be quite close to 0.020 ev, whereas that for the second-level measurements is believed to be worse, ranging between the limit 0.025 ev and 0.040 ev. Thus, the true width of the distribution of scattered neutrons due to the line width is close to 0.025 ev for the first level, but for the second level we can only specify that the level width lies in the range 0.030 ev to 0.045 ev. If the potential well is harmonic, the second level width should be $\sqrt{2}$ times the first level width and thus would be about 0.035 ev. Anharmonic binding effects would broaden the second level. The uncertainty in the width of the second level makes any firm conclusion on the shape of the potential well unlikely from the present data.

For a one-phonon theoretical treatment of the scattering due to the first bound level, one finds that the frequency distribution $\rho(E_o-E)$ is given as:

$$\frac{d^2\sigma}{dEd\Omega} = A\left(\frac{E}{E_o}\right)^{\frac{1}{2}} \exp(-\kappa^2\alpha/2)\ \frac{\kappa^2\alpha}{2}\ \frac{\rho(E_o-E)\exp\left[-(E_o-E)/2T\right]}{2(E_o-E)\ \sinh\left[(E_o-E)/2T\right]}$$

$$= A\,B(E_o,E,\theta)\,\rho(E_o-E) \qquad (15)$$

where

A = a proportionality constant
$\hbar = k = 1$
$E_o > E$, and
κ^2, E_o, E, α, and T are as previously defined.

One can evaluate the frequency distribution for zirconium hydride from experimental distributions, such as are given in Fig. 22, using the kinematic corrections contained in $B(E_o,E,\theta)$. Figure 23 shows the magnitude of this correction. The resulting frequency distribution for the first excited level in zirconium hydride is given in Fig. 24. Since the instrumental resolution is independently evaluated to be 0.023 ev, the observed width for $\rho(\omega)$ at half maximum of 0.036 ev gives a true width in the frequency distribution of 0.028 ev.

One parameter of considerable interest in reactor calculations is the quantum $\underline{h\nu}$ for the hydrogen oscillator. As noted in Section 4.1, our previous values have ranged between 0.130 ev ± 0.004 ev and 0.137 ev. Brockhouse [15] has reported a value of 0.140 ev for his energy-loss scattering measurements. The present series of experiments give values of $\underline{h\nu}(1)$ in the range 0.140 ev to 0.145 ev, depending on whether the peak in frequency distribution (0.145 ev) or in the energy distribution (0.140 ev)

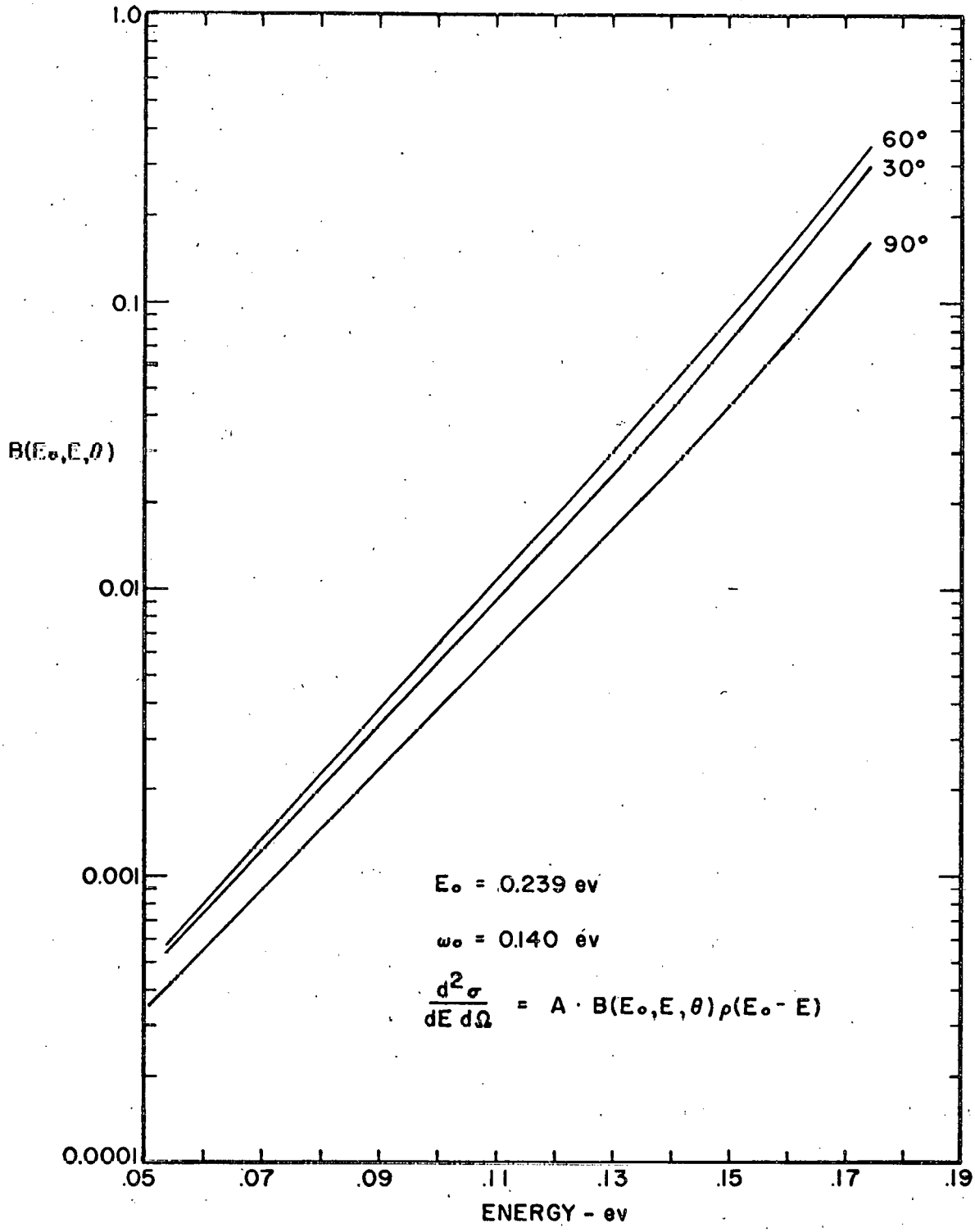

Fig. 23--Typical set of correction terms $B(E_o, E, \theta, \omega_o)$ to be used to derive a frequency distribution $\rho(\omega)$ for ZrH. The E_o was taken as 0.239 ev and ω_o was taken as 0.140 ev.

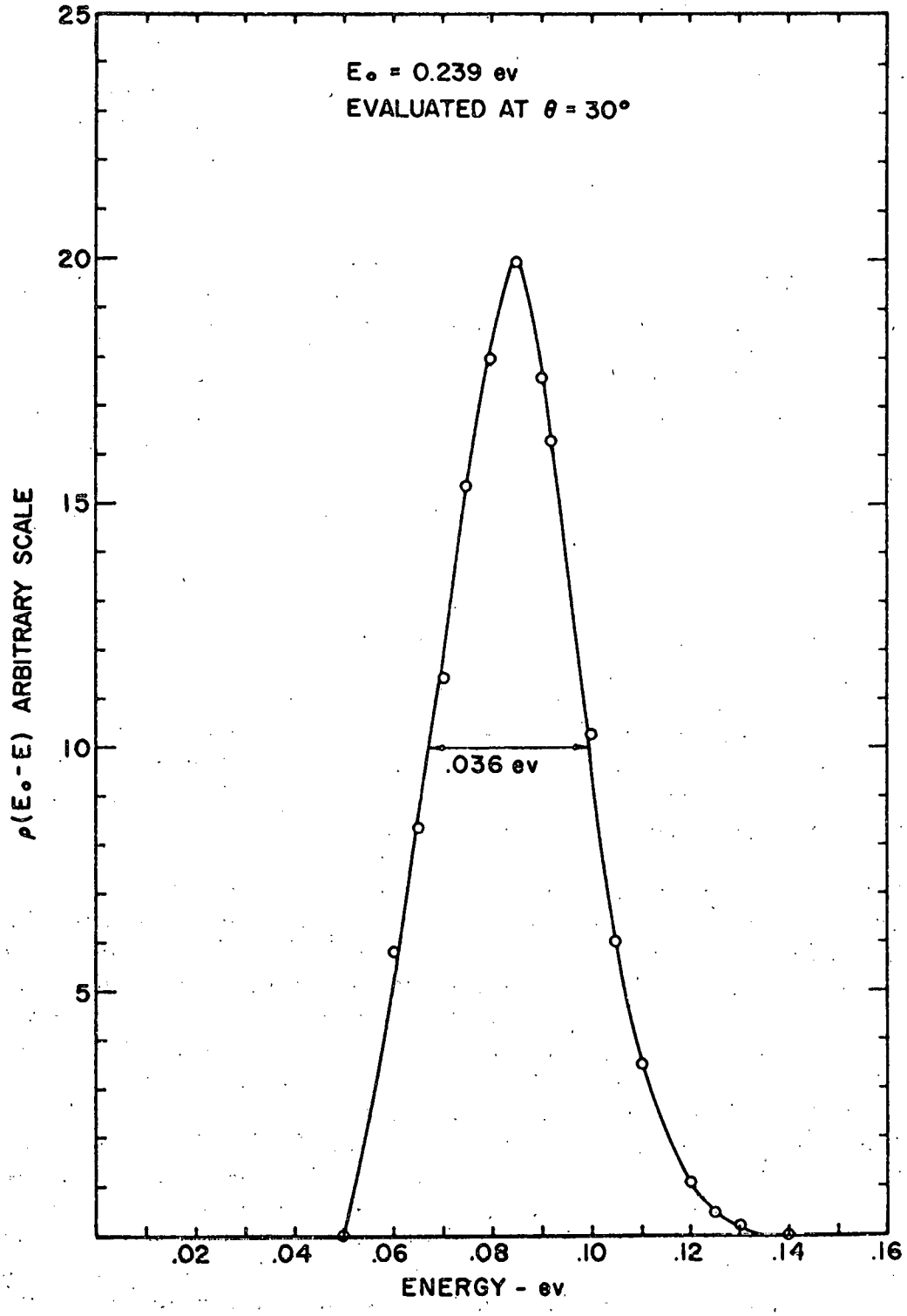

Fig. 24--Experimentally determined frequency distribution for ZrH. E_o = 0.239 ev. This curve includes a contribution due to instrumental resolution; note, however, that the width at half maximum is broader than the distribution in final energy shown in Fig. 22.

of scattered neutrons is used. In considering the above data, we conclude that the value of 0.130 ev is somewhat too low and that a value of about 0.140 ev is more nearly correct. The value of $h\nu(2)$, determined from the peak of the distribution of neutrons scattered by the second bound level of hydrogen, appears to be 0.285 ev for E_o = 0.335 ev, and 0.291 ev for E_o = 0.386 ev. Since the distributions are quite broad, it is difficult to pick a unique, meaningful value. Consequently, we cannot determine whether the second level $h\nu(2)$ is a simple integral multiple of the first level $h\nu(1)$, although there is some slight evidence that the ratio is slightly larger than 2.0.

A measurement was made of the scattering from the first bound level of ZrH as a function of the temperature of the specimen. The incident neutron energy was 0.239 ev. The two temperatures of the sample were 300°K and 90°K. Figure 25 shows that, in the time-of-flight distributions, a real decrease in line width occurs for this change in ambient temperature. Similar data exist at other scattering angles. It should be noted that Brockhouse[15] has published results which indicate no change in line width, within his accuracy, for a similar change in temperature. The reasonable conjecture is that Brockhouse's sample thickness was great enough to give much multiple scattering and thus masked the relatively small change in width caused by a change in temperature. In this same connection, it may be noted that the line width reported by Brockhouse for the second bound level is more than a factor of two wider than found in the present experiments, probably for the same reason.

For the present measurements, we have calculated that the corrected line width of the first scattered level is 0.025 ev for a temperature of 300°K. The data in Fig. 25 give a line width of 0.020 ev after resolution corrections for T = 90°K. The ratio of these line widths is about 1.25. The predicted decrease in width due to Doppler broadening effects is obtained from $(\kappa^2\bar{T}/M)^{\frac{1}{2}}$, where $\bar{T}$ is defined by Eqs. (8) and (9). Equation (9) is valid within 5 percent for all $\bar{T}$ greater than $\theta/4$. From Eq. (9), we note that the ratio of $\bar{T}$ for these two temperatures gives a value of 2.25. Thus the ratio of the resulting level widths at 300°K and 90°K is 1.50, much larger than the observed experimental value of 1.23. However, the magnitude of M above is believed to be so large as to make the magnitude of the predicted level width much too small due to these Doppler effects. Furthermore, it should be noted that a Doppler broadening of the level will also introduce an angular dependence for the line width because of the momentum transfer. For the present case, with E_o = 0.239 ev, E - 0.10 ev, and θ = 30 deg and 90 deg, one predicts that the line width should increase by a factor of 2.2 for scattering at 90 deg compared to 30 deg. Experimentally, one observes that the line width is practically independent of the scattering angle (from 30 deg to 90 deg) for T = 90°K and increases only slightly ($\approx$10 percent) with angle for T = 300°K. All of these observations are at variance with

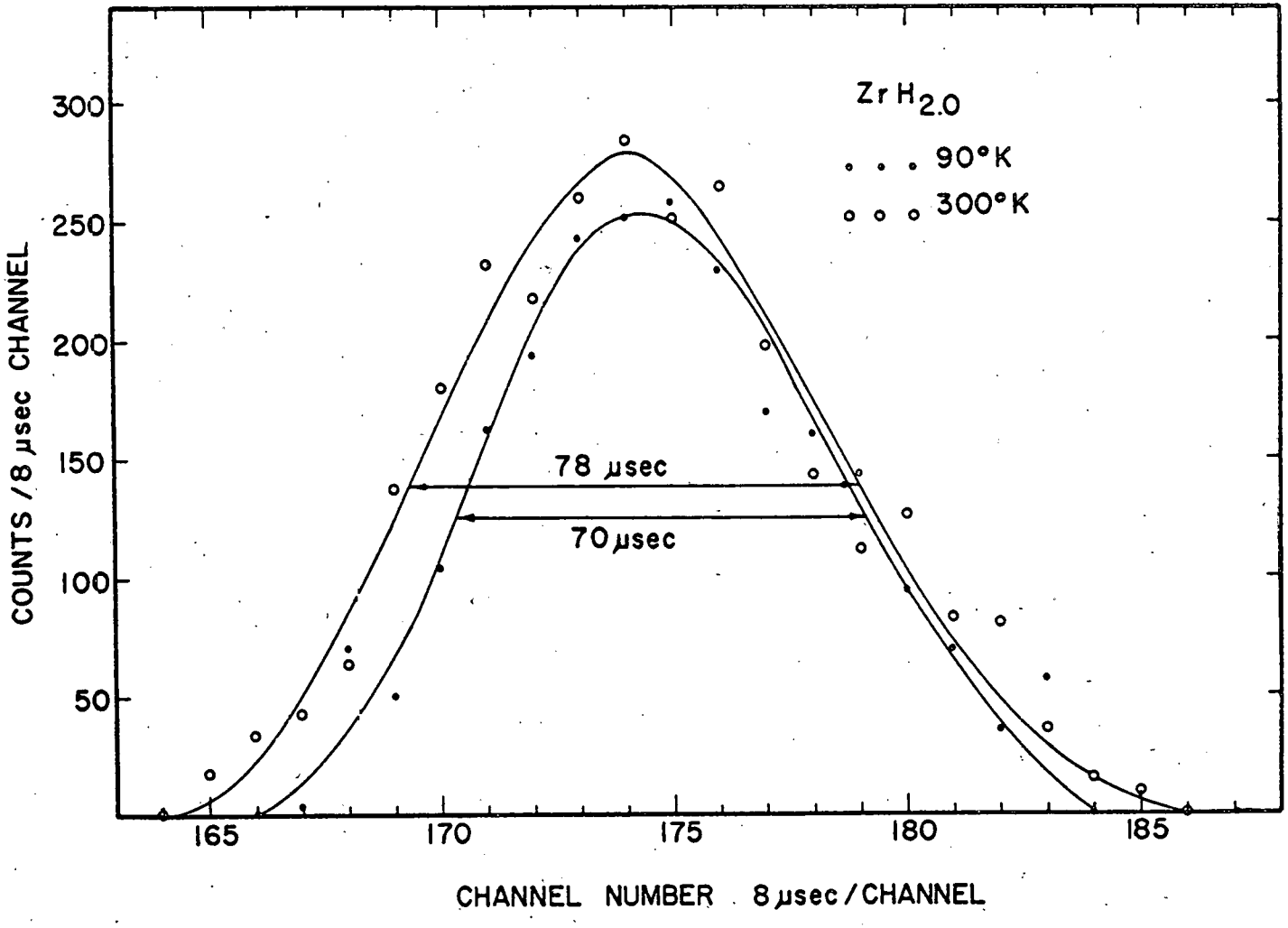

Fig. 25--Experimental distribution in time-of-flight for scattering from the first bound level in ZrH shown as a function of sample temperature. Note that the width at half maximum is noticeably narrower for the lower temperature of 90°K.

those predicted on the basis of simple Doppler broadening of the optical band. A more detailed consideration of the exact phonon distribution is needed for comparison with the present experimental data.

1. $h\nu(1) = 0.140$ to 0.145 ev.
   $h\nu(2) = 0.285$ to 0.291 ev.

2. In the temperature range from $300^{\circ}K$ to $690^{\circ}K$, the width of the first bound level is observed to change with temperature nearly as predicted by $(\kappa^2 \bar{T}/M)^{\frac{1}{2}}$, where κ is the magnitude of the momentum transfer and $\bar{T}$ is related to the average energy of an H atom in the Debye crystal. In the temperature range between 90° and $300^{\circ}K$, the width of the first bound level is observed to change by a factor of 1.25 whereas a Doppler-broadened level would be expected to change its width by a factor of 1.5.

3. A true Doppler broadening of the level also requires an angular variation of the level width. This is nearly absent at $90^{\circ}K$ in the present sample for angles in the range of 30 deg to 90 deg and much smaller at $T = 300^{\circ}K$ than the predicted factor of 2.2.

4. The natural line width due to the finite mass of the zirconium is 0.0007 ev or less, whereas the observed width at $300^{\circ}K$ at half maximum of the distribution of scattered neutrons is 0.025 ev. The observed width for the second level is uncertain within the limits of 0.030 and 0.050 ev. It is thus not certain whether the ratio of the level widths is $\sqrt{2}$ as is expected for harmonic lattice vibrations.

5. The calculated experimental half width of the frequency distribution $\rho(\omega)$ for the first level is 0.028 ev for $T = 300^{\circ}K$.

6. The cross sections of the first and second bound level vary with scattering angle in a manner quite different than that predicted for a pure harmonic oscillator. Differences of a factor of four are observed.

7. The angular dependence of the cross section for purely elastic scattering ($E_o = E$) does <u>not</u> vary linearly with $\sin^2(\theta/2)$ as prescribed for an harmonic oscillator.

8. Items (1), (4), and (5) are consistent with pure harmonic motion of the hydrogen but do not necessarily rule out anharmonic and/or anisotropic motion. On the other hand,

items (6) and (7) are inconsistent with harmonic motion and indicate anharmonic binding of the hydrogen in ZrH. Items (2) and (3) indicate that the level width is not due solely to Doppler broadening.

THIS PAGE

WAS INTENTIONALLY

LEFT BLANK

V. NEUTRON INTERACTIONS IN POLYETHYLENE

For a number of years, the present program has maintained an interest in polyethylene. At present, data on the Scattering Law is being analyzed for the higher incident-neutron energies (> 0.15 ev). Within the next month or two, a complete Scattering Law for polyethylene will be presented and comparisons will be made with the theoretical treatment of Parks.

Polyethylene (CH_{2n}) has been of interest as a neutron moderator for a number of years because of the close similarity which it bears to water (H_2O). Early in this program, the specific differences from H_2O which CH_{2n} exhibits as a moderator were demonstrated in the experimentally-determined slowing-down power $\xi\sigma$. Since these differences are real and are not particularly small, and since polyethylene is still used on occasion to simulate water reactor assemblies, a quantitative study of moderation in polyethylene has been carried on under this program.

5.1 SUMMARY OF PREVIOUS MEASUREMENTS ON POLYETHYLENE MADE UNDER THIS PROGRAM

Before the present experimental arrangement was available, a number of preliminary experiments were made on different aspects of neutron interactions in polyethylene. Most of these have been reported in previous Annual Summary Reports.[1][9] Specifically,

(1) The total cross section as a function of neutron energy in the range $0.0005 < E_o < 0.30$ ev was reported in Fig. 13 of Ref. 9.
(2) The comparison of the logarithmic energy decrement for scattering at 90 deg by H_2O and CH_{2n} was reported in Fig. 35 of Ref. 9.
(3) Cold neutron scattering measurements concentrating on the acoustic spectrum in CH_2 were made and reported in Figs. 30 and 32 of Ref. 9.

Additional measurements of this type were possible but involved inefficient use of the Linac. Consequently, serious work on polyethylene was postponed until this reporting period during which considerably more information has been obtained, some of which is reported here.

5.2 COLD NEUTRON SCATTERING IN CH_2

Using the neutron velocity selector to provide monoenergetic neutrons with $E_o = 0.009$ ev, an experiment was performed to study the inelastic

scattering by polyethylene. Figure 26 shows the experimental results for a very-highly-crystalline specimen of CH_{2n} (≈75 percent long-chain molecules). Figure 27 illustrates the nature of the expected neutron distribution based on the frequency distribution derived by Wunderlich[19] from specific heat data and shown in Fig. 28. Table 4 shows some of the various frequencies pertinent for polyethylene. The double "hump" in the theoretical acoustic spectrum is a result of the exact features of the frequency distribution and will be replaced by a single hump if the sharp discontinuities in the frequency range 50 cm^{-1} should be substantially reduced.

Table 4

MOTION IN POLYETHYLENE*

Mode	Frequency Limit (cm^{-1})	T_{equiv} (°K)
CH_2 rocking	720 - 1168	1368 - 1681
C - C stretch	870 - 1150	1453 - 1655
CH_2 twist	1060 - 1295	1687 - 1863
CH_2 wagg	1175 - 1415	1863 - 2040
CH_2 bend	1460	2100
CH_2 symm stretch	2855	4108
CH_2 assym stretch	2925	4208

*Reference 19.

5.3 SCATTERING LAW FOR CH_{2n}

Numerous earlier measurements of inelastic scattering on CH_{2n} were made for only a single scattering angle (90 deg). A typical scattering pattern for E_o = 0.022 ev is shown in Fig. 29. In this figure, one sees evidence for energy loss as well as energy gain scattering. Other scattering patterns in this earlier data were reported in Ref. 1. A Scattering Law has been calculated from some of these data. More recent data have been collected for other scattering angles and for higher incident energies, but the Scattering Law calculations are not available at this writing.

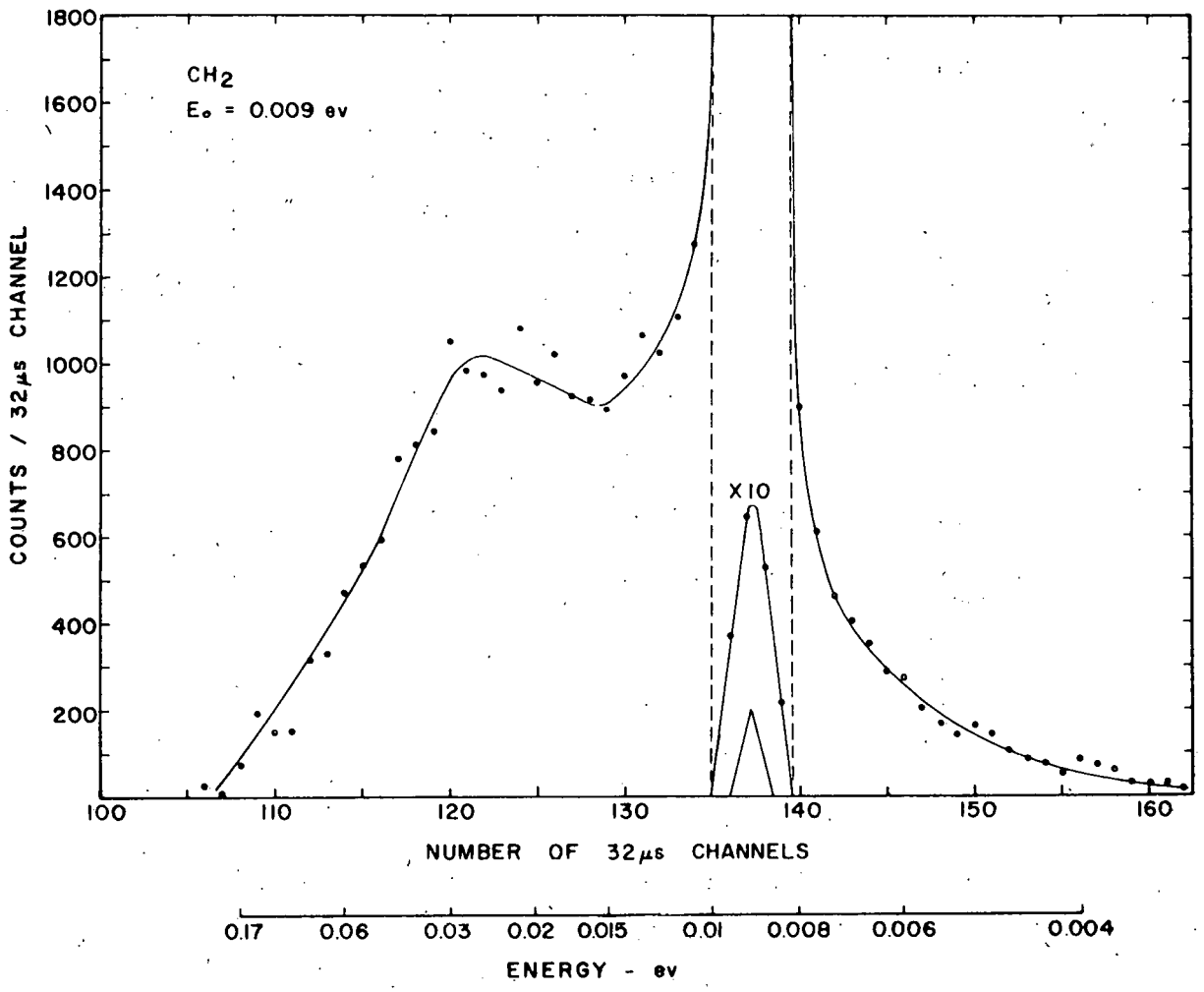

Fig. 26--Scattering of 0.009 ev neutrons from a specimen of polyethylene with 75 percent crystallinity. The resolution of the incident beam as determined by scattering from V is shown by the small triangle.

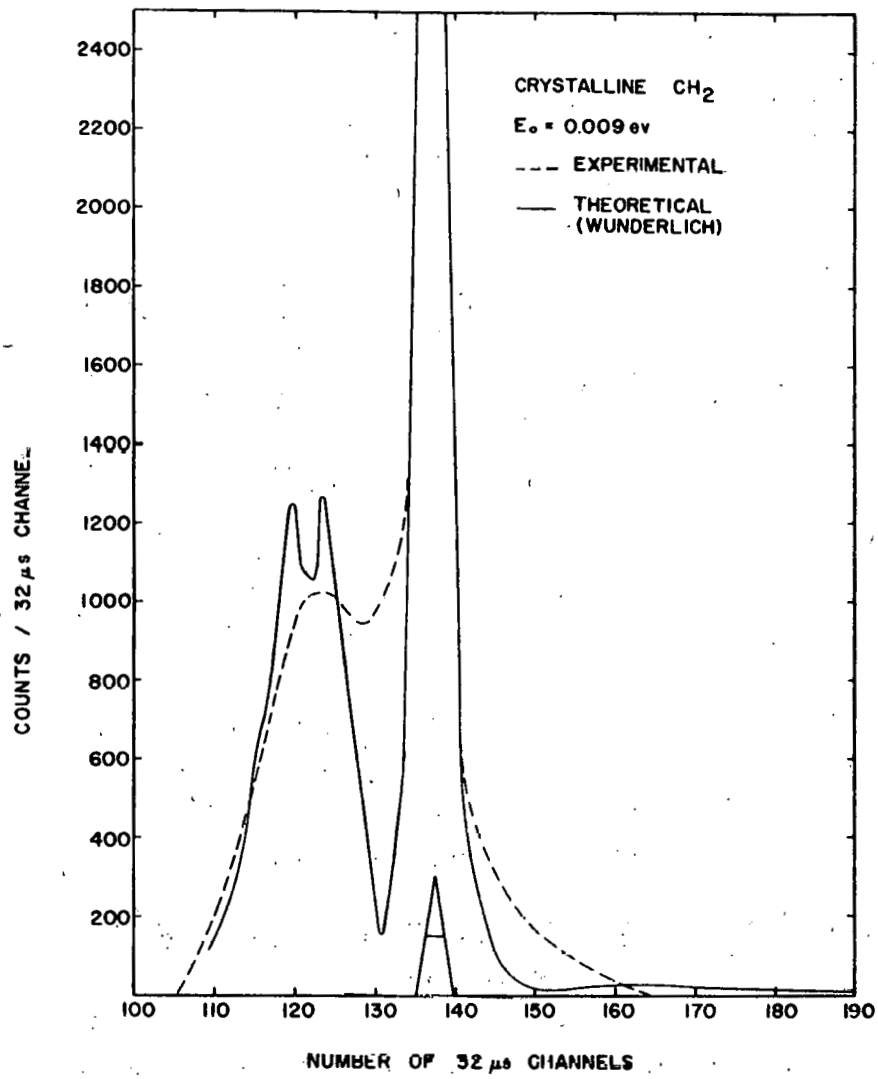

Fig. 27--Time-of-flight scattering pattern for crystalline polyethylene observed at 90 deg for E_o = 0.009 ev. The theoretical curve for 100 percent crystalline CH_{2n}, shown along with the experimental data, takes into account the known experimental resolution shown as a small triangle.

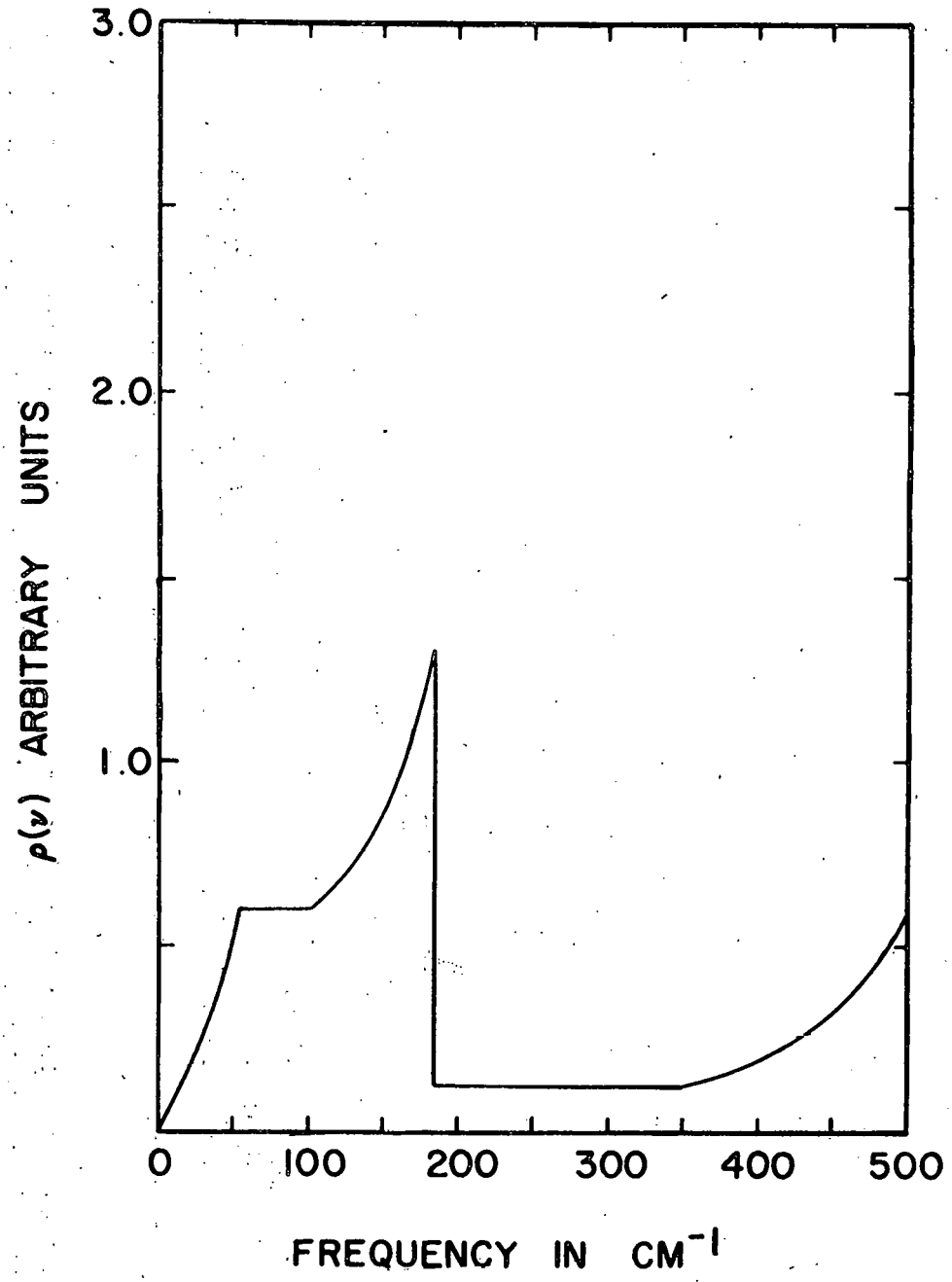

Fig. 28--Molecular frequency distribution derived for polyethylene by Wunderlich and based on specific heat data

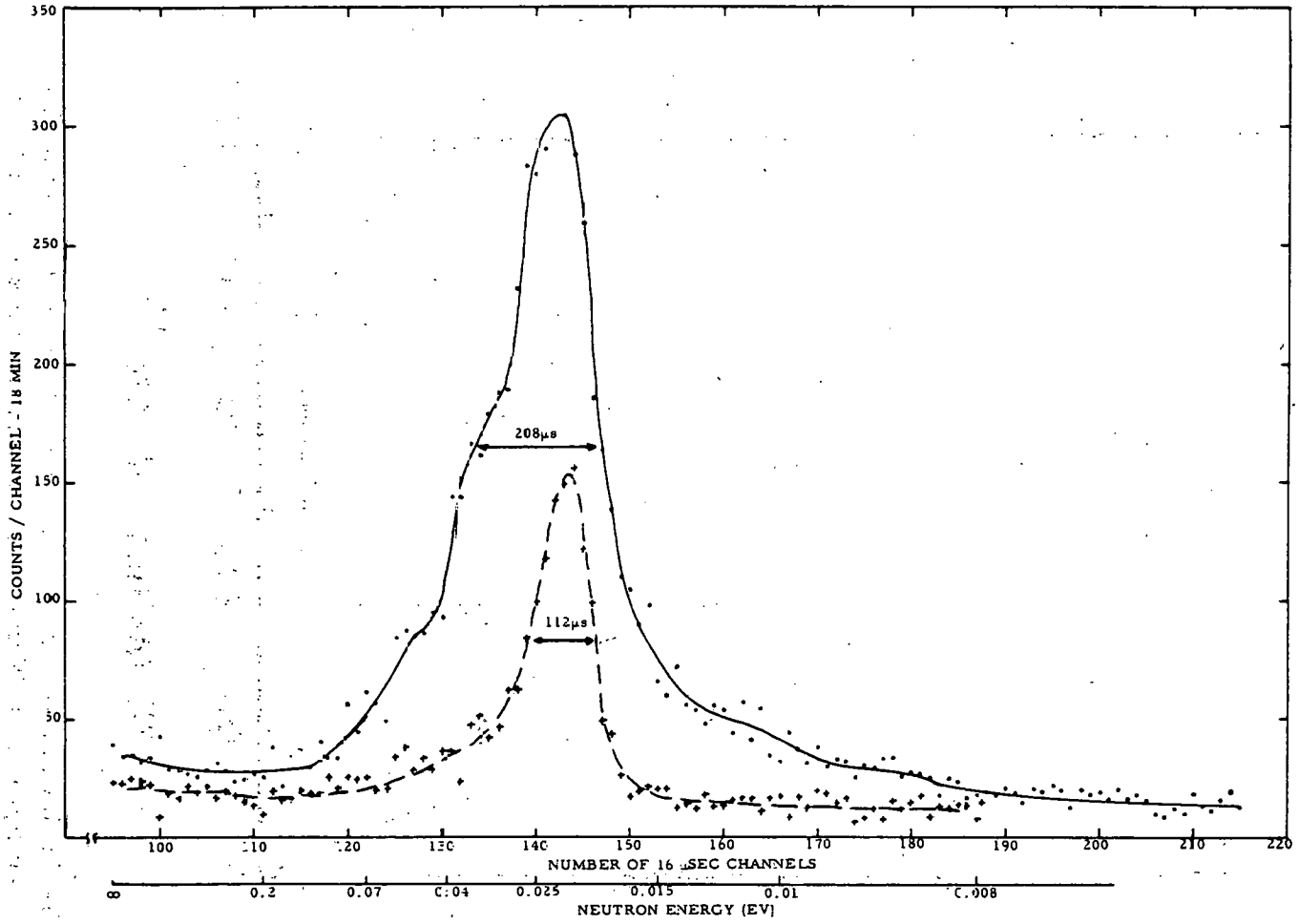

Fig. 29--The time-of-flight distribution of neutrons with $E_o = 0.022$ ev, scattered at $\theta = 90$ deg by a thin specimen of amorphous polyethylene. The incident beam resolution is shown by the scattering from V. Note that the resolution as determined by V is poorer for this experiment than for that shown in Fig. 26 because the chopper rotational speed was slower for this experimental run.

5.3.1 Theory

Goldman[20] has developed a Scattering Law for polyethylene using essentially a perfect gas model for the carbon-hydrogen molecule incorporating the frequencies shown in Table 5. The results of Goldman's calculations are shown in Fig. 30. For small values of α, all values of $S(\alpha, \beta)/\alpha$ decrease abruptly as is characteristic of a perfect gas model. Parks has derived a different representation of the Scattering Law data using the frequency distribution of Wunderlich.[21] These results are shown in Fig. 31. The important differences between these two representations are immediately evident. First, Parks' data extrapolate to finite values of $S(\alpha, \beta)/\alpha$, and second, all values of Parks' calculation of $S(\alpha, \beta)/\alpha$ are noticeably smaller than Goldman's work for the same α and β.

Table 5

FREQUENCIES OF MOTION FOR POLYETHYLENE*

Level	E(ev)
rotation	0.089
vibration	0.187
vibration	0.354
vibration	0.533

*Reference 20.

5.3.2 Experimental Results

An example of more recently obtained scattering patterns for CH_{2n} is exhibited in Fig. 32. From these data, one can readily see evidence for interactions with the higher lying levels (see particularly the data at 90 deg). The data obtained earlier for scattering at $\theta = 90$ deg have been analyzed for use in the Scattering Law evaluation. These data have been reduced to the usual Scattering Law representation, using the relation:

$$\sigma(E_o, E, \theta) = \frac{\sigma_b}{4\pi}\left(\frac{E}{E_o}\right)^{\frac{1}{2}} \exp(-\beta/2) S(\alpha, \beta) \qquad (16)$$

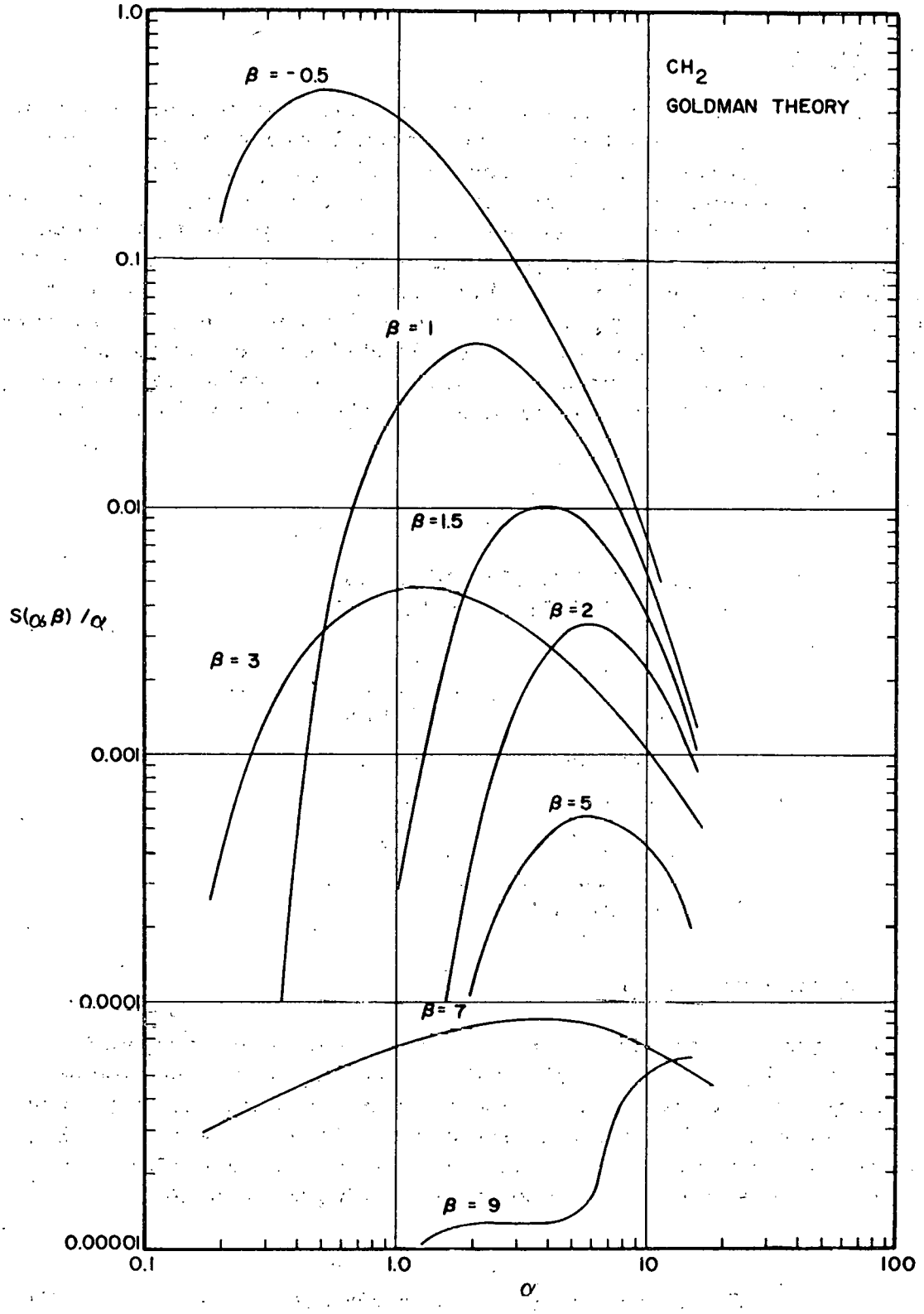

Fig. 30--Theoretical Scattering Law for polyethylene derived by Goldman

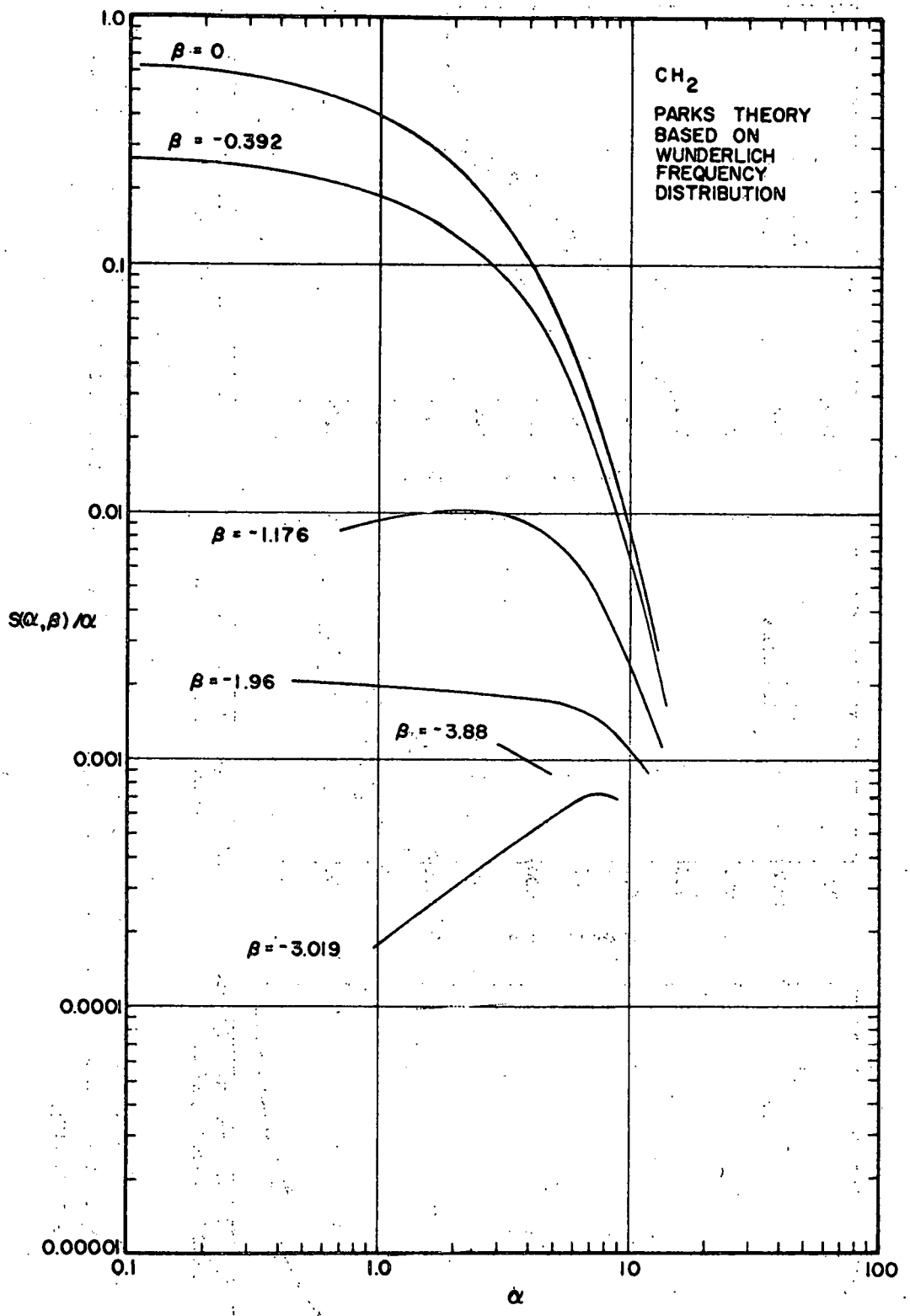

Fig. 31--Theoretical Scattering Law for polyethylene derived by Parks, using Wunderlich's frequency distribution

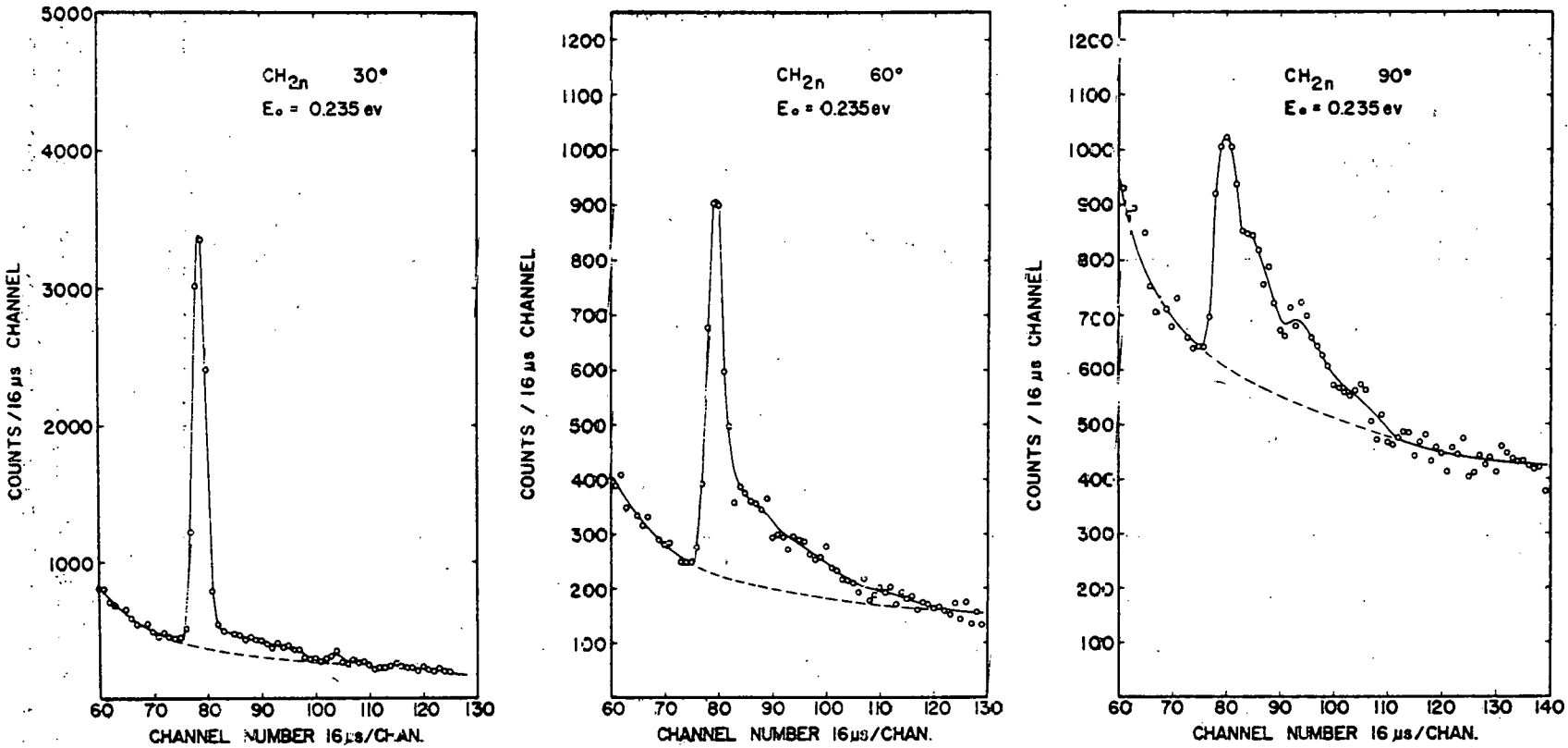

Fig. 32--Set of time-of-flight scattering patterns for amorphous polyethylene obtained for E_o = 0.235 ev. Note the scattering by the bound levels in polyethylene, particularly for data obtained at θ = 90 deg.

where $S(\alpha, \beta)$ is the Scattering Law,

$$\alpha = \frac{h^2\kappa^2}{2k_BT} = \frac{E_o+E-2\sqrt{E_oE}\cos\theta}{k_BT}$$

$$\beta = \frac{E-E_o}{k_BT}$$

σ_b = bound cross section per atom

$$\sigma(E_o, E, \theta) = \frac{d^2\sigma}{dEd\Omega}$$

In the process of deriving $S(\alpha, \beta)$, it has been necessary to evaluate the absolute differential cross sections measured at θ = 90 deg. Table 6 gives the deduced relations between $\frac{d\sigma}{d\Omega}\Big|_{90^o}$ and E_o, together with $4\pi\frac{d\sigma}{d\Omega}\Big|_{90^o}$, and our measured values of σ_{total} for CH_{2n} molecules taken from Fig. 13 in Ref. 9. It will be observed that $4\pi\frac{d\sigma}{d\Omega}\Big|_{90^o}$ is meaningful only if the scattering is isotropic in the laboratory system; otherwise, it only serves to indicate in some degree the anisotropy in the scattering. In Table 6, it will be seen that the normalization is not proper for E_o = 0.128 ev. Something went wrong with the monitor electronics during this run; however, the data can be used for $S(\alpha, \beta)$ calculations if the data of Table 6 is used to normalize the curve consistent with the other data.

Table 6

OBSERVED VALUES FOR CH_2 MOLECULES OF $\frac{d\sigma}{d\Omega}\Big|_{90^o}$, $4\pi\frac{d\sigma}{\sigma\Omega}\Big|_{90^o}$, AND σ_{total}

E_o (ev)	$\frac{d\sigma}{d\Omega}\Big\|_{90^o}$ (barns/sterad)	$4\pi\frac{d\sigma}{d\Omega}\Big\|_{90^o}$ (barns)	σ_{total} (barns)
.0090	9.95	125.0	120
.0136	8.66	109.0	110
.022	7.30	91.5	91
.038	6.76	85.0	80
.071	4.71	59.6	66
.089	4.50	56.5	60
.108	3.95	49.7	51
.128	9.03	113.0	50
.170	3.37	42.5	48

In Fig. 33, we have shown a typical curve of $S(\alpha, \beta)$ versus β and α as determined from Eq. 16. Figure 34 shows two plots of $S(\alpha, \beta)/\alpha$ versus α for different values of β. Also shown on these plots are the calculated curves of Goldman.[20] It is seen that the experimental curves agree rather well with the theory for $\beta = -\frac{1}{2}$ and $\beta = -1$ for $\alpha \gtrsim 1$. For smaller values of α, there is indication from the experimental data that a significant deviation from the theoretical results occur as expected since the Goldman model should fail to represent solid CH_{2n} for small α. For all areas of comparison, the theoretical calculation of Parks[21] should be used for the Scattering Law comparisons since an actual "solid" model was used for the frequency distributions. These will be used in all of our future work on CH_{2n}. In Fig. 35 we have compared three curves for $\beta = 0$, -0.5 and -1.0. These data together with many others will be included in a more complete treatment of polyethylene in the near future.

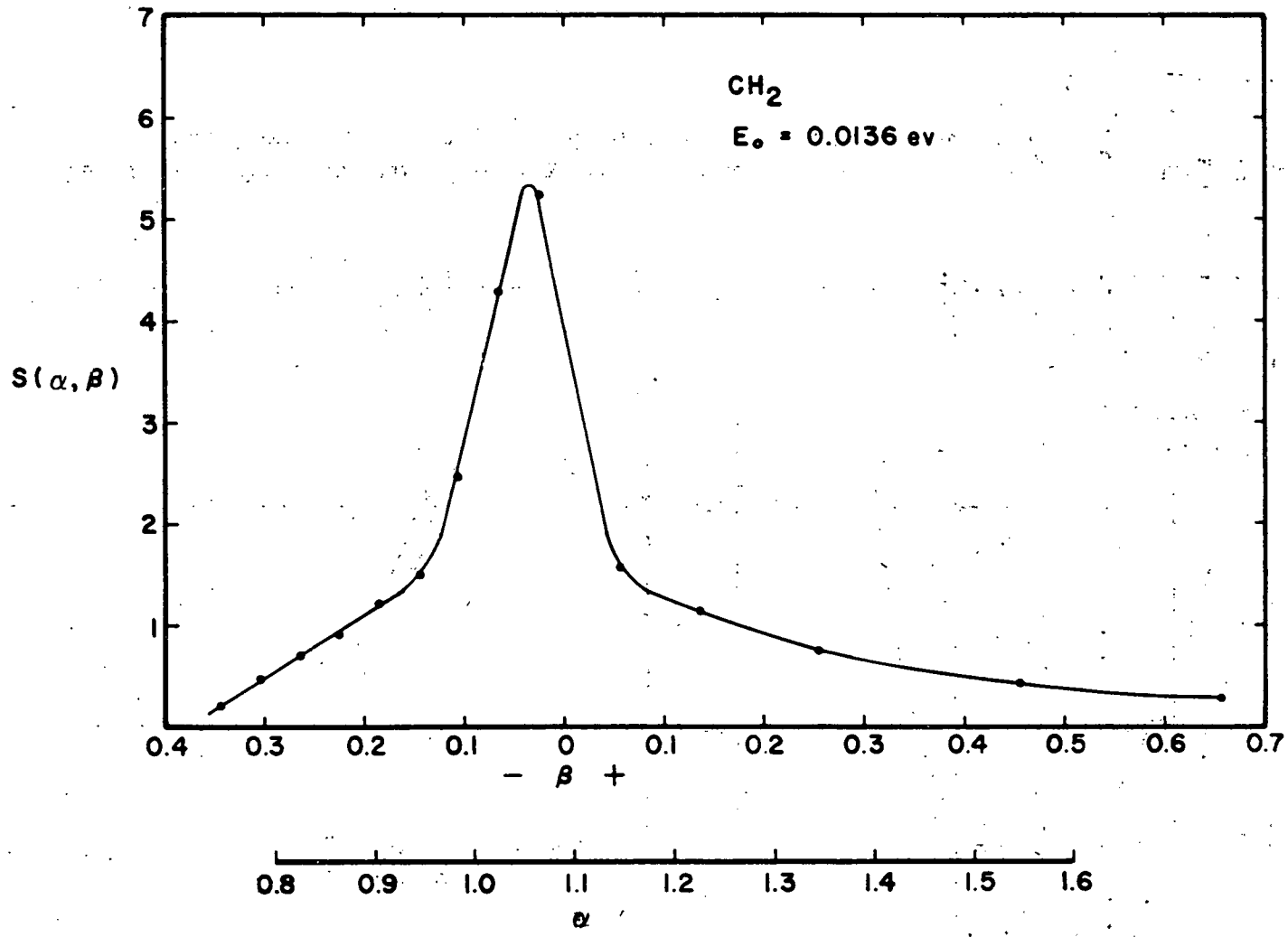

Fig. 33--Plot of the Scattering Law $S(\alpha, \beta)$ versus β and versus α for amorphous polyethylene at 300°K. The incident energy was 0.0136 ev for this experimental run and the scattering angle was 90 deg.

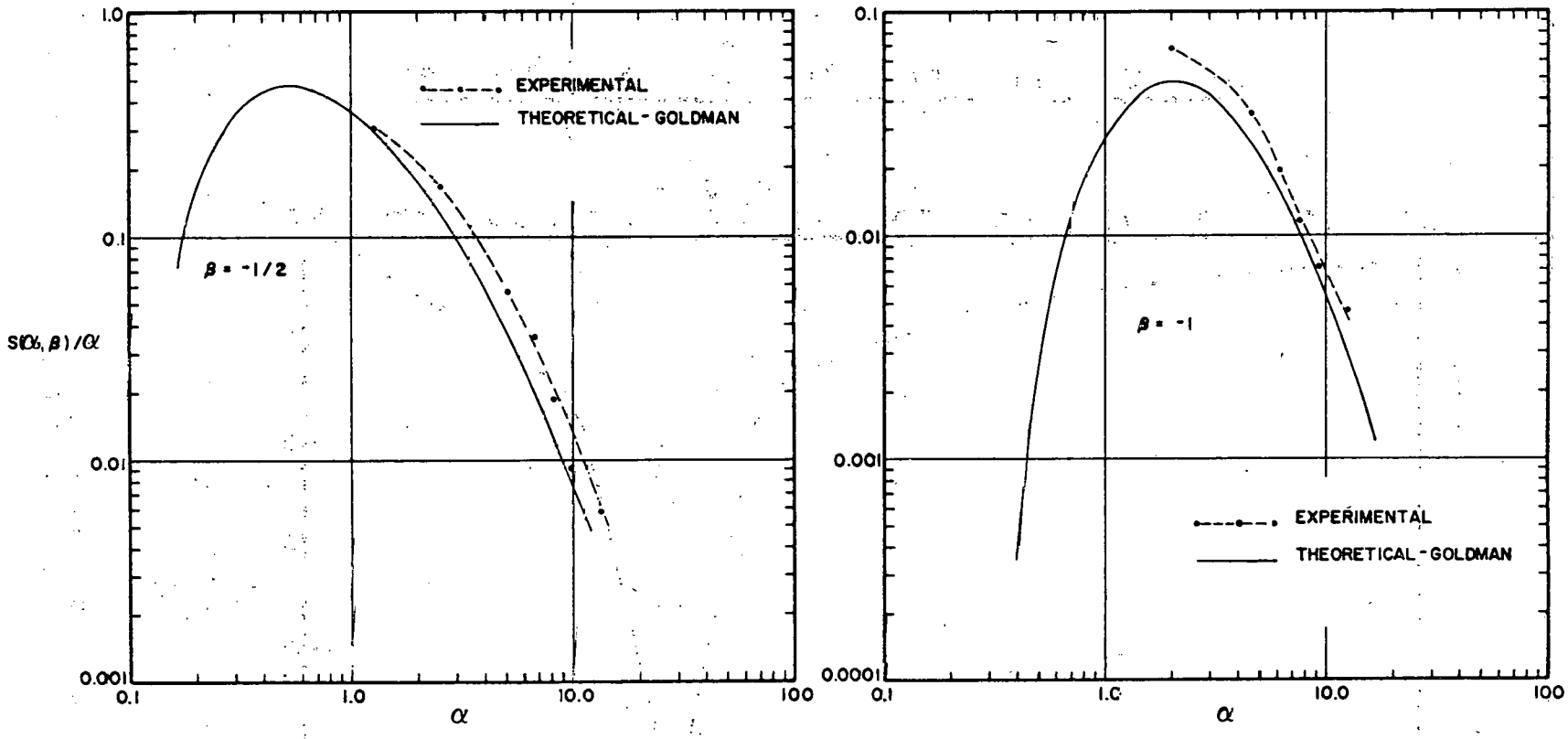

Fig. 34--Plot of the Scattering Law $S(\alpha, \beta)/\alpha$ versus α for $\beta = -1/2$ and $\beta = -1$, showing a comparison of the theory of Goldman with the experimental data

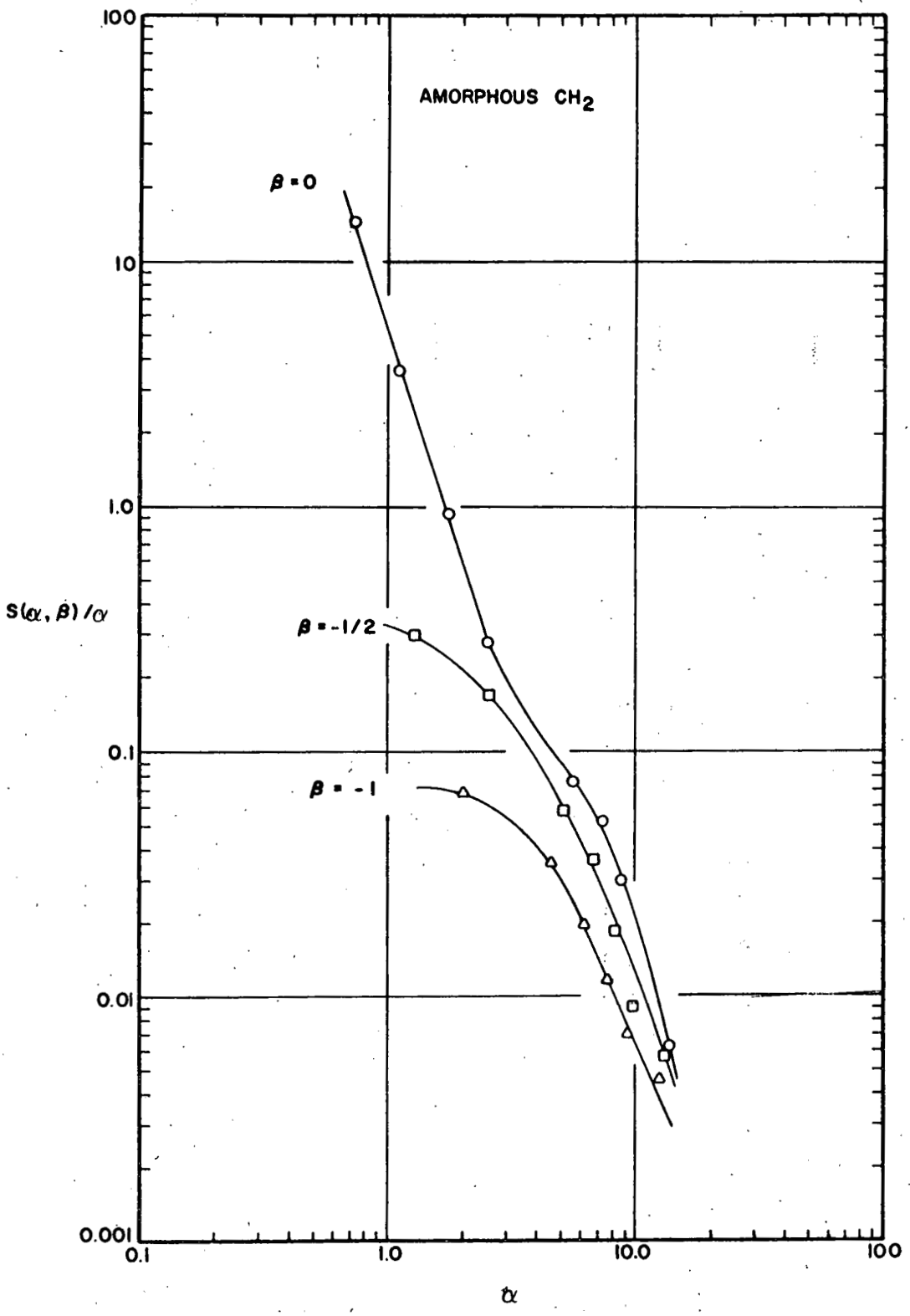

Fig. 35--Plot for polyethylene of experimental values of the Scattering Law $S(\alpha, \beta)/\alpha$ versus α for $\beta = 0, -1/2, -1$

THIS PAGE

WAS INTENTIONALLY

LEFT BLANK

REFERENCES AND FOOTNOTES

1. Whittemore, W. L., "Differential Neutron Thermalization," Annual Summary report covering the period October 1, 1961 through September 30, 1962, on Contract AT(04-3)-167, Proj. Agreement No. 10. (General Atomic report GA-3409). 1962.

2. Zimmermann, K. A., "Actual Entry Time-of-Flight Adapter." Submitted to Review of Scientific Instruments.

3. Sarma, G., in Inelastic Scattering of Neutrons in Solids and Liquids, proceedings of symposium at Vienna, Oct. 11-14, 1960; sponsored by the International Atomic Energy Agency. (I.A.E.A., Vienna, Austria, 1961) p. 397ff.

4. Sjölander, S., Arkiv Fysik 14, 315 (1958).

5. Egelstaff, P. A., in Inelastic Scattering of Neutrons in Solids and Liquids, proceedings of symposium at Chalk River, Sept. 10-14, 1962; sponsored by the International Atomic Energy Agency. (I.A.E.A., Vienna, Austria, 1963) Vol. I, p. 284, Discussion.

6. Schwinger, J., and E. Teller, Phys. Rev. 52, 286 (1937).

7. Webb, F. J., Nuclear Sci. and Eng. 9, 120 (1961).

8. McReynolds, A. W., and W. L. Whittemore, in Inelastic Scattering of Neutrons in Solids and Liquids, proceedings of symposium at Vienna, Oct. 11-14, 1960: sponsored by the International Atomic Energy Agency. (I.A.E.A., Vienna, Austria, 1961)pp.421ff. General Atomic report GA-1690).

9. Whittemore, W. L., and A. W. McReynolds, "Differential Neutron Thermalization," Annual Summary report covering the period of October 1, 1960 through September 30, 1961, on Contract AT(04-3) -167, Proj. Agreement No. 10. (General Atomic report GA-2503) 1961.

10. Squires, G. L., and A. T. Steward, Proc. Roy. Soc. (London) A230, 19 (1955). This work contains many references to previous published reports.

11. Rogalska, Z., "Slow Neutron Scattering by Molecules of Liquid Methane." Institute of Nuclear Physics, Cracow. Report No. 215, 1962.

REFERENCES AND FOOTNOTES (Cont.)

12. Krieger, T. J., and M. S. Nelkin, Phys. Rev. 106, 290 (1957).

13. Whittemore, W. L., and H. R. Danner, in Inelastic Scattering of Neutrons in Solids and Liquids, proceedings of symposium at Chalk River, Sept. 10-14, 1962; sponsored by the International Atomic Energy Agency. (I.A.E.A., Vienna, Austria, 1963.) Vol. I, pp. 283ff. (General Atomic report GA-3371).

14. Bouquet, V. H., "An Investigation of Slowing-down Parameters for Neutrons in Liquid Hydrogen." North Carolina State College, Raleigh, 1963.

15. Woods, A. D. B., B. W. Brockhouse, M. Sakamoto, and R. N. Sinclair, in Inelastic Scattering of Neutrons in Solids and Liquids, proceedings of symposium at Vienna, Oct. 11-14, 1960; sponsored by the International Atomic Energy Agency. (I.A.E.A., Vienna, Austria, 1961.) pp.487ff.

16. Fermi, E. Ric. sci. 7, pt. 2, 13 (1963).

17. Marshall, W., and R. N. Stuart, "The Scattering of Neutrons from Polycrystalline Materials," U. of C. Radiation Laboratory, Livermore, Report UCRL-5586, April 8, 1959.

18. Whittemore, W. L., et al., Phys. Rev. 108, 1092 (1957).

19. Wunderlich, B., J. Chem. Phys. 37, 1203 (1962).

20. Goldman, D., Knolls Atomic Power Laboratory, private communication.

21. Parks, D. E., General Atomic, private communication.

SELECTED BIBLIOGRAPHY

Papers on Differential Neutron Thermalization under Contract AT(04-3)-167, Project Agreement No.10, and related General Atomic Programs (1959 - 1963).

Pelah, I., W. L. Whittemore, and A. W. McReynolds, "Energy Distribution of Neutrons Scattered by Liquid Lead," Phys. Rev. 113, 767 (1959).

Whittemore, W. L., and A. W. McReynolds, "Effects of Chemical Binding on the Neutron Cross Section of Hydrogen," Phys. Rev. 113, 806 (1959).

McReynolds, A. W., and W. L. Whittemore, "Slow Neutron Scattering by Hydrogen," presented at American Physical Society meeting, Washington, April 30-May 2, 1959. Bull. Am. Phys. Soc. 4, 246 (1959).

Whittemore, W. L., A. W. McReynolds, and I. Pelah, "A Neutron Time-of-Flight Study of the Einstein Energy of Several Metal Hydrides," presented at American Physical Society meeting, April 30-May 2, 1959. Bull. Am. Phys. Soc. 4, 246 (1959).

Parks, D. E., D. H. Perkel, and N. F. Wikner, "Thermal-Neutron Spectra in Polycrystalline Graphite," presented at American Nuclear Society meeting, Gatlinburg, Tennessee, June 15-17, 1959. Trans. Am. Nuc. Soc., 2, 244 (1959).

Nelkin, M. S., "Neutron Thermalization in Water," General Atomic report GA-1180, January 13, 1960.

Whittemore, W. L., and A. W. McReynolds, "Measurement of Neutron Transport Cross Section by Crystal Spectrometer Techniques," presented at American Physical Society meeting, New York, January 27-30, 1960. Bul. Am. Phys. Soc. 5, 17 (1960).

Nelkin, M. S., "The Scattering of Slow Neutrons by Water," Phys. Rev. 119, 741 (1960).

Nelkin, M. S., and D. E. Parks, "The Effects of Chemical Binding on Nuclear Recoil," Phys. Rev. 119 , 1060

SELECTED BIBLIOGRAPHY (Cont.)

McReynolds, A. W., and W. L. Whittemore, "Linac Measurements of Hydrogen Bonding Effects on Neutron Thermal Inelastic Scattering," presented at Conference on Neutron Diffraction in Relation to Magnetism and Chemical Binding, Gatlinburg, Tennessee, April, 1960.

McReynolds, A. W., and W. L. Whittemore, "Inelastic Scattering of Neutrons from Very Cold Materials," presented at the International Atomic Energy Agency Conference on Inelastic Scattering of Neutrons in Solids and Liquids, Vienna, Oct. 11-14, 1960, in Inelastic Scattering of Neutrons in Solids and Liquids (I.A.E.A., Vienna, Austria, 1961), pp. 421ff.

Whittemore, W. L., and A. W. McReynolds, "Inelastic Scattering of Thermal Neutrons Produced by an Accelerator," presented at the International Atomic Energy Agency Conference on Inelastic Scattering of Neutrons in Solids and Liquids, Vienna, Oct. 11-14, 1960, in Inelastic Scattering of Neutrons in Solids and Liquids (I.A.E.A., Vienna, Austria, 1961), pp. 511ff.

Whittemore, W. L. "A Small Neutron Beam Chopper," General Atomic report GAMD-1961, January 18, 1961.

McReynolds, A. W., and W. L. Whittemore, "Structure and Dynamics of Liquid Hydrogen by Neutron Scattering," presented at American Physical Society Meeting, Washington, April, 1961. Bull. Am. Phys. Soc. 6, 262 (1961).

Whittemore, W. L., and A. W. McReynolds, "Neutron Scattering by Low-Temperature H_2O," presented at American Physical Society Meeting, Washington, April, 1961. Bull. Am. Phys. Soc. 6, 262 (1961).

McReynolds, A. W., and W. L. Whittemore, "Structure and Dynamics of Liquid Hydrogen by Neutron Scattering," presented at the International Atomic Energy Agency Conference on Inelastic Scattering of Neutrons in Solids and Liquids, Chalk River, Canada, September 10-14, 1962, in Inelastic Scattering of Neutrons in Solids and Liquids (I.A.E.A., Vienna, Austria, 1963) Vol. I, pp. 263ff.

Whittemore, W. L., and H. R. Danner, "Neutron Interactions in Liquid Para- and Ortho-Hydrogen," presented at the International Atomic Energy Agency Conference on Inelastic Scattering of Neutrons in Solids and Liquids, Chalk River, Canada, September 10-14, 1962, in Inelastic Scattering of Neutrons in Solids and Liquids (I.A.E.A., Vienna, Austria, 1963) Vol. I, pp. 273ff.

SELECTED BIBLIOGRAPHY (Cont.)

Whittemore, W. L., "Neutron Inelastic Scattering in Liquid Methane and Liquid Parahydrogen," General Atomic report GA-4292. Submitted to Nuclear Science and Engineering. An oral presentation of part of this report was made at the Washington meeting of the American Physical Society, April, 1963.

Zimmermann, K., "Actual Entry Time-of-Flight Adapter for a 1024 Channel Analyzer." Submitted to Review of Scientific Instruments.

Papers in preparation, with publication anticipated prior to the end of the current contract year:

1. "The Scattering Law for Zirconium Hydride."
2. "Experimental and Theoretical Scattering Law for Polyethylene."
3. "Neutron Scattering by Hydrogen Bound in Zirconium Hydride."
4. "The General Atomic Neutron Velocity Selector for Pulsed Thermal Beams Using an Electron Linear Accelerator."